01/17/97 FRI 16:14 FAX 512 916 5529 ONR AUSTIN 0 13060 002

# REPORT DOCUMENTATION PAGE

Form Approved
OMB No. 0704-0188

Public reporting burden for this collection of information is estimated to average 1 hour per response, including the time for reviewing instructions, searching existing data sources, gathering and maintaining the data needed, and completing and reviewing the collection of information. Send comments regarding this burden estimate or any other aspect of this collection of information, including suggestions for reducing this burden to Washington Headquarters Services, Directorate for Information Operations and Reports, 1215 Jefferson Davis Highway, Suite 1204, Arlington, VA 22202-4302, and to the Office of Management and Budget, Paperwork Reduction Project (0704-0188), Washington, DC 20503.

**1. AGENCY USE ONLY** *(Leave blank)*

**2. REPORT DATE** 05-27-97

**3. REPORT TYPE AND DATES COVERED** Final

**4. TITLE AND SUBTITLE**
Theory and Simulation of the Structure and Dynamical Properties of Electronic Materials

**5. FUNDING NUMBERS**
G- N00014-95-1-0906

**6. AUTHOR(S)**
Sokrates T. Pantelides

**7. PERFORMING ORGANIZATION NAME(S) AND ADDRESS(ES)**
Vanderbilt University
6631 Stevenson Center
Nashville, TN 37235

**8. PERFORMING ORGANIZATION REPORT NUMBER**

**9. SPONSORING/MONITORING AGENCY NAME(S) AND ADDRESS(ES)**
ONR-Atlanta Regional Office
101 Marietta Street, Suite 2805
Atlanta, GA 30323

**10. SPONSORING/MONITORING AGENCY REPORT NUMBER**

**11. SUPPLEMENTARY NOTES**

**12a. DISTRIBUTION / AVAILABILITY STATEMENT**

APPROVED FOR PUBLIC RELEASE; DISTRIBUTION IS UNLIMITED.

**12b. DISTRIBUTION CODE**

**13. ABSTRACT** *(Maximum 200 words)*

During the course of this grant, research focused on using available theoretical tools to explore and elucidate complex dynamics of impurities in Si. In particular, we studied clustering of As in heavily-doped Si, segregation of As in Si grain boundaries and the migration of oxygen in Si. In addition we carried out atomic-scale nonequilibruim heat flow simulations and mesoscopic calculations of void growth in polycrystalline metal lines.

DTIC QUALITY INSPECTED 2

19970616 105

**14. SUBJECT TERMS**
semiconductors, silicon, impurities

**15. NUMBER OF PAGES** 56

**16. PRICE CODE**

| 17. SECURITY CLASSIFICATION OF REPORT | 18. SECURITY CLASSIFICATION OF THIS PAGE | 19. SECURITY CLASSIFICATION OF ABSTRACT | 20. LIMITATION OF ABSTRACT |
|---|---|---|---|
| unclassified | unclassified | unclassified | unlimited |

Final Report on ONR Grant N00014-95-1-0906

# Theory and Simulation of the Structure and Dynamical Properties of Electronic Materials

Sokrates T. Pantelides
Department of Physics and Astronomy
Vanderbilt University

## 1. Introduction

During the grant period, the research focus was to use existing computational tools and explore atomic-scale dynamics, defect reactions, and diffusion in solids. These tools include state-of-the-art first-principles calculations (density functional theory in the local density approximation for exchange-correlation with pseudopotentials and supercells) as well as classical molecular dynamics.

In particular, we addressed: a) the dynamics of dopant impurities in Si in the heavily-doped limit, including dopant deactivation through clustering, thermal reactivation, and enhanced diffusion; b) the segregation of dopants in Si grain boundaries and dislocation, where we predicted selective segregation in particular columns in the form of pairs or ordered chains -- the prediction was subsequently verified by atomic-resolution transmission electron microscopy; c) the mechanism of oxygen migration in crystalline Si where we found enormous complexity and coupled barriers in a seemingly very simple atomic jump; d) the flow of heat across a grain boundary using molecular dynamics which led to a direct calculation of the Kapitza resistance of a grain boundary; and e) mesoscopic calculations of void growth under electromigration conditions.

Brief descriptions of the main results are given below. More detailed discussion is given in the attached Appendices.

## 2. Dynamical phenomena in heavily As doped Si

In the dilute limit, As impurities occupy substitutional sites and act as donors. It has been possible by non-equilibrium techniques to incorporate As impurities as substitutional donors at very high concentrations, as high as $10^{21}$ $cm^{-3}$. However, moderate heating (~300-400°C) leads to rapid deactivation. Partial reactivation is possible by heating to higher temperatures (>800°C). Early work attributed the deactivation to the formation of $As_nV_m$ clusters (where V stands for a vacancy), but there has been no consensus about the values of m and n for the dominant defect. Another major puzzle has been the fact that, in the dilute limit, there is no observable diffusion in the 300-400°C temperature range. Thus, some other diffusion mechanism must be operating in the heavily-doped limit to enable the As atoms to migrate and form clusters. Early diffusion measurements in heavily-doped samples, however, found that the diffusion constant increases gradually with increasing As concentration, but then begins to drop for As concentrations above ~$3x10^{20}$ $cm^{-3}$. More recent experiments using rapid thermal annealing techniques,

found a sharp increase in the value of the diffusion constant beginning at the same concentration. References to all the relevant experimental work can be found in Appendix A. Though explanations for some of the observations have been proposed by earlier workers, no comprehensive account of all the data has been possible.

A set of comprehensive calculations carried out by Ramamoorthy and Pantelides provided a systematic account of all the perplexing observations and made additional predictions. The detailed results are discussed in Appendix A. In particular, it was found that:

i) Complexes of the form $As_nV_m$ have a negative formation energy for n>2. For all such complexes, the binding energy of each As atom (relative to an isolated substitutional site in the bulk crystal) is ~1.5 eV. These results mean that As-doped Si is a metastable system at all As concentrations. If it were not for kinetic constraints, all As atoms would decorate vacancies and multivacancies. The result is a consequence of the chemical valency of As which makes threefold-coordinated As energetically favored.

ii) It has long been known that, in the dilute limit, As diffusion is mediated by AsV pairs. The pair migrates as follows: The vacancy loops around a six-member ring and positions itself "in front" of the As; the As atom jumps into the vacant site; the vacancy again loops around another six-member ring and again positions itself "in front" of the As atom. The activation energy for diffusion by this mechanism (formation plus migration energy of the pair) was computed to be 3.9 eV, in excellent agreement with experimental data.

iii) In the heavily doped limit, Mathiot and Pfister[1] proposed that the same mechanism operates, but the activation energy is lowered by the presence of nearby As atoms. In particular, during migration, as the vacancy loops around a six-member ring, it is likely to pass by another As atom. Mathiot and Fister recognized, however, that such proximity with another As atom would require extremely high concentrations. They resolved this quandary by invoking percolation theory, according to which an infinite percolation network with very high As concentrations forms when the total concentration exceeds ~$3 \times 10^{20}$ $cm^{-3}$. The activation energy for the mechanism proposed by Mathiot and Pfister was computed to be ~1 eV lower than the simple AsV pair mechanism. It would appear, therefore, that the percolation model can account for the mobility of As atoms leading to clustering at moderate temperatures and the observed enhanced diffusion at high concentrations. The model, however, does have a problem in that enhanced diffusion within the percolation network would quickly lead to the formation of $As_nV_m$ clusters that would break up the continuity of the network. In contrast, the experiments show that the clustering process persists for long times.

iv) Calculations reported demonstrated that $As_2V$ complexes are mobile and can, therefore, mediate As diffusion. The net activation energy was computed to be 2.8 eV, i.e. essentially the same as in the mechanism advocated by Mathiot and Pfister. The key difference is that diffusion mediated by $As_2V$ complexes does

not need a continuous percolation network but only high-concentration regions. Such regions may exist, for example, when the average concentration is just below the percolation threshold (pre-percolation patches) or after an initial rapid diffusion for average concentrations that exceed the percolation threshold (post-percolation patches). In the latter case, the initial diffusion leads to clustering that breaks up the percolation network, but $As_2V$ complexes continue to mediate diffusion by traveling both through and between patches.

v) Mobile $As_2V$ complexes account for all the observed phenomena in a systematic way (see Appendix A for more details). In addition, they lead to predictions on the nature of the dominant complexes in deactivated samples. The complexes AsV, $As_2V$ and $As_3V$ are the only one which can break up into an isolated substitutional As and a mobile complex. In each case, the energy to "peel off" an As atom is ~1.5 eV, which is the same as the value of the reactivation activation energy Schwenker et al.[2] extracted from their experimental data.[1] Since EXAFS data established that in deactivated samples virtually all As atoms are second neighbors to each others, we conclude that the dominant complexes in deactivated samples are $As_2V$ and $As_3V$. Higher-order complexes also exist and are the ones that persist during reactivation at 1000°C because the energy needed to break them up is much larger than 1.5 eV.

3. Segregation of As atoms in Si grain boundaries

This is worked carried out by Pantelides in collaboration with A. Maiti, S. J. Pennycook and M. Chisholm at Oak Ridge National Laboratory and is described in detail in Appendix B, where references to original literature can be found. The issue is that virtually 99% of As in polycrystalline Si segregates in grain boundaries. This is undesirable because As in grain boundaries is electrically inactive and one normally would like to dope polycrystalline Si very heavily to be used as contact.

The segregation energy (defined to be the energy difference per As atom between As atoms in the grain boundary and the bulk crystal) is measured to be ~0.5 eV and is responsible for the observed behavior. It is worthwhile to determine if this large segregation energy is an intrinsic property of grain boundaries in Si or it is a consequence of defects or steps where As atoms bind preferentially. This question became particularly relevant when it was determined by both theory and experiment that tilt grain boundaries in Si without steps or impurities relax to configurations where all Si atoms are fourfold-coordinated.

Recent theoretical work by Arias and Joannopoulos[3] found that As atoms placed at fourfold-coordinated sites in a fully relaxed $\Sigma=5$ grain boundary in Ge remain fourfold and lower their energy by a minimal amount over bulk sites (~0.1 eV). They suggested that the observed large segregation energy is likely to be caused by defects or steps.

The main objective of our work was to explore the possibility that As atoms can be incorporated in threefold coordination in otherwise perfect grain boundaries. It was found that threefold coordination is possible if As atoms are incorporated in pairs. The phenomenon is quite intriguing. Two nearest-neighbor substitutional As

atoms repel each other trying to achieve threefold coordination (their preferred chemical valence) at a cost of elastic energy in the distorted back bonds. The calculations show that in the bulk crystal and energy gain and cost roughly balance out. In the grain boundary, however, the cost is a bit less. The net result is that a dimer binds in the grain boundary through repulsion! The segregation energy of such dimers was found to be in the range 0.1-0.2 eV. For chains of dimers, however, the segregation energy increased to 0.35 eV (for a case where one actually perfectly ordered As atoms with equal As-As distances) and to 0.5 eV.

The dimer calculations were done for two distinct $\Sigma=5$ boundary structures, both of which have all Si atoms fourfold coordinated, with total energies that are very close (one is higher by 0.15 eV/atom). The As chains with the highest segregation energy are in fact in the grain boundary structure with the slightly higher energy. This result leads to the intriguing suggestion that As atoms segregating in a grain boundary may actually induce a structural transformation of the entire grain boundary.

In addition to theoretical investigations of As impurities in Si grain boundaries, an experimental search was undertaken by Chisholm and Pennycook for evidence of As segregation. Arsenic was implanted and annealed for a prolonged period of time. Micrographs obtained with high-resolution transmission microscopy using the Z-contrast technique reveal evidence of chains of As atoms.

Finally, calculations have been performed to investigate whether the ordering of As impurities in grain boundaries occurs also in isolated dislocations. The results indicate that chains of As dimers again form along the dislocation pipe with very large segregation energies (~1 eV). These results are described in detail in Appendix C.

4. Oxygen migration in Si

This is a case that on the face appears very simple, yet turns out to hide enormous complexity. The work was carried out by Ramamoorthy and Pantelides and is described in detail in Appendix D, where references to the original literature can be found.

Oxygen has long been known to occupy a bridge site between neighboring Si atoms, forming a buckled Si-O-Si chain virtually identical to the Si-O-Si chains in $SiO_2$. Its migration has been measured over a range of more than 1000 degrees and has been found to have a simple Arrhenius behavior with a 2.5-eV activation energy. The migration ought to be a simple process: the O atom jumps from one bridge site to the next. The saddle point should be at the midpoint of the O path.

Theory over the years has stumbled on this one. Calculations of the activation energy have ranged from 1.2 eV to 4.1 eV. Some authors found 2.5 eV. Then, a paper by Jiang and Brown in 1995 reported calculations using classical interatomic potentials. These authors stepped the O atom along its entire path, relaxing the Si atoms at each step. They found that the maximum energy, i.e. the saddle point was at a point after the O atom passed the midpoint of its path. This saddle point energy

was 2.5 eV. However, Jiang and Brown[4] did not notice that the total-energy profile they computed along the path did not satisfy a basic symmetry requirement, namely time reversal, which requires that the energy profile be symmetric about the midpoint of the path.

We performed systematic first-principles calculations and unveiled an enormous amount of complexity while accounting for both the experimental data and the earlier theoretical work. It was found that the motion of the O atom is intimately coupled to the motion of the "central Si atom" – the one that participates in both the initial and the final Si-O-Si chain. Both these atoms face barriers. In order to describe the migration process one needs a total-energy hypersurface in several dimensions that reveals a multiplicity of paths and a "saddle ridge" with a height of ~ 2.5 eV. Details and figures can be found in Appendix D.

More recent work (Appendix E) examined the effect of H on O diffusion. It was found that H also occupies a buckled bridge position next to the O. Migration of the O atom now proceeds as follows: the O atom heads toward the bridge site occupied by H; the latter moves toward the next bridge site in front of it. This synergism led to a lowering of the activation by about 1 eV, in agreement with observations.

## 5. Atomic-scale simulation of heat flow

Most molecular dynamics simulations are carried out within one of the equilibrium ensembles of statistical mechanics. In order to carry out simulations of a nonequilibrium process such as heat flow one has to meet significantly more stringent requirements. We have pursued heat flow calculations by maintaining a difference in temperature at the two ends of a slab of Si and demonstrated that by using long simulations it is possible to establish local equilibrium in thing layers and set up a smooth temperature gradient. We pursued such calculation for a grain boundary in Si using classical interatomic potentials and demonstrated that it is possible to compute the corresponding Kapitza resistance. Details are given in Appendix F.

## 6. Mesoscopic calculations of void growths

Electrical current is known to induce atomic diffusion which leads to void growth or extrusions that can sever or short metal interconnects in integrated circuits. Our work focused on void growth. Results are described in Appendix G.

REFERENCES


1. D. Mathiot and J. C. Pfister, J. Appl. Phys. 55, 3518 (1984).
2. O. Schwenker, E.S. Pan and R. F. Lener, J. Appl. Phys., 42, 3195 (1971).
3. A. Arias and J. D. Joannopoulos, Phys. Rev. B 49, 4525 (1994).
4. Z. Jiang and R. A. Brown, Phys. Rev. Lett. 74, 2046 (1995).

## Published Articles

M. Ramamoorthy and S.T. Pantelides, "Coupled-Barrier Diffusion: The Case of Oxygen in Silicon", Phys. Rev. Lett. 76, 267-270 (1996).

M. Ramamoorthy and S.T. Pantelides, "Complex Dynamical Phenomena in Heavily Arsenic Doped Silicon", Phys. Rev. Lett. 76, 4753-4756 (1996).

A. Maiti, M.F. Chisholm, S.J. Pennycook, and S.T. Pantelides, "Dopant segregation at semiconductor grain boundaries through cooperative chemical rebonding", Phys. Rev. Lett. 77, 1306-1309 (1996).

A. Maiti, T. Kaplan, M. Mostoller, M.F. Chisholm, S.J. Pennycook, and S.T. Pantelides, "Ordering of As impurities in a Si dislocation core", Appl. Phys. Lett. 70, 336-338 (1997).

D. Maroudas, M. N. Enmark, C. M. Leibig and S. T. Pantelides, "Analysis of Damage Formation and Propagation in Metallic Thin Films Under the Action of Thermal Stresses and Electric Fields", Journal of Computer-Aided Materials Design 2, 231-258 (1996).

A. Maiti, G.D. Mahan, and S.T. Pantelides, "Dynamical Simulations of Nonequilibrium Processes - Heat Flow and the Kapitza Resistance Across Grain Boundaries", Solid State Comm. 102, 7, 517-521 (1997).

S.T. Pantelides, "Point Defects in Semiconductors -- Then and Now", Solid State Phen. 47-48, 237-246(1995).

D. Maroudas and S. T. Pantelides, "Microstructure Evolution in Polycrystalline Conducting Films", in Proceedings of Electrochemical Society Symposia (1996).

S.T. Pantelides, M. Ramamoorthy, A. Maiti, M. Chisholm, and S.J. Pennycook, "Complex Impurity Dynamics in Si", in CAS '96 Proceedings, (IEEE, 1996), p. 13.

S. T. Pantelides, "Computational Physics for Microelectronics – The Old and the New Challenges," in Semiconductor Characterization – Present and Future Needs, edited by W.M. Bullis, D.G. Seiler and A.C. Diebold, (AIP Press, New York, 1996), p. 141.

## Invited talks at conferences

"Materials Modeling for Microelectronics -- The Old and the New Challenges", Workshop on Characterization of Microelectronics Materials, Washington, D.C., February 1995.

"Microstructure Simulation in Polycrystals", D. Maroudas and S.T. Pantelides, given by collaborator D. Maroudas, Spring Meeting of the Materials Research Society, San Francisco, April 1995.

Complex Diffusive Processes in Semiconductors", 4th International Congress on Advanced Materials, Cancun, Mexico, August 1995.

"Point Defects in Semiconductors - Then and Now", 5th Conference on Gettering and Defect Engineering in Semiconductor Technology, Berlin, Germany, September 1995.

"Point Defects in Semiconductors", International School in Semiconductor Physics, Crimea, Ukraine, Septemeber 1995 (declined)

"Mesoscopic Dynamics in Polycrystalline Metallic Films", 5th Euroconference on Complex Materials, Patras, Greece, September 1995.

"The Si-$SiO_2$ Interface - A First-Principles Approach", Fall MRS Meeting, Boston, MA, December 1995.

"Oxygen Migration in Silicon: a Case of Coupled barriers," given by post-doc M. Ramamoorthy, APS March Meeting, St. Louis, MO, March 1996.

"Oxygen in Silicon – A Very Complex Simple Jump", given by post-doc M. Ramamoorthy at Oxygen-96, a NATO Workshop in Exeter, England, March 1996.

"Complex Diffusive Phenomena in Si", M. Ramamoorthy and S.T. Pantelides, given by post-doc M. Ramamoorthy at the 5$^{th}$ Lakeview Conference on Computational Materials Science, Morgantown, WV, May 1996.

"Reminisces of the Lund Conferences", Symposium in honor of retiring professor H. Grimmeiss, Lund, Sweden, May 1996.

"The Wonderful World of Diffusion in Solids", 25$^{th}$ Annual Jasowiec Conference on Semiconductor Physics, Jasowiec, Poland, May 1996.

"Theory and Simulation of Microstructure Evolution in Polycrystalline Metal Films", D. Maroudas and S. T. Pantelides, given by collaborator D. Maroudas at the Electrochemical Society Meeting, Los Angeles, CA, May 1996.

"Theory and Simulation of Radiation - Matter Dynamics", Theory Workshop on Synchrotron Radiation, Argonne, IL, June 1996.

"Complex Diffusive Processes in Semiconductors", DI-MAT '96, Nordkirchen, Germany, July 1996.

"Oxygen Migration in Si - A Very Complex Simple Jump", Gordon Conference on Point and Line Defects in Semiconductors, Plymouth, NH, August 1996.

"Complex Impurity Diffusion Processes in Silicon", 19th International Semiconductor Conference (CAS-1996), Sinaia, Romania, October 1996.

"New Theoretical Tools Suitable for Nanoclusters", 5th Consortium for Nanostructured Materials, Nashville, TN, October 1996.

"Complex Atom Dynamics in Solids", Southeastern Section APS annual meeting, Atlanta, GA, November 1996.

"Arsenic Segregation in Silicon Grain Boundaries – Theory and high-resolution Imaging" given by post-doc A. Maiti at the MRS Fall Meeting, Boston, December 1996.

"High Resolution Scanning Transmission Electron Microscopy" (S. J. Pennycook, M F Chisholm, P D Nellist, A. Maiti and S. T. Pantelides) American Physical Society March Meeting, St. Louis. MO, March 1997

"Probing structure-property relationships at interfaces by atomic resolution Z-contrast imaging, EELS, and theory", (S. J. Pennycook, M.F. Chisholm, P. D. Nellist, A. Maiti and S.T. Pantelides) at the Workshop on Electron Microscopy, Arizona State University, January 1997.

"Impurity Segregation and Diffusion in Grain Boundaries", DiBoS '97, Moscow, Russia, May 1997.

"Impurity Segregation and Diffusion in Grain Boundaries," by post-doc A. Maiti at the Lakeview Conference on Computational Materials Science, Morgantown, WV, May 1997.

"Theory of the Nucleation and Growth of $SiO_2$ in Si: Application to SOI", International Symposium on "Silicon-On-Insulator Technology and Devices, Paris, France, August 1997.

## Contributed talks at conferences

"Impurity Clustering and Dynamics in Heavily-Doped Silicon", M. Ramamoorthy and S. T. Pantelides, Conference on Microsructure in Maerials, Baca Raton, LA, February 1996.

"Classical Molecular Dynamics without Pair Potentials", J.S. McCarley and S.T. Pantelides, APS March Meeting, St. Louis, MO, March 1996.

"Dipole Moments of Polyatomic Systems", R. Winkler and S.T. Pantelides, APS March Meeting, March 1996.

"Theory and simulation of the interaction of intense infrared fields with molecules", M. Ferconi and S.T. Pantelides, APS March Meeting, St. Louis, MO, March 1996.

"Oxygen Diffusion in Silicon", M. Ramamoorthy and S. T.Pantelides, Workshop on Electronic Structure Theories, Minneapolis, MN, June 1996.

"Thermal-Donor Formation And Oxygen-Precipitate Nucleation In Si", MRS 1996 Annual Fall Meeting, Boston, MA, December 1996.

"Classical Molecular Dynamics without Pair Potentials", J.S. McCarley and S.T. Pantelides, APS March Meeting, Kansas City, MO, March 1997.

"Infrared Field Driven Dynamics of Solids", R. Winkler and S.T. Pantelides, APS March Meeting, Kansas City, MO, March 1997.

"Nonlinear Dynamics of Systems in Intense Electromagnetic Radiation via a Time-Dependend Car-Parrinello Technique", M. Ferconi and S.T. Pantelides, APS March Meeting, Kansas City, MO, March 1997.

"Dynamical Simulations of Nonequilibrium Processes -- Heat Flow and the Kapitza Conductance Across Grain Boundaries", A. Maiti, G.D. Mahan and S.T. Pantelides, APS March Meeting, Kansas City, MO, March 1997.

## Colloquia/seminars at Universities and Research Centers

Oak Ridge National Laboratory, Oak Ridge, TN, January 1995.
University of Kentucky, Lexington, KY, April 1996
Michigan Technological University, April 1996 (declined)
Materials Science Institute, Demokritos Research Center, Athens, Greece, May 1996.
Institute of Semiconductor Physics, Frankfurt/Oder, Germany, August 1996.
Western Kentucky University, Bowling Greene, KY, October 1996.

# Complex Dynamical Phenomena in Heavily Arsenic Doped Silicon

Madhavan Ramamoorthy and Sokrates T. Pantelides
*Department of Physics and Astronomy, Vanderbilt University, Nashville, Tennessee 37209*
(Received 7 February 1996)

Several complex dynamical phenomena have been observed in heavily doped Si, but a comprehensive account of the underlying atomic-scale processes is lacking. We report a wide array of first-principles calculations in terms of which we give such a comprehensive account. In particular, we find that vacancies ($V$), As$V$ pairs, $As_2V$ complexes, and higher-order $As_nV_m$ complexes play distinct roles in the observed dopant deactivation, reactivation, and anomalous diffusion. The latter is mediated by mobile $As_2V$ complexes that form in "prepercolation" patches of a very high dopant concentrations and gives rise to fast As clustering at moderate temperatures. Our results are quantitative and in agreement with experimental numbers where available. [S0031-9007(96)00428-0]

PACS numbers: 68.35.Bs, 61.72.Ji, 68.35.Dv, 73.20.At

For some time now it has been possible to prepare Si specimens with very high concentrations of dopants such as As (as high as $10^{21}$ cm$^3$; i.e., roughly one As atom per 50 host atoms) with a corresponding high conductivity. Such specimens exhibit a wide array of complex dynamical phenomena that have been investigated extensively over the last 25 years. These investigations fall into two distinct categories.

(i) Beginning in the 1970s, a number of investigators [1–4] found that annealing of heavily doped samples at moderate temperatures (400–500 °C) results in a dramatic drop in conductivity. The phenomenon has been universally attributed to the formation of electrically inactive As complexes. This deactivation of dopants is partially reversible by heating to higher temperatures (800–1000 °C). The major focus of most investigations has been the identification of the dominant electrically inactive complex. There is extensive experimental evidence that the dominant defect is an $As_nV$ complex, where $V$ stands for a vacancy, but there is no consensus on the value of $n$ [5–11]. The most perplexing feature of the observations is that at 400–500 °C, in lightly doped Si, As diffusion is negligible. Yet, somehow, at these temperatures, in heavily doped specimens, the As atoms are rapidly rearranged [1–3] from isolated substitutional sites to form $As_nV$ clusters [9–11] and precipitates [12], generating silicon self-interstitials [11]. No atomistic mechanism for the deactivation and subsequent reactivation has been proposed so far.

(ii) A different set of investigators studied As diffusion in heavily doped samples at temperatures in the range of 1000–1100 °C. Early investigations [5] showed that the As diffusion constant increased linearly with dopant concentration $n$ for $n < 3 \times 10^{20}$ cm$^{-3}$. For $n > 3 \times 10^{20}$ cm$^{-3}$ the diffusion constant *decreased*. This was ascribed to clustering [5]. However, later rapid thermal annealing (RTA) experiments [13,14] revealed *increased* As diffusivity for $n > 3 \times 10^{20}$ cm$^{-3}$. Other RTA studies [15] of the diffusion of small concentrations of As in heavily P-doped Si also showed a dramatic increase in As diffusivity for donor concentrations above $\sim 2 \times 10^{20}$ cm$^{-3}$. The most intriguing suggestion to account for the observed enhanced dopant diffusion above a critical doping threshold is the formation of a percolation network of dopant atoms [15,16]. However, other theories [17] account for the enhanced diffusion without invoking percolation. No attempt has been made thus far to give a unifying interpretation of the diffusion data *and* the deactivation or reactivation data.

In this Letter, we report a comprehensive set of first-principles calculations in terms of which we obtain a detailed description of the dynamical atomic-scale processes that occur in heavily As-doped Si. These results allow us to give a systematic account of both the deactivation-reactivation observations and the anomalous diffusion data. In particular, we find that vacancies, As$V$ pairs, $As_2V$ complexes, and higher-order $As_nV_m$ complexes play distinct roles in the observed deactivation, reactivation, and anomalous diffusion phenomena. A percolation network, which in principle may exist in heavily doped specimens prior to any thermal treatments, would in fact quickly break up due to the formation of $As_nV_m$ complexes and thus would not sustain long-term As diffusion and clustering. We find that fast As diffusion at high doping levels is mediated by mobile $As_2V$ complexes that form in "prepercolation" patches of very high dopant concentrations and give rise to rapid As clustering at moderate temperatures. Our predictions are quantitative and in agreement with experimental numbers, where available.

The calculations were based on the density functional method, using the local density approximation. Pseudopotentials [18] were used for Si and As. Electronic wave functions were expanded in a plane wave basis, with a 15 Ry cutoff. Tests for bulk Si gave a lattice parameter of 5.42 Å and a bulk modulus of 0.99 Mbar. Defect configurations were simulated using the supercell method. The formation energies of individual defects changed by only 0.25 eV on going from 16 to 32 site supercells, indicating that the results from 32 site supercells were well

 © 1996 The American Physical Society 

converged. Two special $k$ points were used [19]. Migration energies of the As-vacancy complexes were calculated using 64 site supercells. Calculated forces on atoms were used to relax each structure to equilibrium.

First, we report our calculations of the formation energies of defect clusters containing As atoms and native point defects in Table I. Our results show that As atoms have negligible affinity for each other but bind strongly to vacancies and interstitials. The binding energy per As atom in a cluster containing a vacancy is appreciably larger than that containing an interstitial, reflecting the preference of As for threefold coordination. In fact, each time an As atom is taken from an isolated substitutional fourfold-coordinated site and placed next to a vacancy, there is an energy gain of about 1.5 eV. All $As_nV_m$ complexes with $n > 2m$ have negative formation energies, including the $As_4V$ complex, where our result is in agreement with the calculation reported by Pandey *et al.* [9]. These authors studied only the $As_4V$ complex and asserted that, because of its negative formation energy, it is the dominant defect in deactivated samples. However, as we see, this complex is only one among a hierarchy of such complexes. In these results, we observe a clear trend: *At any doping level, compared with isolated fourfold-coordinated configurations, thermodynamics would favor the agglomeration of As atoms with vacancies in the form of* $As_nV_m$ *complexes or the attachment of As atoms to microvoid surfaces.* In other words, As-doped Si is metastable at any doping level and the preparation of electrically active samples is possible only because of *kinetic limitations.*

The results presented above allow us to conclude that the defects that underlie deactivation and reactivation of heavily doped Si are $As_nV_m$ complexes. This conclusion is fully consistent with earlier analysis of experimental data [6,8–11]. It is clear, however, that formation energies alone (thermodynamics) do not tell us what role each $As_nV_m$ complex plays, which one is dominant if any, what are the mechanisms that allow them to form only in heavily doped materials, and how diffusion is enhanced. We must, therefore, investigate the *dynamical processes* (kinetics) that are possible only in heavily doped materials.

TABLE I. The formation energies, in eV, of the complexes of As atoms with a vacancy.

| Defect complex | Formation energy | Binding energy per As atom |
|---|---|---|
| $As_2$ | 0.10 | 0.05 |
| $As_4$ | −0.10 | −0.03 |
| $V$ (vacancy) | 3.78 | |
| $AsV$ | 2.47 | 1.31 |
| $As_2V$ | 0.82 | 1.48 |
| $As_3V$ | −0.53 | 1.44 |
| $As_4V$ | −2.39 | 1.54 |
| $V_2$ (divacancy) | 6.07 | |
| $As_2V_2$ | 2.70 | 1.69 |
| $As_4V_2$ | −0.54 | 1.65 |
| $As_6V_2$ | −3.23 | 1.57 |
| $I$ (interstitial) | 4.14 | |
| $As_2I$ | 3.76 | 0.19 |
| $As_4I$ | 2.19 | 0.49 |

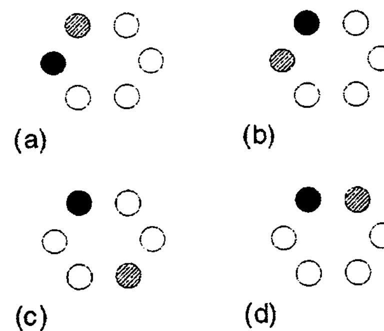


FIG. 1. Migration of $AsV$. Si: white circle, As: dark circle, $V$: shaded circle. (a) Initial configuration; (b) As and $V$ have exchanged positions; (c) saddle configuration: $V$ is third neighbor of As; (d) final configuration; one diffusion step is complete.

It is helpful to start with the process that underlies As diffusion in lightly doped Si. It is well known that diffusion proceeds primarily by the formation and migration of $AsV$ pairs [20]. The migration of $AsV$ is illustrated in Fig. 1: The vacancy loops around the As atom for the pair to make one step. The diffusion activation energy of the $AsV$ complex is the sum of its formation energy and migration energy. From Table I, the formation energy of the $AsV$ complex is 2.5 eV. The migration energy is made up of two contributions: the change in energy when the vacancy goes from the nearest neighbor to the third neighbor position of the As atom and the energy of vacancy migration, which we calculate to be 0.9 and 0.5 eV, respectively. This gives a net activation energy for $AsV$ diffusion of 3.9 eV, in good agreement with experiment [20]. With such a large activation energy, negligible As migration occurs at moderate temperatures.

In the heavily doped limit, Mathiot and Pfister (MP) [16] have suggested that enhanced diffusion comes about as follows: $AsV$ pairs during their migration are not isolated. Specifically, MP considered the case there two As atoms are fifth neighbors. If one of these As atoms is connected to a vacancy, then, during the migration of the $AsV$ pair, when the $V$ is a third neighbor of one As atom, it would be a second neighbor of the other. The net effect is a lowering of the migration energy. For a uniform As distribution, such a cluster would not occur even at an As concentration as high as $10^{21}$ cm$^{-3}$, for As atoms would be eighth neighbors, on average. MP proposed a resolution to this quandary by invoking percolation theory. They found that when the As concentration exceeds $\sim 3 \times 10^{20}$ cm$^{-3}$, fluctuations in the As distribution would result in the presence of an infinite network of As atoms in the sample, in which any two As atoms are fifth neighbors of each

other (or closer). They described a scenario for enhanced As diffusion above this critical doping threshold, due to accelerated diffusion of vacancies through this "infinite percolation network." We have performed the relevant calculations in this limit using supercells and found that both the formation and migration energy of an As$V$ pair are lowered, leading to a decrease in the diffusion activation energy of about 1 eV. This is consistent with the number obtained by MP [16] from simulations. A simple calculation, assuming no significant change in the preexponential factor in the expression for the diffusion coefficient [$D = D_0 \exp(-Q/k_b T)$], indicates that *the rate of As diffusion in a heavily doped specimen at* ~450 °C *is comparable to that in a lightly doped specimen at* ~900 °C. This can explain how fast As migration can occur at moderate temperatures.

However, there is a problem with the above scenario. The percolation model yields a quantitative account of enhanced diffusion for As concentrations above $\sim 3 \times 10^{20}$ cm$^{-3}$, but it is not consistent which the fact that enhanced diffusion causes As clustering with vacancies. Such clustering would break up the percolation network into high concentration patches and halt enhanced diffusion and further clustering after a few seconds of annealing. This would be in contradiction with deactivation observations [1,2] that indicate continued As clustering over many hours at moderate temperatures.

We note that other workers have claimed to account for enhanced diffusion [17] in heavily doped specimens without invoking percolation. Here, we propose an atomistic mechanism that does not require a fully connected percolation cluster and yet explains the diffusion data [5,14], namely, *a mobile* $As_2V$ *complex*. The formation energy of $As_2V$, from Table I, is 0.8 eV. Its migration is illustrated schematically in Fig. 2. Two basic steps are depicted: the sequence (abcd) and the sequence (abef), with comparable migration energies. The net diffusion activation energy is 2.7 eV for the $As_2V$ complex, which is 1.2 eV lower than that of the As$V$ pair. This is virtually identical to the result we obtained for As$V$ migration in the percolation network. Thus, based on activation energies alone, one cannot distinguish between the percolation model and the migration of $As_2V$. While earlier investigators [5,7,10] had proposed that $As_2V$ complexes [21] are present in deactivated specimens, they were not considered mobile. In modeling diffusion of Sb in P-doped Si, Larsen and Weyer [22] had considered diffusion mediated by SbP$V$ complexes, but in later work [15] abandoned this mechanism in favor of the percolation model. *We believe, however, that* $As_2V$ *plays a key role in enhanced diffusion in heavily doped Si as it does not need a continuous percolation network, something that would not be sustained when As agglomeration into* $As_nV_m$ *complexes occurs.* We propose that enhanced As diffusion starts below the percolation threshold, calculated by MP [16] to be $3 \times 10^{20}$ cm$^{-3}$. High-concentration "prepercolation patches" in which two As atoms are fifth neighbors or closer enable the formation of large numbers of $As_2V$ complexes. These $As_2V$ complexes can migrate fast through the sample, even at moderate temperatures. During their motion, they react with other defects to form larger, immobile complexes. Modeling diffusion data on the basis of these reactions is beyond the scope of this Letter.

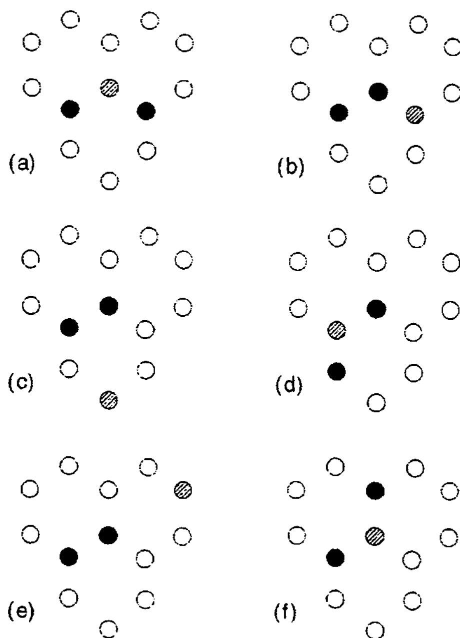


FIG. 2. Migration of $As_2V$. (a) Initial configuration; (b) one As and $V$ have exchanged positions; (c),(d) translation; (e),(f) reorientation starting with configuration (b).

We now summarize the main experimental observations and how the theory described above accounts for them.

*(1) Diffusion data.*—Early observations [5] showed that the diffusion constant of As decreased for dopant concentrations greater than $3 \times 10^{20}$ cm$^{-3}$. However, later RTA experiments [14] on As-implanted Si found fast As redistribution (within 20 s) which reduced the peak As concentration to $(2.5-3) \times 10^{20}$ cm$^{-3}$, if the as-implanted peak As concentration exceeded this value. Otherwise, negligible As migration was observed. RTA experiments [15] on small concentrations of As in heavily P-doped Si found enhanced diffusion for donor concentrations greater than $\sim 2.0 \times 10^{20}$ cm$^{-3}$. The early diffusion studies were carried out over several hours. The decreased As diffusivity at high doping levels was correctly attributed to As clustering [5]. The fast As migration observed in RTA experiments is due to $As_2V$ migration over a very short time scale (6–60 s), during which extensive clustering does not occur. The investigations of As diffusion in heavily P-doped Si establish that the onset of enhanced dopant diffusion is indeed below the percolation threshold. The enhanced As diffusion observe din these latter experiments is mediated by AsP$V$ complexes. The extracted activation energy [15] of 2.7 eV is identical to that of the $As_2V$ complex.

*(2) Deactivation data.*—During deactivation at moderate temperatures (400–600 °C), the rate of deactivation is

highest initially and then continues at a slower rate [1,2,4]. Initially As atoms are close to each other in prepercolation patches. Migrating $As_2V$ complexes have a high cross section for reaction inside such patches, giving rise to larger immobile complexes. Thus, the initial deactivation rate is high. Once a degree of clustering takes place, As atoms are further from each other, on average, and $As_2V$ complexes have to travel greater distances to cause further deactivation. At some point, deactivation becomes extremely slow and effectively stops. The distribution of complexes is determined by kinetics, for the system does not reach thermodynamic equilibrium at these temperatures.

*(3) Reactivation data.*—Annealing of deactivated specimens at elevated temperatures (800–1000 °C) is found to reactivate carriers. Schwenker, Pan, and Lever [1], assuming that one complex is predominant in deactivated specimens, obtained the activation energy for the reactivation to be 1.6 eV and the number of As atoms in the complex to be between 1.7 and 2.8 As atoms. For concentrations of order $2 \times 10^{20}\ \mathrm{cm}^{-3}$, most of the initial As concentration is reactivated. Reactivation is a result of the breakdown of complexes formed at lower temperatures, releasing As atoms, and requires the removal of an $AsV$ pair or an $As_2V$ complex, for these are the mobile species. From Table I, we find that the energy required to break up $AsV$ ($AsV \rightarrow As + As$), $As_2V$ ($As_2V \rightarrow AsV + As$), and $As_3V$ ($As_3V \rightarrow As_2V + As$), are all about 1.5 eV, in excellent agreement with the data. Larger complexes do not decompose into $As + X$, as $X$ is not mobile. They would have to break up into larger fragments and that requires more energy. Therefore, we conclude that $AsV$, $As_2V$, and $As_3V$ may be present in deactivated specimens. $AsV$ is ruled out by experiments [9,11] which find that most As atoms in deactivated specimens have another As atom as a second neighbor. The fact that most of the As atoms were reactivated at a doping level of $2 \times 10^{20}\ \mathrm{cm}^{-3}$ indicates that $As_2V$ and $As_3V$ are the dominant complexes in deactivated specimens, near the enhanced-diffusion threshold.

*(4) The saturation of the carrier concentration.*—The carrier concentration in heavily doped Si does not exceed $\sim 3 \times 10^{20}\ \mathrm{cm}^{-3}$ at elevated temperatures (1000 °C) [3], even if the total As concentration exceeds this value. This concentration, as MP [16] showed, marks the threshold above which an infinite percolation network of As atoms is present initially in the sample. If the initial As concentration exceeded this value, then, in the very early stages of annealing, a very high flux of vacancies would flood the sample along the percolation network. Thus, the As concentration in excess of the critical value would become bound very rapidly in $As_nV_m$ complexes with $n > 2m$ (like $As_4V$). Such complexes would not decompose even at 1000 °C.

In conclusion, we reported extensive calculations of formation energies, migration energies, and defect reaction energies in terms of which we have been able to give a systematic account of the major observations of both deactivation or reactivation and enhanced diffusion in heavily doped Si.

This work was supported in part by Office of Naval Research Grant No. N00014-95-1-0906. Supercomputing time was provided by the Pittsburgh Supercomputing Center under Grant No. DMR950001P.

[1] R. O. Schwenker, E. S. Pan, and R. F. Lever, J. Appl. Phys. **42**, 3195 (1971).
[2] W. K. Chu, Appl. Phys. Lett. **36**, 273 (1980).
[3] A. Lietoila, J. F. Gibbons, and T. W. Sigmon, Appl. Phys. Lett. **36**, 765 (1980).
[4] K. Itoh *et al.*, Jpn. J. Appl. Phys. **21**, L245 (1982).
[5] R. B. Fair and G. R. Weber, J. Appl. Phys. **44**, 273 (1973).
[6] S. M. Hu, in *Atomic Diffusion in Semiconductors,* edited by D. Shaw (Plenum, New York, 1973), p. 306.
[7] W. K. Chu and B. J. Masters, in *Laser-Solid Interactions and Laser Processing,* edited by S. Ferris, H. J. Leamy, and J. M. Poate, AIP Conf. Proc. No. 50 (AIP, New York, 1979), p. 305.
[8] M. Y. Tsai, F. F. Morehead, J. E. E. Baglin, and A. E. Michel, J. Appl. Phys. **51**, 3230 (1980).
[9] K. C. Pandey *et al.*, Phys. Rev. Lett. **61**, 1282 (1988).
[10] Th. Wichert and M. L. Swanson, J. Appl. Phys. **66**, 3027 (1989).
[11] D. W. Lawther *et al.*, Appl. Phys. Lett. **67**, 3575 (1995).
[12] A. Lietoila *et al.*, Appl. Phys. Lett. **35**, 532 (1979).
[13] J. L. Hoyt and J. F. Gibbons, Mater. Res. Soc. Symp. Proc. **52**, 15 (1986).
[14] A. N. Larsen, S. Yu. Shiryaev, E. S. Sorensen, and P. Tidemand-Peterson, Appl. Phys. Lett. **48**, 1805 (1986).
[15] A. N. Larsen, K. K. Larsen, P. E. Andersen, and B. G. Svensson, J. Appl. Phys. **73**, 691 (1993). The study of small concentrations of As in heavily P-doped Si was motivated by the high solubility of P in Si, which at 1000 °C is $\sim 4 \times 10^{20}\ \mathrm{cm}^{-3}$. Thus, enhanced dopant diffusion can be studied at high donor concentrations, without clustering. See R. B. Fair, Inst. Phys. Conf. Ser. **46**, 559 (1979); D. Nobili, A. Armigliato, M. Finetti, and S. Solmi, J. Appl. Phys. **53**, 1484 (1982).
[16] D. Mathiot and J. C. Pfister, J. Phys. (Paris), Lett. **43**, L-453 (1982); Appl. Phys. Lett. **42**, 1043 (1983); J. Appl. Phys. **66**, 970 (1989).
[17] E. Antoncik, Appl. Phys. A **56**, 291 (1993); S. T. Dunham and C. D. Wu, J. Appl. Phys. **78**, 2362 (1995).
[18] D. Vanderbilt, Phys. Rev. B **41**, 7892 (1990).
[19] D. J. Chadi and M. L. Cohen, Phys. Rev. B **8**, 5747 (1973).
[20] P. M. Fahey, P. B. Griffith, and J. D. Plummer, Rev. Mod. Phys. **61**, 289 (1989).
[21] Fair and Weber [5] considered $V^0$ combining with two neutral As atoms whereas Chu and Masters [7] considered $V^{--}$ combining with two $As^+$ atoms to form $As_2V$. As a thermodynamic quantity, the formation energy of $As_2V$ is independent of the charge states of the constituent defects.
[22] A. N. Larsen and G. Weyer, Mater. Sci. Forum **83–87**, 273 (1992).

# Dopant Segregation at Semiconductor Grain Boundaries through Cooperative Chemical Rebonding

A. Maiti,[1,2] M. F. Chisholm,[1] S. J. Pennycook,[1] and S. T. Pantelides[1,2]
[1]*Solid State Division, Oak Ridge National Laboratory, Oak Ridge, Tennessee 37831*
[2]*Department of Physics and Astronomy, Vanderbilt University, Nashville, Tennessee 37235*
(Received 25 March 1996)

Recent theoretical work found that isolated As impurities in Ge grain boundaries exhibit minimal binding, leading to the suggestion that the observed segregation is likely to occur at defects and steps. We report *ab initio* calculations for As in Si and show that segregation is possible at defect-free boundaries through the cooperative incorporation of As in *threefold-coordinated* configurations: As dimers, or *ordered chains* of either As atoms or As dimers along the grain boundary dislocation cores. Finally, we find that As segregation may drive structural transformations of certain grain boundaries. [S0031-9007(96)00811-3]

PACS numbers: 61.72.Mm, 68.35.Dv, 68.55.Ln, 71.15.Pd

Polycrystalline semiconductors are used in microelectronics. Dopants, which control the electrical properties of these materials, are known to segregate in grain boundaries in electrically inactive configurations [1–4]. The fraction of dopants in the grain boundaries is governed by the *segregation energy,* i.e., the energy difference between a dopant atom in the grain boundary and a dopant atom in the bulk crystal. For the specific case of As segregation in Si and Ge grain boundaries, experimental values of the segregation energies range from 0.41 to 0.65 eV [1–4].

Clearly it would be very important for technologists to know if the large segregation energy is an intrinsic property of a defect-free grain boundary or is caused by defects that could, in principle, be avoided. The origin of the segregation energy has not, however, been accounted for so far. Experiment [5] and theory [6,7] have established that tilt grain boundaries in undoped Si and Ge rebond so that all host atoms are fourfold coordinated. The only first-principles theoretical study of segregation was reported recently by Arias and Joannopoulos [8]. These authors examined the segregation energies of isolated As atoms placed at different substitutional sites in a Ge grain boundary and found values only of order 0.1 eV. They proposed that the observed segregation energies are likely to arise from As atoms bound to steps or other defects. No calculations were pursued to explore such possibilities.

The motivation for the present work was the recognition that the observed large segregation energies may occur in defect-free grain boundaries because As atoms achieve their preferred threefold coordination, as they are known to do in amorphous Si and Ge [9]. Simple bond counting suggests that if a single As atom were to achieve threefold coordination in a Si or Ge grain boundary, at least one Si (Ge) atom would have to have odd coordination (3 or 5), which is energetically costly. Clearly threefold-coordinated As atoms would be far more likely if they were incorporated in a grain boundary in a *cooperative* manner, at least two at a time. The simplest possibility would be two As atoms at nearest-neighbor sites. We have performed systematic first-principles calculations for such possibilities in Si, which is technologically more important, and found that As dimers do form in grain boundaries with segregation energies up to 0.2 eV per As atom. Dimer binding occurs through *repulsion:* The two As atoms repel each other seeking to achieve threefold coordination (Fig. 1); the energy gain from this *chemical rebonding* is larger than the elastic energy cost from backbond distortions. Furthermore, we find that larger segregation energies (0.3–0.5 eV per As atom) are achieved through the formation of chains of As dimers or fully ordered chains of threefold-coordinated As atoms. Finally, we find that the formation of such chains may induce a structural transformation of certain grain boundaries.

Calculations were performed for a $\Sigma = 5\{310\}\langle 001\rangle$ symmetric tilt boundary in Si. This grain boundary is parallel to the {310} plane of the original crystalline lattice. It has a minimum periodicity of one conventional lattice parameter ($a = 5.431$ Å) in the $\langle 001\rangle$ direction and a periodicity of $a\sqrt{5/2} = 8.587$ Å in the direction perpendicular to the $\langle 001\rangle$ axis. In the discussion below, we follow the convention that the $x$ axis is perpendicular to the grain boundary plane, the $z$ axis is parallel to the $\langle 001\rangle$ axis of the original crystalline lattice, and the $y$ axis runs parallel to the grain boundary plane in a direction perpendicular to the $z$ axis. We used periodic supercells that contain two oppositely oriented $\Sigma = 5$ grain boundaries. In a supercell with $N$ planes of atoms along

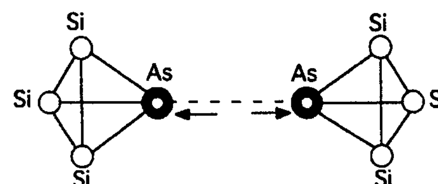


FIG. 1. Schematic showing how the member atoms of an As dimer placed substitutionally in neighboring Si sites would move away from each other into threefold coordination, and thus lower energy.

 0031-9007/96/77(7)/1306(4)$10.00 © 1996 The American Physical Society

the $x$ direction, the grain boundaries are separated by $N/2$ planes. The actual supercells used in the calculations will be discussed later.

The calculations were based on density functional theory [10] with local exchange-correlation energy as parametrized by Perdew and Zunger [11]. The atomic cores are represented by nonlocal, norm-conserving pseudopotentials of the Kerker type [12] in a separable Kleinmann-Bylander form [13], and defined on a real-space grid [14]. The calculations were performed using the code CETEP [15], which was run on 128 processors of the Intel Paragon XP/S 35 at Oak Ridge National Laboratory. The integration over the Brillouin zone was performed using two special $k$ points chosen according to the Monkhorst-Pack scheme [16]. The electronic wave functions were expanded in a plane wave basis set with an energy cutoff of 150 eV, verified to yield accurate lattice constant and bulk modulus for the pure crystal. For each geometry the electronic wave functions were first relaxed by the conjugate gradient scheme of Payne *et al.* [17] until they reached a local minimum (the Born-Oppenheimer surface). The ions were then moved according to the Hellman-Feynman forces until the largest force on any ion in any direction was less than 0.08 eV/Å. Energy changes due to changes in supercell dimensions, known to be small [8], were neglected.

Calculations were performed with $N = 30$ and 40 planes of atoms, with the corresponding supercells containing, respectively, 60 and 80 atoms for the minimum periodicity in the grain boundary plane. Computed segregation energies changed by less than 0.02 eV, indicating that the two grain boundaries in the supercell are adequately isolated from each other. In order to isolate the As dimers from each other in the grain boundary plane, calculations were performed with double the primitive cell and $N = 30$. Most calculations were performed using only the primitive cell in the grain boundary plane and $N = 40$, resulting in chains of interacting dimers.

The calculations for the undoped $\Sigma = 5$ grain boundary yielded a fully relaxed structure, which we label GB1, that is the same as described in Ref. [8] for Ge. We found, however, a second low-energy structure, which we label GB2, with a total energy that is higher by only 0.15 eV per periodic segment of the grain boundary plane. Figures 2 and 3 display $xy$ projections of the structures. The two structures differ in the relative $z$ shift of the two grains forming the boundary, by $a/8 = 0.68$ Å, and also in the nature of the dislocation cores comprising the boundaries. The cores of GB1, formed by terminating planes coming from the same grain, are of the pure edge type ($\mathbf{b} = \frac{a}{2}\langle 100\rangle$). The cores of GB2 are formed by terminating planes coming from different grains, have the Burger's vector at 45° to the $z$ direction ($\mathbf{b} = \frac{a}{2}\langle 101\rangle$), and therefore have mixed screw and edge character.

We studied segregation of As atoms in both GB1 and GB2 because the two structures contain different dislocation cores that are components of many different grain boundaries. Figures 1 and 2 show labels for the sites where As atoms were placed: [a] through [e] are sites in the GB1 grain boundary, whereas [f] and [g] are sites in the bulk; [a′] through [f′] denote corresponding sites for GB2. Symmetry has been used to reduce the number of possible distinct As sites and site pairs. Thus using the symbol "$\sim$" to indicate symmetry equivalence, we have for GB1: a $\sim$ c and d $\sim$ e. It follows that for GB1 the possible distinct sites for atom segregation are [a] ([c]), [b], and [d] ([e]). The distinct site pairs for dimer segregation are [a, c], [a, d], [b, c], and [d, e]. In addition, we have also studied the dimer [f, g] where two atoms are placed at nearest-neighbor sites in the bulk crystal. For GB2 we have the equivalence $b' \sim c' \sim e'$. The resulting distinct site pairs are [a′, d′], [d′, e′], [b′, c′], and [a′, c′].

The results for isolated As substitutionals are shown in the top halves of Tables I and II. We find that all sites except [a] ([c]) on GB1 and [a′] on GB2 have a binding energy of $\sim$0.1 eV, the same value obtained for isolated

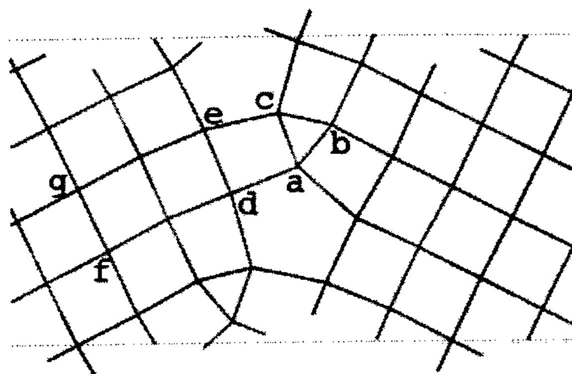


FIG. 2. 2D projection (normal to the tilt axis) of an atomically relaxed structure of the $\Sigma = 5\{310\}\langle 001\rangle$ symmetric grain boundary of Si in its ground state (GB1). In the actual 3D structure, the atoms in the bulk lie on four different planes. The letters a–g denote various sites at which segregation of isolated As atoms and As dimers are investigated. The dislocation cores comprising this grain boundary are of the pure edge type.

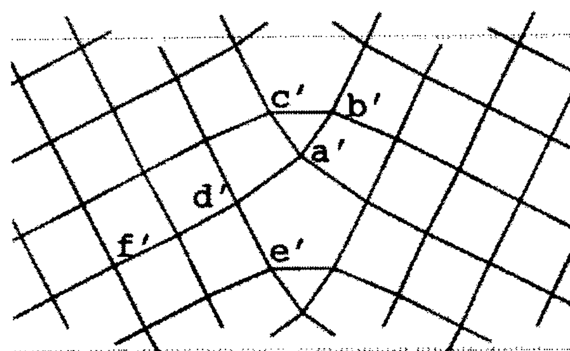


FIG. 3. Grain boundary of Fig. 2 in a metastable state (GB2) in the same projection view. The letters a′–f′ denote various sites at which segregation of isolated As atoms and As dimers are investigated. The dislocation cores comprising this grain boundary have mixed screw and edge characters.

TABLE I. Segregation energies (normalized per As atom) for isolated As atoms and As dimers placed at various sites on GB1. The equilibrium As-As distance for the dimers is also indicated. The sites are described in Fig. 2.

| As site(s) | Segregation energy eV/As atom | As-As distance (Å) (dimer geometries) | As-As* distance (Å) (dimer geometries) |
|---|---|---|---|
| [f] | 0.00 | | |
| [a], [c] | 0.03 | | |
| [b] | 0.11 | | |
| [d], [e] | 0.11 | | |
| [f, g] | −0.01 | 2.71 | 4.59 |
| [a, d] | 0.10 | 2.71 | 5.20 |
| [d, e] | 0.19 | 2.79 | 4.70 |
| [a, c] | 0.20 | 2.89 | 3.76 |
| [b, c] | 0.32 | 3.43 | 3.43 |

As atoms in a similar boundary in Ge [8]. The smaller binding of [a] can be explained from the *similarity* of its environment, characterized by the surrounding bond-length and bond-angle distribution, to that of a bulk site [f] or [g], while an opposite effect occurs for [a′]. In all cases of isolated As substitutionals, the lattice is found to undergo only a very small relaxation, in agreement with the results of Ref. [8].

We now turn to the dimer configurations. As we noted earlier, we performed calculations with both minimal and double periodicity in the grain-boundary plane, corresponding to dimer chains and isolated dimers, respectively. The latter calculations are extremely time consuming even on the Paragon supercomputer and were therefore performed only for selected pairs of sites. We found that dimer formation in the grain boundary is energetically favored. If two As atoms are placed at neighboring substitutional sites in the bulk crystal, they repel each other seeking to achieve threefold coordination (pair [f, g] in Table I). The equilibrium As-As distance is 2.71 Å compared to a Si-Si bond length of 2.35 Å. The overall energy goes up by a tiny amount (0.01 eV per As atom) as compared with isolated substitutional atoms because of the elastic energy cost. In contrast, As dimers in the grain boundary lead to an overall lowering of the energy. The selected calculations we performed for the isolated dimers yielded net binding of order 0.05–0.2 eV/atom, indicating that the elastic energy cost in the grain boundary can be smaller than in the bulk. Dimer formation in the grain boundary is the result of *repulsion* between neighboring As atoms and occurs because this repulsion can be accommodated easier in the grain boundary than in the bulk crystal.

The results for chains of As dimers are even more dramatic and are displayed in detail in Tables I and II for the two grain-boundary structures, respectively. We see that segregation energies range from 0.1 to 0.5 eV/atom, the latter being in agreement with the measured values [1–3]. In Tables I and II, the third column contains the As-As distance in the dimer, which is to be compared with the normal Si-Si distance of 2.35 Å. The fourth column contains the As-As* distance between As atoms of neighboring dimers (dimers in neighboring supercells).

We note three classes of results: (i) Cases where the As-As* distance is significantly larger than the As-As distance, suggesting that the dimers in the chain are fairly well separated. The segregation energy is small, less than 0.2 eV/atom, comparable to that of truly isolated dimers that we discussed earlier. (ii) Cases where the As-As and As-As* distances are comparable but different (e.g., [a, c] in GB1 and [a′, c′] in GB2) where the segregation energy ranges from 0.2 to 0.5 eV/atom. (iii) A case where the As-As and As-As* distances are identical ([b, c] in GB1), corresponding to a fully ordered chain of As atoms, with an intermediate segregation energy of 0.32 eV/atom. Figure 4 displays the electronic charge density in a slice passing through the plane containing the As atoms in the [b, c] geometry of GB1. There is no significant charge

TABLE II. Segregation energies and As-As distance at various sites on GB2 (Fig. 3).

| As site(s) | Segregation energy eV/As atom | As-As distance (Å) (dimer geometries) | As-As* distance (Å) (dimer geometries) |
|---|---|---|---|
| [f′] | 0.00 | | |
| [b′], [c′], [e′] | 0.12 | | |
| [d′] | 0.13 | | |
| [a′] | 0.22 | | |
| [a′, d′] | 0.08 | 2.43 | 5.25 |
| [d′, e′] | 0.09 | 2.72 | 4.84 |
| [b′, c′] | 0.11 | 2.42 | 4.29 |
| [a′, c′] | 0.52 | 2.76 | 3.54 |

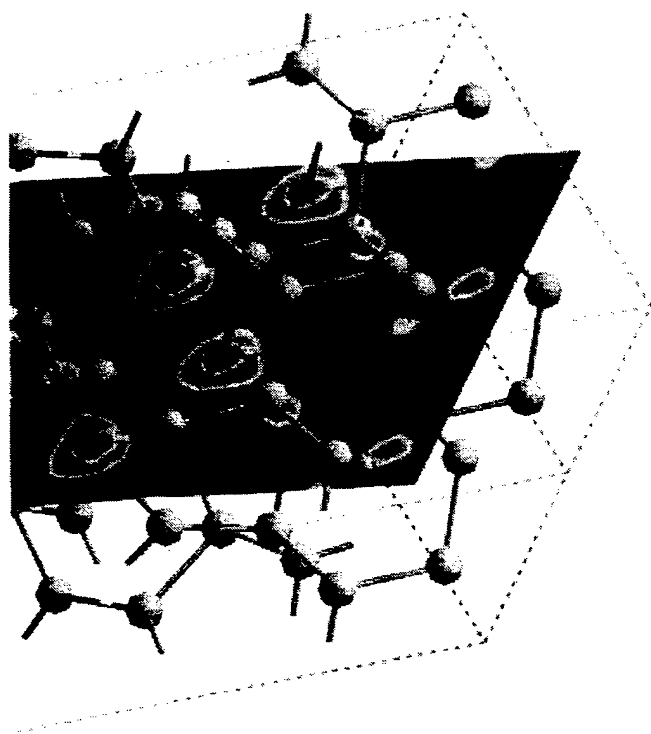

FIG. 4(color). A 2D plot of the electronic charge density on a slice passing through the perfect As chain [b, c] in GB1. The As atoms are magenta and Si atoms gray. The color scheme is red → yellow → green → light blue → deep blue for maximum to minimum charge density.

in the region between two neighboring As atoms in the chain, proving conclusively the threefold coordination of each As atom. The charge density for all other dimer configurations is qualitatively similar.

An examination of the local three-dimensional topologies corresponding to Fig. 2 and 3 suggests that the most stable dimer geometries in a chain are the ones in which one or both of the component As atoms can relax *into* the dislocation cores, where the average atomic density is lower than the crystalline bulk. Such relaxation reduces the strain in the Si backbonds, thereby yielding a larger segregation energy. It is interesting to note that the most stable chain of dimers [a′, c′] in GB2 has its component atoms on two different dislocation cores, a configuration possible only in relatively large-angle grain boundaries, while the chain of dimers [b, c] on GB1 has only one of its atoms (c) lying on a dislocation core, and could occur in any dislocation core of the perfect edge type.

Finally, it is particularly interesting to note that the highest segregation energy in GB2 is significantly larger than in GB1 and might actually drive a structural transformation. In other words, the injection of a high concentration of As into polycrystalline Si may convert a grain boundary with perfect edge dislocations into one with mixed dislocations. Similar solute-induced grain boundary transformations have long been known to occur in metals [18], but we are not aware of any prior reports in semiconductors. From the relative total energies of the two grain boundaries we estimate that the transformation from GB1 to GB2 would require a critical As concentration of ~19% in the column of the favored dimer sites. However, such a transformation involves a relative shift (sliding) of the two grains at the boundary, and the above estimate does not take into account any elastic energy cost that may be required to maintain integrity at triple junctions during the sliding process.

In summary, cooperative phenomena involving chains of threefold-coordinated As atoms or dimers result in much larger segregation energies than isolated As substitutionals. Segregation energies thus obtained are in agreement with experimental values. This provides a mechanism for As segregation that does not require the presence of steps or other defects. Chains of As dimers in mixed dislocation cores have lower energies, raising the intriguing possibility that As segregation may drive a structural transformation in grain boundaries containing pure edge dislocations.

We would like to thank V. Milman for help with the CETEP code, and the ORNL Center for Computational Sciences for providing valuable supercomputer hours. This research was supported in part by Lockheed Martin Energy Research Corp. under DOE Contract No. DE-AC05-96OR22464, and ONR Grant No. N00014-95-1-0906.

[1] C. R. M. Grovenor, J. Phys. C **18**, 4079 (1985).
[2] C. R. M. Grovenor, P. E. Batson, D. A. Smith, and C. Y. Wang, Philos. Mag. A **50**, 409 (1984).
[3] M. M. Mandurah, K. C. Saraswat, C. R. Helms, and T. I. Kamins, J. Appl. Phys. **51**, 5755 (1980).
[4] J.-L. Maurice, in *Polycrystalline Semiconductors II,* edited by J. H. Werner and H. P. Strunk, Springer Proceedings in Physics Vol. 54 (Springer, Berlin, 1992), p. 166.
[5] A. Bourret and J. L. Rouvière, Springer Proc. Phys. **35**, 8 (1989).
[6] M. Kohyama, Phys. Status Solidi B **141**, 71 (1987).
[7] A. T. Paxton and A. P. Sutton, J. Phys. C **21**, L481 (1988).
[8] T. A. Arias and J. D. Joannopoulos, Phys. Rev. B **49**, 4525 (1994).
[9] N. F. Mott, Adv. Phys. **16**, 49 (1967).
[10] P. Hohenberg and W. Kohn, Phys. Rev. **136**, B864 (1964).
[11] J. P. Perdew and A. Zunger, Phys. Rev. B **23**, 5048 (1981).
[12] G. P. Kerker, J. Phys. C **13**, L189 (1980).
[13] L. Kleinmann and D. M. Bylander, Phys. Rev. Lett. **48**, 1425 (1982).
[14] R. D. King-Smith, M. C. Payne, and J. S. Lin, Phys. Rev. B **44**, 13 063 (1991).
[15] L. J. Clarke, I. Stich, and M. C. Payne, Comp. Phys. Commun. **72**, 14 (1992).
[16] H. J. Monkhorst and J. D. Pack, Phys. Rev. B **13**, 5188 (1976).
[17] M. C. Payne, M. P. Teter, D. C. Allan, T. A. Arias, and J. D. Joannopoulos, Rev. Mod. Phys. **64**, 1045 (1992).
[18] V. Vitek and G. J. Wang, Surf. Sci. **144**, 110 (1984); K. E. Sickafus and S. L. Sass, Acta Metall. **35**, 69 (1987); C. Rottman, J. Phys. (Paris) **49**, C5, 313 (1988).

Appendix C

# Ordering of As impurities in a Si dislocation core

A. Maiti,[a] T. Kaplan, M. Mostoller, M. F. Chisholm, and S. J. Pennycook
*Solid State Division, Oak Ridge National Laboratory, Oak Ridge, Tennessee 37831*

S. T. Pantelides
*Department of Physics and Astronomy, Vanderbilt University, Nashville, Tennessee 37235*

(Received 5 July 1996; accepted for publication 13 November 1996)

We demonstrate by *ab initio* calculations that segregation of As in a dislocation core in Si occurs in the form of an ordered chain of As atoms running along the dislocation pipe. All As atoms in the chain achieve threefold coordination and the segregation energy is close to 1 eV per As atom. © *1997 American Institute of Physics.* [S0003-6951(97)01003-6]

Plastically deformed materials release excess strain by creating extended defects such as dislocations. In semiconductor devices, dislocations can severely affect the behavior of dopant impurities because: (1) the dislocation cores may provide a fast diffusion pathway to impurities, which severely influences the dopant profile in an uncontrolled way, and (2) impurities may get trapped in the core regions leading to preferential segregation and electrical deactivation of the impurity.

It has generally been believed that impurities get trapped at sites with imperfect bond order in dislocation cores. However, experimental[1–3] and theoretical[4–12] work has established that dislocations and grain boundaries in Si and Ge actually reconstruct in such a manner that all atoms are fourfold coordinated. Therefore, a single impurity atom occupying a substitutional site in the core does not experience any appreciable difference from its environment in the bulk material away from the core, resulting in small segregation energies. For example, in the case of As segregation in a symmetric tilt boundary in Ge, the segregation energy was found to be only of order 0.1 eV.[12] However, in a very recent *ab initio* study[13] we found that As impurities form ordered chains of As dimers (a periodically repeated array of two substitutional As atoms at neighboring sites), or in some cases, perfectly ordered chains of As atoms along the grain boundary cores, with segregation energies as high as 0.5 eV per As atom. In such chain configurations, each As atom relaxes away from its partner atom in the dimer through repulsion, and attains its preferred threefold coordination, thereby lowering energy. It was also found that isolated As dimers lead to threefold coordination, but the excess binding energy over single substitutional As atoms is small, ~0.1 eV per atom, and sometimes there is no energy gain at all. It follows that the energy gain from attaining threefold coordination is largely cancelled by the elastic energy cost of distorting the Si backbonds. However, a significant additional energy gain occurs through chain formation.

In this letter, we show that As segregation at an isolated dislocation core in Si occurs in the same manner as in grain boundaries, namely in the form of ordered chains of threefold-coordinated As atoms. In fact, the strains associated with isolated dislocation cores are in general much larger than in grain boundaries. These strains lead to larger segregation energies in a dislocation core than in the grain boundary, as high as ~0.9 eV per As atom. In earlier work using cluster calculations, Jones *et al.*[7] found that As and P dimers in a dislocation core gain substantial energy by achieving threefold coordination. However, chains of threefold-coordinated impurities were not considered.

Before delving into computational details, a brief introduction to dislocation terminology is in order. The major operative slip system in diamond cubic structures involves the glide of {111} planes along ⟨110⟩ directions. Well separated perfect glide dislocations lie primarily along ⟨110⟩ directions, and are either screw or 60° dislocations, the latter deriving its name from the fact that the angle between the dislocation line direction and the Burgers vector **b** is 60°. In materials with low stacking fault energy, the 60° dislocation is often found to be dissociated into two Shockley partial dislocations separated by a stacking fault. These two Shockley partials have their Burgers vectors ($\mathbf{b}=\frac{a}{6}\langle 112\rangle$) aligned, respectively, at 30° and 90° to their ⟨110⟩ line direction, and are commonly referred to as the 30° and 90° partials.[14] In this work, we have chosen the 90° partial dislocation core in Si as a concrete system to perform our segregation study.

As in our previous work,[13] the total energy calculations and structural relaxations were carried out using density functional theory with the exchange and correlation energy treated in the local density approximation. We used a noncubic periodic supercell with two oppositely oriented 90° partial cores separated by a distance of 13 Å (Fig. 1). An energy cutoff of 150 eV was used, and the Brillouin zone integration was performed using two special $k$ points, chosen according to the Monkhorst–Pack scheme.[15] Atoms were re-

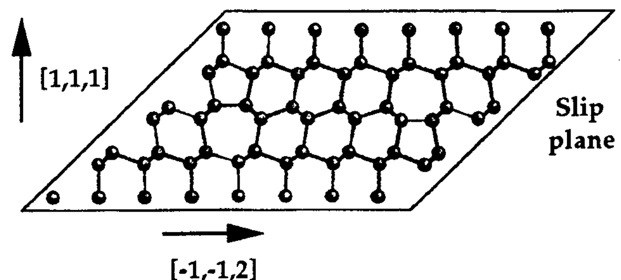


FIG. 1. View along the dislocation line of a periodic supercell containing two oppositely oriented 90° partials with the asymmetric reconstruction; the supercell for the symmetric reconstruction appears almost identical in the same view. The supercell contains 64 atoms and the cores are separated by 13 Å.

[a]Electronic mail: nnd@ornl.gov

 0003-6951/97/70(3)/336/3/$10.00 © 1997 American Institute of Physics

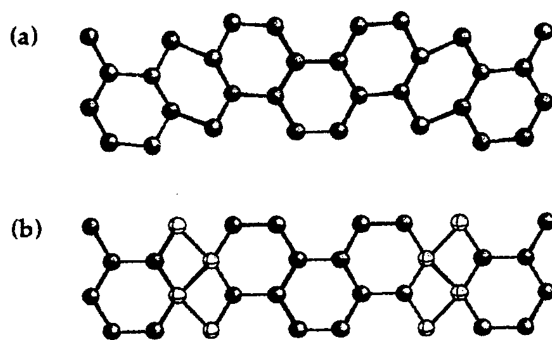


FIG. 2. Bonding structure of the 90° partial dislocation dipole in the slip plane, shown by doubling the supercell periodicity in Fig. 1 along the dislocation line for : (a) asymmetric reconstruction and (b) symmetric reconstruction. In the three-dimensional geometry, the asymmetric reconstruction [Fig. 2(a)] has all atoms fourfold coordinated, while the symmetric reconstruction [Fig. 2(b)] has some atoms, distinguished by lighter shading, quasi-fivefold-coordinated. See text.

laxed in small steps until the magnitude of the largest force component was less than 0.07 eV/Å.

Previous studies found two models of reconstruction in the 90° partial dislocation core: (1) the asymmetric reconstruction, in which the mirror symmetry along the dislocation line is broken,[16,17] and (2) the symmetric reconstruction, in which the mirror symmetry is kept intact.[18] The asymmetric structure has all the atoms fourfold coordinated, while the symmetric structure has two quasi-fivefold-coordinated atoms per periodic segment of the core. Both these reconstructed cores look almost the same in the projection along the dislocation line (Fig. 1), but are clearly distinguishable in the bonding structures in the slip plane (Fig. 2). From *ab initio* relaxations we found that the asymmetric structure was stable, while the symmetric structure spontaneously transformed into the asymmetric structure, in agreement with an earlier *ab initio* study.[19] All our segregation studies were thus performed exclusively on the asymmetric structure.

Single As atoms and As dimers were, respectively, placed at various sites and nearest neighbor site pairs of the dislocation core, as indicated in Fig. 3. In all cases, the energy of the relaxed structure was calculated relative to the geometry in which the As atoms in the core were exchanged with Si atoms in the bulk, i.e., away from the core. The negative of this energy, known as the segregation energy, is

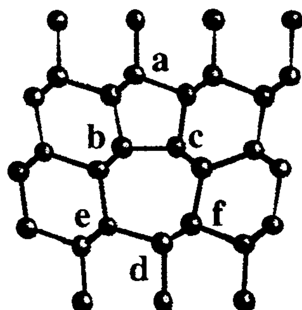


FIG. 3. Various sites of an isolated 90° partial core, viewed along the dislocation line, on which single As atoms and As dimers are placed. Segregation energies are listed in Table I.

TABLE I. Segregation energies of single As atoms and As dimers placed substitutionally at various sites of an asymmetrically reconstructed core. For the dimer geometries the relaxed distance between the two dimer companion atoms ($d_{As-As}$) and the corresponding distance between the first As atom and the periodic image of its dimer companion ($d_{As-As*}$) are also indicated. See Fig. 3 for site denominations.

| As site (s) | Segregation energy (eV/As atom) | $d_{As-As}$ (Å) (Dimer geometries) | $d_{As-As*}$ (Å) (Dimer geometries) |
|---|---|---|---|
| Bulk | 0.00 | | |
| [d] | −0.15 | | |
| [a] | 0.14 | | |
| [b], [c] | 0.33 | | |
| [d,f] | 0.01 | 2.57 | 2.42 |
| [d,e] | 0.13 | 2.90 | 4.53 |
| [b,c] | 0.88 | 2.87 | 2.95 |

listed in Table I for all different As configurations considered.

Let us first consider the single As atoms in the dislocation core. Four different sites were chosen. The strain distribution is very different at different sites, as is apparent from comparing the site-associated bond lengths with the bulk Si–Si bond length of 2.35 Å, making the segregation energy strongly site dependent. Thus the strain is: (i) compressive at site a, with bond lengths (2.29, 2.31, 2.31, and 2.34) Å; (ii) tensile at site d, with bond lengths (2.37, 2.41, 2.43, and 2.44) Å; (iii) mixed compressive/tensile at sites b and c with bond lengths (2.31, 2.34, 2.41, and 2.43) Å. The resulting segregation energy for As is largest for sites b and c, moderate but positive at site a, and even negative for site d. The largest segregation energy of 0.33 eV (sites b,c) is much larger than the average binding at a grain boundary.[12,13] Also, the wide variation of segregation energy from site to site is to be contrasted with a much smaller dispersion in a grain boundary,[13] where the strain distribution is much more uniform. In all cases of single substitutional As, the relaxation from the initial Si site is very small, just as in a grain boundary.

Segregation studies of periodic chains of As dimers yield more dramatic results. To interpret these results, it should be reemphasized that two As atoms placed on nearest neighbor Si sites, which we call As dimers, seek to repel and relax away from each other. In this way, each As atom achieves its preferred threefold coordination, leaving all the Si atoms fourfold coordinated.[13] The three largest bonds in the dislocation core, i.e., [d,f], [d,e], and [b,c] were chosen for investigation. Table I displays the segregation energies for these three dimers. It also lists, for each relaxed geometry, the distance of an As atom from: (a) its dimer companion (column 3), and (b) the nearest periodic image (As*) of the dimer companion in the dislocation line direction (column 4). The distinct behaviors of the three dimers are clearly evident from Table I, as discussed below:

(i) [d,f]: In this case the orientation of the dimer is such that site d is the nearest neighbor of both f and its nearest periodic image $f^*$ in the dislocation line direction. Thus, in the periodic chain of dimers, all the As atoms are too close to each other. This allows only a small stretching of the As–As separation, to only

2.57 Å, while the As–As* distance (2.42 Å) changes very little from the equilibrium Si–Si bond distance of 2.35 Å. Consequently, the relaxed structure consists of a chain of essentially fourfold-coordinated As atoms, resulting in negligible binding.

(ii) [d,e]: In this case the orientation of the dimer is nearly perpendicular to the dislocation line direction, and sites d and e* are only second neighbors. This allows the As dimer atoms to relax away from each other, stretching the As–As separation to 2.90 Å, thereby leading to threefold coordination of each As atom. However, the transverse orientation of the dimer keeps it well separated from its periodic images in the dislocation line direction, as is evident from the large As–As* distance. We therefore have an array of nearly isolated As dimers. This leads to a positive but low segregation energy (0.13 eV per As) , just as in a grain boundary.[13]

(iii) [b,c]: In this case the dimer is oriented such that although b and c* are second nearest neighbors, their distance before relaxation is much less than the separation of d and e* in case (ii). Consequently, the As–As stretch is accompanied by As and As* getting closer to each other. In the final relaxed geometry, the As–As* separation (2.95 Å) is only slightly larger than the As–As separation (2.87 Å) and we have a nearly perfect chain of As atoms leading to a large segregation energy (0.88 eV per As).

In order to elucidate further the source of energy gain through the formation of dimer chains, we have examined the electronic energy levels in the As dimers in the dislocation core and compared them with those of isolated As atoms in the bulk. As one would expect, the isolated As atom has a shallow donor level at less than 0.1 eV below the conduction band edge. In the [b,c] dimer chains, on the other hand, each As atom has an electron at a level in the midgap region.[20] Further analysis indicates that the level in the gap is a member of the lone-pair states that As atoms have when they are threefold coordinated. Because of the close proximity of the threefold coordinated As atoms, these lone-pair states split, with half of them in the band gap and half of them in the valence band. Thus, the gain in energy could be viewed as a result of the shallow donor level being driven deep into the band gap by the lattice relaxation accompanying dimer formation, or, equivalently, as arising from the fact that dimer formation leads to lone-pair states that are lower in energy than the states that are available when an As atom is fourfold coordinated.

In summary, using the 90° partial dislocation as a concrete example, we find that As likes to decorate a core in Si in an ordered chain fashion. All As atoms in the chain achieve threefold coordination through repulsion between alternating As atoms. Overall behavior of single impurities, isolated dimers, and chains in the dislocation core is similar to the behavior we found in a Si grain boundary.[13] However, the segregation energy of both single As atoms and those in a chain are much larger in the dislocation core, with the result for the chain being as high as 0.9 eV per As atom.

We would like to thank the ORNL Center for Computational Sciences for providing valuable supercomputer hours. This research was supported in part by Lockheed Martin Energy Research Corp. under DOE Contract No. DE-AC05-96OR22464, and ONR Grant No. N00014-95-1-0906, and by an appointment to the ORNL Postdoctoral Research Associates Program administered jointly by ORNL and ORISE.

[1] P. B. Hirsch, Mater. Sci. Technol. **1**, 666 (1985), and references therein.
[2] Papers in *Structure and Properties of Dislocations in Semiconductors*, Institute of Physics Conference Series No. 104, (Bristol, 1989).
[3] A. Olson and J. C. H. Spence, Philos. Mag. A **43**, 945 (1980).
[4] F. Louchet and J. Thibault-Desseaux, Rev. Phys. Appl. **22**, 207 (1987).
[5] S. Marklund, Phys. Status Solidi B **100**, 77 (1980).
[6] M. Heggie, R. Jones, and A. Umerski, Philos. Mag. A **63**, 571 (1991).
[7] R. Jones, A. Umerski, P. Stich, M. I. Heggie, and S. Oberg, Phys. Status Solidi A **137**, 389 (1993).
[8] K. W. Lodge, A. Lapiccirella, C. Battistoni, N. Tomassini, and S. L. Altmann, Philos. Mag. A **60**, 643 (1989).
[9] K. Masuda, K. Kojima, and T. Hoshino, Jpn. J. Appl. Phys. 1 **22**, 1240 (1983).
[10] M. Mostoller, M. F. Chisholm, and T. Kaplan, Phys. Rev. Lett. **72**, 1494 (1994); Phys. Rev. B **50**, 12183 (1994).
[11] F. Liu, M. Mostoller, V. Milman, M. F. Chisholm, and T. Kaplan, Phys. Rev. B **51**, 17192 (1995).
[12] T. A. Arias and J. D. Joannopoulos, Phys. Rev. B **49**, 4525 (1994).
[13] A. Maiti, M. F. Chisholm, S. J. Pennycook, and S. T. Pantelides, Phys. Rev. Lett. **77**, 1306 (1996).
[14] J. P. Hirth and J. Lothe, *Theory of Dislocations* (McGraw-Hill, New York, 1982).
[15] H. J. Monkhorst and J. D. Pack, Phys. Rev. B **13**, 5188 (1976).
[16] R. Jones, J. Phys. (France) Colloq. **40**, C6 (1979).
[17] P. B. Hirsch, J. Phys. (France) Colloq. **40**, C6 (1979).
[18] M. S. Duesbery, B. Joos, and D. J. Michel, Phys. Rev. B **43**, 5143 (1991).
[19] J. R. K. Bigger, D. A. McInnes, A. P. Sutton, M. C. Payne, I. Stich, R. D. King-Smith, D. M. Bird, and L. J. Clarke, Phys. Rev. Lett. **69**, 2224 (1992).
[20] In the local density approximation used in the calculations, the band gap is smaller than the experimental band gap, so we cannot unambiguously determine the precise location of the level relative to the conduction band edge. Note that, however, for total-energy calculations performed here, only the occupied states are pertinent.

# Coupled-Barrier Diffusion: The Case of Oxygen in Silicon

Madhavan Ramamoorthy and Sokrates T. Pantelides
*Department of Physics and Astronomy, Vanderbilt University, Nashville, Tennessee 37209*
(Received 9 August 1995)

Oxygen migration in silicon corresponds to an apparently simple jump between neighboring bridge sites. Yet extensive theoretical calculations have so far produced conflicting results and have failed to provide a satisfactory account of the observed 2.5 eV activation energy. We report a comprehensive set of first-principles calculations that demonstrate that the seemingly simple oxygen jump is actually a complex process involving coupled barriers and can be properly described quantitatively in terms of an energy hypersurface with a "saddle ridge" and an activation energy of ~2.5 eV. Earlier calculations correspond to different points or lines on this hypersurface.

PACS numbers: 66.30.Jt, 31.15.Ar, 61.72.–y, 81.60.Cp

Oxygen in silicon has long been known to occupy a bridge position between neighboring Si atoms, with an Si-O-Si configuration similar to those in $SiO_2$ [1,2]. Its diffusion, measured to have an activation energy of 2.5 eV [3], is generally believed to consist of simple jumps between neighboring bridge positions on the (110) plane defined by the corresponding Si-Si bonds (Fig. 1). In terms of the angle $\theta_O$ defined in Fig. 1, the midpoint of the jump is at $\theta_O = 90°$.

Most calculations to date [4–8] assumed such a simple adiabatic jump, with reflection symmetry about the vertical axis shown in Fig. 1. Thus, the saddle point was assumed to have the O atom at $\theta_O = 90°$ and the central Si atom at $\theta_{Si} = 90°$. The remaining degrees of freedom and the positions of the other Si atoms were determined by total-energy minimization. The resulting total energy, measured from the energy of the equilibrium configuration, represents the adiabatic activation energy for diffusion. Some authors [4,5] reported activation energies around 2.5 eV, while others [6–8] reported smaller values ranging from 1.2 to 2.0 eV.

In Ref. [8], Needels *et al.* found a value of 1.8 eV and attributed the discrepancy with experiment to dynamical phenomena, i.e., the neighboring Si atoms do not relax fully along the O trajectory. They reported model dynamical calculations for a "generic" nonadiabatic path in which the O atom was given an initial "kick," i.e., an initial velocity corresponding to a kinetic energy of 2.0, 2.3, or 2.7 eV. They found that when the kick energy was <2.5 eV, the O atom went past the saddle point but then returned to the original bridge position. When the kick was >2.5 eV the O atom migrated to the next bridge site. They concluded that their results suggested that dynamical effects are important in O migration, but did not constitute definitive evidence.

In a recent paper, Jiang and Brown (JB) [9] sought to resolve the issue by exploring the entire migration path. They performed total-energy minimizations by stepping the oxygen atom from one bridge site to the next. They found that the total energy attains a value of only ~1.2 eV at $\theta_O = 90°$, but then keeps rising to a maximum value (saddle point) of ~2.5 eV at $\theta_O = 113°$. In addition, they computed the diffusion constant and found it to agree very well with experiment over 12 decades. They concluded that the saddle point of O migration is past the midpoint of the path and that their results account for all the experimental data.

At first glance, JB's results account nicely for the experimental data without the need to invoke dynamical effects. Nevertheless, the pronounced asymmetry of JB's total-energy profile about $\theta_O = 90°$ raises a serious question: If the global minimum of the total energy was indeed obtained at each point of the O path, the energy profile would be symmetric about $\theta_O = 90°$. Clearly, JB's minimization procedure yielded a secondary minimum for each $\theta_O > 90°$, not the global minimum. The energy at the global minimum for $90° + \alpha$ is by symmetry equal to that at $90° - \alpha$. If an energy profile were constructed using global minima along the entire path, it would have a maximum of only 1.2 eV at $\theta_O = 90°$. This value would be in poor agreement with experiment. We conclude that there is still no satisfactory account of the observed 2.5 eV

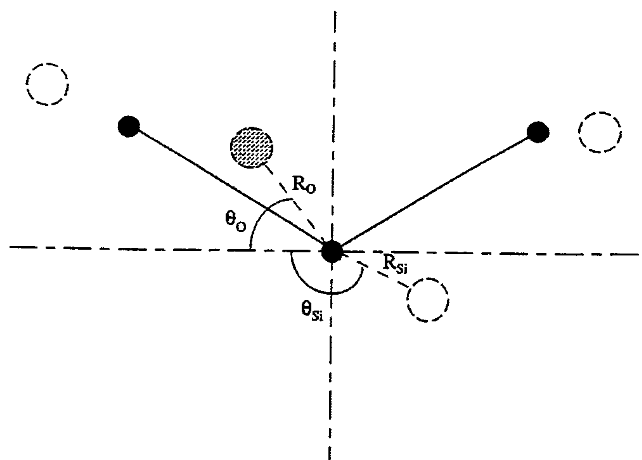


FIG. 1. The geometry of O migration in a (110) plane. The solid dots are the nominal positions of Si atoms in the perfect crystal. The open circles show the positions of the Si and O atoms in the equilibrium configuration.

 © 1996 The American Physical Society 

activation energy, or of the mutually conflicting theoretical results published so far on oxygen diffusion in silicon.

In this paper, we report a series of first-principles total-energy calculations which show that the process of O migration is far more complex than has been recognized so far, but is still adiabatic. During the migration process, *both* the O atom and the central Si atom perform jumps and face large barriers. As a result, a quantitative description of the process requires a calculation of the total-energy hypersurface as a function of the positions of both atoms. We will show slices of this hypersurface that reveal a "saddle ridge" in multidimensional space. The migration process is adiabatic and occurs along a multiplicity of paths over this ridge with a predominant barrier of ~2.5 eV. Finally, we find that the results of earlier authors correspond to different points or lines on the hypersurface.

We performed calculations using density functional theory and the local-density approximation for exchange and correlation, using the form for the exchange-correlation potential given by Ceperley and Alder [10]. The ultrasoft pseudopotentials of Vanderbilt [11] were used for Si and O. These pseudopotentials have been thoroughly tested in several extensive investigations [12–14]. The calculations employed a plane wave basis set and converged results were obtained with an energy cutoff of 25 Ry. A bcc supercell with 32 Si atoms and one O atom was used. Each structure was relaxed until the force on each atom was less than 0.5 eV/Å. All calculations were first done with one special $k$ point at (0.5, 0.5, 0.5) in the irreducible Brillouin zone [15]. The key calculations were repeated with two $k$ points at (0.75, 0.25, 0.25) and (0.25, 0.25, 0.25) [15]. The energy differences changed at most by about 0.2 eV, with all the qualitative results obtained with one $k$ point being unchanged. Hence, the results with one $k$ point were taken to be converged with respect to $k$-point sampling, and used in all the figures in this paper.

Our results for the equilibrium configuration of O, shown schematically in Fig. 1, are in agreement with earlier work [2]. We find a very flat minimum at $\theta_O \sim 55°$. The Si-O bond length is 1.6 Å, the Si-Si length is 3.2 Å (compare with the value of 2.35 Å in bulk silicon), and the Si-O-Si bond angle is ~150°. The angle $\theta_{Si}$ is also ~150°. For our purposes here, the key point is that the central Si atom is well to the right of the vertical symmetry axis (see Fig. 1). As the O migrates from the left bridge position to the one on the right, the central Si needs to move from the right to the left, specifically from $\theta_{Si} \sim 150°$ to $\theta_{Si} \sim 30°$. We will see below that *this swing of the central Si atom controls the dynamics of the oxygen migration because the Si atom has to overcome a barrier.*

We demonstrate this key result in Fig. 2, where we plot the total energy of the system as a function of $\theta_{Si}$ when the O atom at $\theta_O = 90°$ [16]. For each $\theta_{Si}$, the total energy was minimized with respect to $R_O$, $R_{Si}$ (see Fig. 1), and the positions of the other Si atoms. We see that it costs only 0.6 eV to place the O atom at the midpoint if the central Si atom is allowed to relax freely either to the left or to the right [17]. As we saw earlier, as the O atom moves from the left bridge position to the one on the right, the central Si atom needs to swing from the right side to the left side. Figure 2 shows that, with $\theta_O = 90°$, the total barrier is 2.2 eV. This barrier corresponds to the two atoms crossing the midpoints of their respective paths at the same time. It could be argued that this configuration constitutes the saddle point, as was assumed in several previous investigations [4–8]. The total barrier of ~2.2 eV is indeed in good agreement with the experimental value. This simple result, however, belies an enormous complexity which we unravel below. The basis of this complexity is that the O atom and the central Si atom need not pass through the midpoints of their paths at the same time.

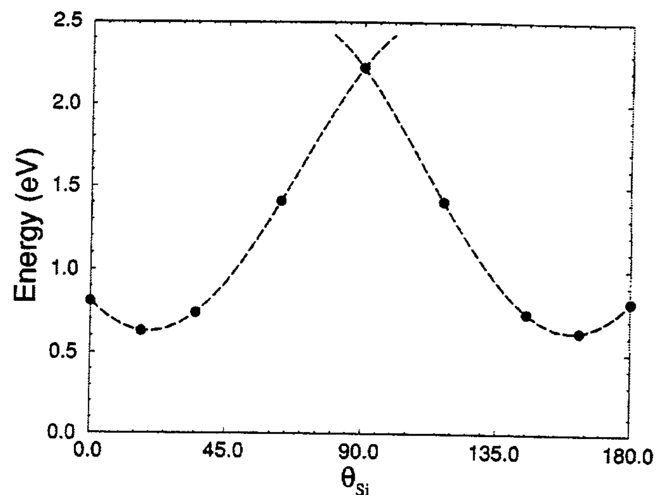


FIG. 2. The total-energy variation of the system, as a function of $\theta_{Si}$ when the O atom is at $\theta_O = 90°$. The zero of the energy in this and in subsequent plots is taken as that of the equilibrium configuration.

The above analysis makes it clear that O migration needs to be described in at least a two-dimensional space defined by $\theta_O$ and $\theta_{Si}$ because the central Si atom also must climb a barrier. This barrier, however, is not simple, but, as shown in Fig. 2, has a cusp at $\theta_{Si} = 90°$, indicative of a Jahn-Teller-like instability with two symmetric total-energy manifolds. These two manifolds correspond to the central Si atom being to the left or the right of the symmetry axis, being bonded to the respective Si atom on the left or the right. For values of $\theta_O$ other than 90°, the two manifolds are not symmetric. In Fig. 3 we trace the evolution of the two total-energy manifolds for a sequence of $\theta_O$ values starting with the O atom near its equilibrium bridge position on the left of the vertical symmetry axis (bottom panel). The central Si atom is on the right side of the axis (the lower-energy manifold). As the O atom progresses along its path (higher panels in Fig. 3), the central Si atom stays in the right manifold. At $\theta_O = 90°$, the two manifolds cross and the central Si atom can switch

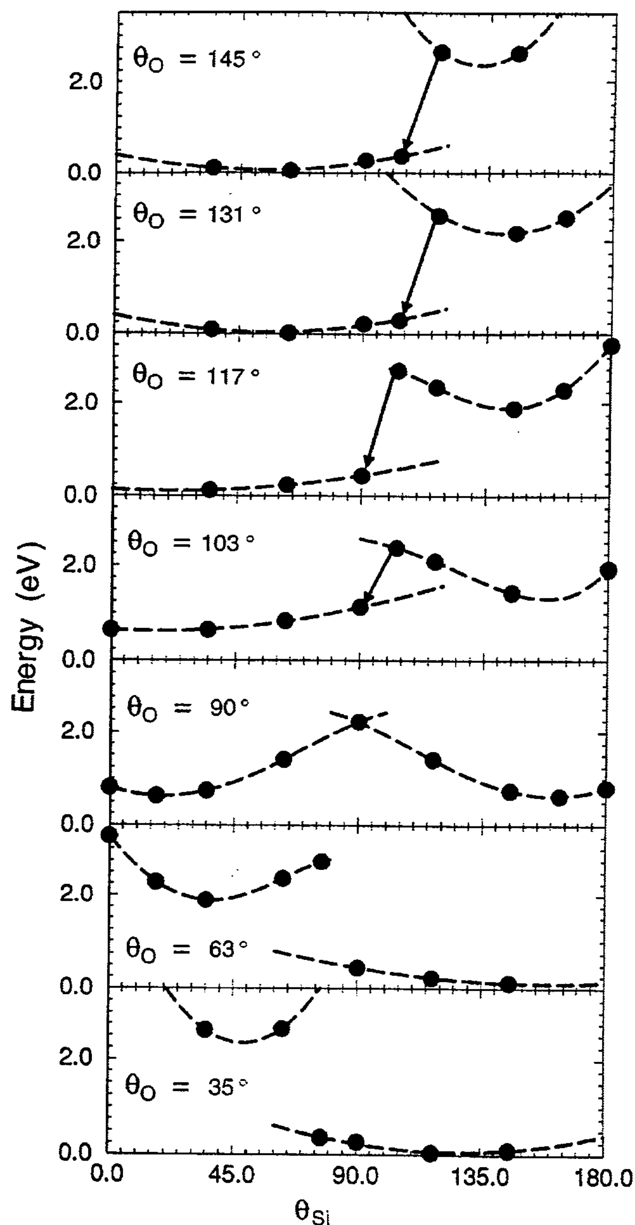


FIG. 3. A series of plots indicating the variation of the total energy as a function of $\theta_{Si}$ for several values of $\theta_O$.

manifolds and swing over to the left of the axis, so that both the O atom and the central Si atom can head for their final destinations. The total barrier for this process is 2.2 eV.

There are additional possibilities, however. The O atom may overshoot the midpoint of its jump without the central Si atom swinging over. The relevant total-energy manifolds are shown in the upper panels of Fig. 3. The central Si atom is now in the high-energy manifold, stuck on the "wrong" side of the vertical axis. Even though the manifolds do not cross, the central Si atom is stable in the higher-energy manifold only up to a certain value of $\theta_{Si}$, marked by the solid arrows. At those points, the calculations show that the central Si atom collapses to the lower-energy manifold, i.e., swings over to the left side of the axis. No matter how much the O atom overshoots (i.e., any of the top four panels), the total energy needed for the central Si atom to swing over is of order 2.3–2.7 eV. In other words, the O atom and the central Si atom *need not move in concert and be at the midpoints of their respective paths at the same time*. They can move independently and still face a net barrier of ~2.5 eV.

The multiplicity of paths is best illustrated with a two-dimensional plot of the total energy as a function of $\theta_O$ and $\theta_{Si}$. For clarity, we show only one of the two manifolds at each pair ($\theta_O$, $\theta_{Si}$), namely, the one corresponding to coupled adiabatic migration. The surface was obtained by interpolating through a sizable number of calculated points. Note the flat regions corresponding to the two equilibrium configurations and the steep drops that correspond to the regions of the solid arrows in Fig. 3. We see that there is a "saddle ridge" with a net energy of ~2.5 eV over a considerable range. At the high symmetry point on the ridge ($\theta_O = 90°$, $\theta_{Si} = 90°$), the total energy is somewhat lower, ~2.2 eV, but this smaller value corresponds to a small fraction of all possible migration paths over the ridge (the resolution of the figure is limited by the complexity of the surface near the ridge). There are two classes of paths: those in which the O atom overshoots the midpoint of its path with the central Si atom trailing and those in which the central Si atom goes over the midpoint of its path first with the O atom trailing. Along all these paths the distance between the O atom and the central Si atom is ~1.7 Å. Thus, the O-Si bond acts like a pogo stick that faces a net barrier of ~2.5 eV no matter how it turns as it attempts to change its tilt from the left to the right.

The collapse from one manifold to the other indicated by the solid arrows in Fig. 3 (steep drops in Fig. 4) was intriguing enough to merit further investigation. The plots in Figs. 3 and 4 were constructed by picking $\theta_O$ and $\theta_{Si}$ and then letting both the O atom and the central Si atom move *radially* until the energy was minimized. It turns out that the two manifolds shown in Fig. 3 correspond to two fairly distinct regions of $R_{Si}$ values. We explored $R_{Si}$ values between these two regions and found that for each $\theta_{Si}$ the energy as a function of $R_{Si}$ has two minima with a barrier that prohibits the central Si atom's motion from one minimum to another, corresponding to a switch between the two energy manifolds. At the critical $\theta_{Si}$ value (solid arrow in Fig. 3), this barrier vanishes and the collapse occurs. The evolution of this radial barrier is also quite intriguing and will be discussed further in a longer article. In fact, a complete description of O migration requires the total energy as a function of four coordinates on the (110) plane: ($\theta_O$, $\theta_{Si}$, $R_O$, $R_{Si}$). Figures 3 and 4 represent slices through this hypersurface.

We now turn to examine the earlier theoretical work in light of the present work. The major point is that all earlier investigators did not recognize the important role of the central Si atom in the migration process. Nevertheless, we can map their results on Fig. 4. References [4–8] assumed that the saddle point is at $\theta_O = \theta_{Si} = 90°$, shown as a dot in Fig. 4. Our value for this point lies

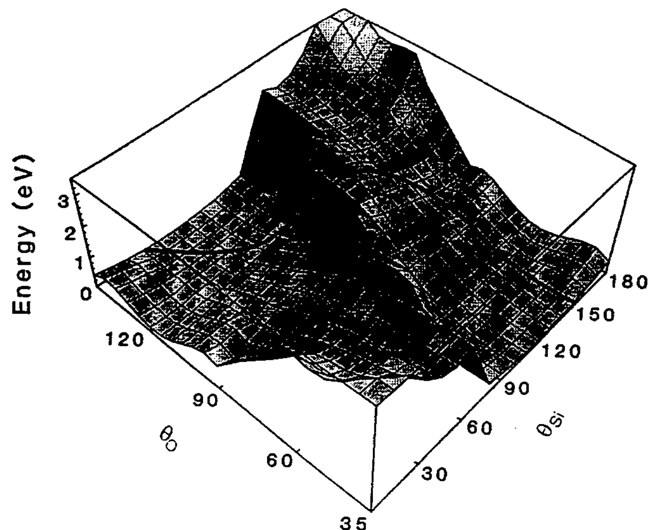


FIG. 4. The total-energy variation as a function of $\theta_O$ and $\theta_{Si}$. The central dot and the hand-drawn path (in the direction of the arrowhead) are discussed in the text.

in the middle of the range of earlier theoretical results (1.8–2.5 eV) [18]. This spread in part reflects the fact that calculations involving oxygen are computationally extremely demanding. The important point to note is that in Fig. 4, the paths that contain the point $\theta_O = \theta_{Si} = 90°$ constitute a small portion of the phase space of all paths going over the ridge. Most of the ridge is somewhat higher, ~2.5 eV, close to the observed activation energy.

Figure 4 also clarifies the "kick" simulations of Needels *et al.* [8] and JB's calculations. Both calculations correspond to the path shown by the hand-drawn line in Fig. 4. Needels *et al.* gave a high kinetic energy to the O atom, whereas JB stepped the O atom gradually. In both cases, the O atom crossed the midpoint of its path before the central Si atom did. In JB's case, the central Si atom crossed over when $\theta_O \sim 115°$. In the case of Needels *et al.*, for kick energies <2.5 eV, the O atom had to turn back because the central Si atom still faced a barrier and could not cross over. In hindsight, one should have given a kick to the central Si atom. In any case, this is not a very likely path because in reality both the O atom and the central Si atom are vibrating about their equilibrium positions, attempting to overcome their respective barriers. As the ridge has roughly a constant height over a considerable range, any point at an energy of ~2.5 eV may be fairly representative of the entire ridge. This might explain the good agreement obtained by JB for the diffusion constant with experiment.

Finally, Needels *et al.* [8] noticed the formation of a metastable configuration at the endpoint of the O path, when the kick was 2.7 eV. The present work shows that this configuration occurs in the right-hand manifold shown in the upper panels of Fig. 3. The metastable configuration is created *during* the migration process for all paths that do not cross $\theta_O = \theta_{Si} = 90°$. Contrary to the findings of Needels *et al.* [8], this configuration collapses to the equilibrium configuration at the end of the migration process.

In summary, we have shown that the total-energy variation during O migration is a very complex hypersurface in a multidimensional space. We have shown slices of this hypersurface along some relevant coordinates, revealing seemingly disconnected manifolds. We believe that the calculations we have done so far have captured essentially all of the very complex physics of the seemingly simple O jump in bulk Si. Our results suggest that such complexity is likely to be present whenever migration of an impurity involves bond breaking and rebonding with different host atoms.

This work was supported in part by Office of Naval Research Grant No. N00014-95-1-0906. Supercomputing time was provided by the Pittsburgh Supercomputing Center under Grant No. DMR950001P.


[1] J.W. Corbett, R.S. Mac Donald, and G.D. Watkins, J. Phys. Chem. Solids **25**, 873 (1964).

[2] E. Martinez, J. Plans, and F. Yndurain, Phys. Rev. B **36**, 8043 (1987).

[3] J.C. Mikkelsen, Jr., Appl. Phys. Lett. **40**, 336 (1982).

[4] L.C. Snyder and J.W. Corbett, Mater. Res. Soc. Symp. Proc. **59**, 207 (1986).

[5] P.J. Kelly and R. Car, Phys. Rev. B **45**, 6543 (1992).

[6] M. Saito and A. Oshiyama, Phys. Rev. B **38**, 10711 (1988).

[7] A. Oshiyama and M. Saito, in *Defect Control in Semiconductors,* edited by K. Sumino (Elsevier Science Publishers, North-Holland, Amsterdam, 1990).

[8] M. Needels, J.D. Joannopoulos, Y. Bar-Yam, S.T. Pantelides, and R.H. Wolfe, Mater. Res. Soc. Symp. Proc. **209**, 103 (1991).

[9] Z. Jiang and R.A. Brown, Phys. Rev. Lett. **74**, 2046 (1995).

[10] D.M. Ceperley and B.J. Alder, Phys. Rev. Lett. **45**, 566 (1980).

[11] D. Vanderbilt, Phys. Rev. B **41**, 7892 (1990).

[12] R.D. King-Smith and D. Vanderbilt, Phys. Rev. B **49**, 5828 (1994).

[13] Feng Liu, S.H. Garofalini, R.D. King-Smith, and D. Vanderbilt, Phys. Rev. B **49**, 12528 (1994).

[14] M. Ramamoorthy, D. Vanderbilt, and R.D. King-Smith, Phys. Rev. B **49**, 16721 (1994).

[15] D.J. Chadi and M.L. Cohen, Phys. Rev. B **8**, 5747 (1973).

[16] In all the calculations reported in this paper, we confined the motion of the O atom and the central Si atom to the (110) plane. Our test calculations showed that, in agreement with Ref. [9], the energy rises if either atom is allowed to go off the (110) plane.

[17] In the symmetrical configuration $\theta_O = \theta_{Si} = 90°$, O is forced to have three bonds, with each Si-O-Si bond angle about 85°. In the configurations corresponding to the minima in Fig. 2, there are only two Si-O bonds with lengths ~1.7 Å and the magnitude of the Si-O-Si bond angle equal to 127°, significantly closer to equilibrium values.

[18] The value 1.2 eV of Ref. [6] was replaced by a more accurate value of 2.0 eV by the same authors in Ref. [7].

Appendix E

# Enhanced Modes of Oxygen Diffusion in Silicon

M. Ramamoorthy and S. T. Pantelides

*Department of Physics and Astronomy, Vanderbilt University*

*Nashville, TN 37235*

(September 17, 1996)

## Abstract

Experiments have established two modes of enhanced oxygen diffusion in silicon, one of unknown origin and the other catalyzed by hydrogen. Existing theories, all based on cluster calculations, have yielded contradictory results for both modes. We report state-of-the-art first-principles calculations and determine migration pathways for a self-enhanced mode via oxygen dimers and for the H-enhanced mode via oxygen-hydrogen complexes. The concerted atomic motions are physically transparent and the corresponding reduced activation energies agree with experiment.

Typeset using REVTEX 3.0



DMR9500001P

Oxygen diffusion in silicon is an important technological process because it leads to the formation of aggregates (small O clusters, $SiO_2$ precipitates) during the thermal processing of crystalline Si wafers.[1] The published experimental data exhibit a number of puzzles.[2] While the diffusion of O atoms has been directly observed[3] to take place with an activation energy of 2.5 eV over a wide range of temperatures (300-1200°C), O clustering at moderate temperatures (350-450°C) takes place with an activation energy of only 1.7 eV.[4–6] Moreover, the observed rates of clustering at these temperatures are several orders of magnitude higher than would be possible by means of the diffusion of isolated O atoms. To resolve this puzzle, different investigators postulated the existence of different candidates for a fast-diffusing defect complex: the $O_2$ molecule,[7,8], an O-vacancy complex,[9] an O-Si-self-interstitial complex,[10] the O dimer.[11] No definitive experiment or theory has established the complex's identity.

Enhanced O diffusion in Si has also been shown to be induced by H in a separate set of investigations,[12] with a low activation energy of $\sim$ 1.2 eV.[13] The catalytic effect of H has been attributed to collisions of fast-diffusing H atoms with O atoms[13] and to oxygen-hydrogen complexes.[14] Again, no definitive explanation has been established.

In all the published theoretical work on enhanced O diffusion in Si, the infinite Si crystal was approximated by a small cluster containing between 30 and 50 Si atoms, with the impurity atoms placed at the center. Pathways were reported for "self-enhanced" O diffusion (i.e. enhanced O migration in the absence of any other impurity or native defect) via the motion of O dimers and for H-enhanced diffusion via the motion of oxygen-hydrogen complexes. The results, however, are mutually contradictory. For self-enhanced O diffusion, Snyder et al.[11], using the semi-empirical MINDO/3 method, found a pathway with a low activation energy of $\sim$ 1.4 eV via the migration of the O dimer. However, Ewels et al.[15], using density functional theory, did not find a lowered activation energy along the same pathway. For H-enhanced O diffusion, Estreicher[14] employed the approximate PRDDO method and Jones et al.[16] employed density functional theory to obtain pathways for the migration of the oxygen-hydrogen complex with low activation energies of $\sim$ 1.5 eV. However, they proposed

completely different configurations for the equilibrium structure of the complex and different pathways for its migration.

In this paper we report a comprehensive investigation of enhanced migration of O in Si using density functional theory, the local density approximation for the exchange-correlation potential and pseudopotentials. The defect configurations are simulated using supercells, which are infinite crystals made up of periodically repeated large cells, containing a defect at the center. This approach has been established over the last decade to be reliable for addressing problems involving the energetics and diffusion of impurities in solids. In particular, a few years ago, this method was adopted by one of the present authors and his then coworkers to resolve numerous controversies concerning the diffusion of H in crystalline Si.[17] More recently, the present authors used the same approach to resolve controversies in the diffusion of the O atom in crystalline Si.[18] Here, we report the results of an extensive investigation of self-enhanced and H-enhanced O diffusion in Si. We show that self-enhancement occurs with a low activation energy of about 1.5 eV, through the motion of O dimers. H-enhanced diffusion occurs through the migration of oxygen-hydrogen complexes. Our results for the equilibrium configurations for the positive, neutral and negative charge states for this complex bear a logical similarity to the published results for isolated H in crystalline Si.[17] For the neutral charge state, we found a diffusion pathway with a low activation energy of only 1.2 eV. The lowered activation energy during of self-enhanced and H-enhanced O diffusion, in comparison with the migration of the O atom, is due to the saturation of a dangling bond on one of the principal Si atoms involved in the migration process. The detailed mechanisms of the two processes, however, are very different.

The theoretical results reported in this article were obtained using density functional theory and the local-density approximation for exchange and correlation. The ultra-soft pseudopotentials of Vanderbilt[19] were used. The calculations employed a plane wave basis set. Converged results were obtained with an energy cutoff of 25 Ry. A 32 site bcc supercell was used, with one k-point at $(0.5, 0.5, 0.5)$ in the irreducible Brillouin zone[20]. Each structure was relaxed until the force on each atom was less than 0.5 eV/Å.

In the following paragraphs, we describe migration pathways which lead to enhanced O migration in Si. Given the complexity of the energy surface describing the migration of each defect complex, we investigated a sequence of configurations which would lead us from one equilibrium configuration to another. The principal atoms driving the migration process were moved in small steps of order 0.1-0.2 Å with the application of suitable constraints, while all the other atoms were allowed to relax to equilibrium.

We were guided in our choice of pathways by the recent comprehensive investigation of the diffusion of an O atom in Si.[18] Here, we summarize the results of that investigation, to motivate the bond-breaking and bond-making processes described in the subsequent discussion. The migration of the O atom is an extremely complex process with both the O atom and a Si neighbor being required to surmount large energy barriers. The process occurs through a multiplicity of paths, all of which have an activation barrier of about 2.5 eV. One path is shown schematically in Fig. 1 where three Si atoms are labelled Si(L), Si(C) and Si(R) respectively. The O atom moves from the bond-center position between Si(L) and Si(C) to the bond-center position between Si(R) and Si(C). The calculated 2.5 eV activation energy of migration for the process is made up of two major contributions:

(i) $\sim$ 0.6 eV to make the O atom threefold coordinated in an intermediate configuration, as shown in Fig. 1 (b);

(ii) $\sim$ 1.6 eV required to allow Si(C) to break its bond with Si(R) and re-form its bond with Si(L), which requires the system to go through an intermediate configuration where Si(C) is only three-fold coordinated (with a dangling bond), as shown in Fig. 1 (c).

We now describe a pathway for self-enhanced O diffusion, through the migration of the O dimer. This is shown schematically in Fig. 2. The principal atoms driving the migration process are the two O atoms and two Si atoms, Si(C) and Si(R), with Si(L) and Si(S) playing a secondary role. In the equilibrium configuration depicted in Fig. 2(a), the two O atoms in the dimer occupy neighboring bond-center positions with a binding energy of 0.3 eV, in agreement with recent theoretical work.[21] All four Si-O bond lengths are $\sim$ 1.65 Å. First, both O atoms move in concert so that they become threefold coordinated at the same time,

as shown in Fig. 2(b). Here the principal atoms lie in a four-membered ring, with each O atom at the nominal midpoint of its migration path (in the absence of the other O atom), vertically above either Si(C) or Si(R).[22] The energy of this configuration is $\sim$ 1.25 eV above equilibrium. This is nearly twice the energy required to make the isolated O atom threefold coordinated. The strong Si-O bonds, drawn with solid lines, are $\sim$ 1.7 Å in length, while the strained ones, drawn with dashed lines, are $\sim$ 1.9 Å in length.

The next event is the gradual re-formation of the bond between Si(C) and Si(L), with the other principal atoms moving to keep the four-membered ring intact.[23] As Si(C) moves, the O atoms rearrange themselves so that Si(C) remains almost four-fold coordinated with one strong Si-O bond of length 1.7 Å and another, considerably strained Si-O bond of length 2.1 Å. The bond between Si(R) and Si(S) becomes elongated during this motion of Si(C). The configuration with the highest energy along this pathway, 1.5 eV above equilibrium, is shown schematically in Fig. 2(c). Here Si(C) is letting go of the second O atom while the bond with Si(L) is close to being formed. After the bond between Si(C) and Si(L) is re-formed, the forces on the two O atoms are such that when they move freely, the system spontaneously rearranges itself to attain the final configuration shown in Fig. 2(d). *The low 1.5 eV activation energy is due to the presence of the second O atom which enables Si(C) to be almost fourfold-coordinated during the migration process.*

We now show how H-enhanced O diffusion takes place through the migration of oxygen-hydrogen complexes. We studied the equilibrium configuration of the oxygen-hydrogen complex in the positive, neutral and negative charge states. Three configurations of the complex are illustrated in Fig. 3. In Fig. 3(a), the O atom and the H atom occupy neighboring bond-center sites. We denote this configuration by BC. In Fig. 3(b), the H atom occupies an antibonding position relative to a Si atom bonded to an O atom, which we denote by AB. In Fig. 3(c), the H atom is directly bonded to the O atom, which we denote by OH. We find that the stability of each configuration and the nature of the equilibrium configuration is strongly dependent on the charge state.

- positive charge state: BC is the equilibrium structure, and is bound by 0.5 eV

compared with isolated, bond-centred O and $H^+$ impurities. OH is about 0.1 eV higher in energy, and is, therefore, also strongly bound compared to the same isolated impurities. AB is unstable with respect to spontaneously distorting into BC.

• **neutral state:** BC is the equilibrium structure, and is bound by 0.3 eV compared with isolated, bond-centred O and $H^0$ impurities. AB is 0.2 eV higher in energy and marginally bound, while OH is about 0.5 eV higher in energy and is unbound, in comparison with the isolated neutral mpurities.

• **negative charge state:** AB is the equilibrium structure, and is bound by 0.4 eV compared with isolated, bond-centred O and the intersititial $H^-$ impurity. OH and AB are both much higher in energy (over 1 eV) and are thus unbound with respect to the isolated impurities.

The above results have a logical consistency with the published results for H in Si.[17] In both cases, $H^+$ and $H^0$ prefer a site midway between two Si neighbors, where the electronic density is high. When the $H^+$ and $H^0$ are placed next to a Si-O-Si bridge, the Si-H-Si unit buckles a little. Finally, $H^-$ in pure Si prefers the tetrahedral interstitial site, where the electron density is low. When placed next to a Si-O-Si bridge the $H^-$ moves towards one of the Si neighbors of the O atom to attain the AB configuration. The OH configuration is not the equilibrium configuration for any charge state, probably because it makes the O atom three-fold coordinated.

A pathway for the migration of the oxygen-hydrogen complex in the neutral state is shown in Fig. 4. The equilibrium BC configuration is shown in Fig. 4 (a). During the migration process, the two impurity atoms move in the following sequence. First, the O atom moves towards the Si-Si bond along which the H atom sits, to take up the bond-center position between Si(C) and Si(R).[24] Owing to the strain created by the proximity of the O atom, the H atom moves into an antibonding position adjacent to Si(C), as shown in Fig. 3(b). This configuration has an energy only 0.3 eV higher than equilibrium. The maximum increase in energy during this stage is only 0.55 eV. Next, Si(C) moves to re-form its bond with Si(L), while the H atom keeps adjusting its position to maintain a strong bond with Si(C). When

the bond between Si(L) and Si(C) is almost re-formed, in order to complete the migration process, the H atom needs to move into a position in-between Si(R) and Si(S). As the H atom climbs the energy barrier to accomplish this, it goes first into an antibonding position with Si(R). The maximum energy during the whole process corresponds to the configuration shown in Fig. 4 (c), which has an energy 1.2 eV above equilibrium. *The low 1.2 eV activation energy for the migration of the oxygen-hydrogen complex is a result of two reasons: (i) the presence of the H atom opens up the bond between Si(C) and Si(R), making it easy for the O atom to move in-between; (ii) the H atom keeps rearranging itself to keep Si(C) nearly fourfold coordinated, throughout the migration process.*

We now compare our results with earlier theory. For the equilbrium structure of the neutral oxygen-hydrogen complex, our results are in agreement with Estreicher[14] and in disagreement with Jones et al.[16]. The energy surface proposed by Estreicher is of questionable quantitative accuracy, given his high estimate of 4.1 eV for the migration energy of the O atom, compared to more accurate estimate of of 2.6 eV of Jones et al. The pathways proposed by both investigators for the migration of the oxygen-hydrogen complex requires the complex to break up and the H atom to diffuse independently of the O atom. The pathway we propose shows that this is unnecessary.

In the case of self-enhanced O diffusion, the pathway that we found has some features in common with that proposed by Snyder et al.[11] They obtained a four-membered ring-like structure, like that shown in Fig. 2 (b), during the migration of the O dimer. However, their semi-empirical method gave them a completely incorrect energy surface. They found the ring-like configuration to be <u>metastable</u> and nearly identical in energy with that of the equilibrium configuration. Our calculations, however, reveal that the ring-like configuration is almost 1.3 eV higher in energy than equilibrium and is <u>unstable</u>.

In conclusion, we have found mechanisms for enhanced O diffusion in Si. Self-enhanced O diffusion proceeds via the migration of O dimers. The calculated activation energy is 1.5 eV, which is close to the experimental estimate[4–6] of 1.7 eV for the activation energy of thermal donor formation. Thus, we conclude that the formation of thermal donors occurs

through the migration of O dimers. H-enhanced O diffusion occurs through the migration of the oxygen-hydrogen complex. The calculated diffusion activation energy is $\sim$ 1.2 eV, again in good agreement with experiment.[13] *In each process, the reduction in the activation energy by about 1.0 eV, in comparison with the 2.5 eV activation energy of the O atom, is the result of the saturation of a dangling bond on one of the principal Si atoms during the migration process.*

## I. ACKNOWLEDGMENTS

This work was supported in part by the Office of Naval Research Grant No. N00014-95-1-0906. Supercomputing time was provided by the Pittsburgh Supercomputing Center under Grant No. DMR950001P.

## REFERENCES


[1] F. Shimura, *Semiconductors and Semimetals* **42**, Academic Press Inc., San Diego, p. 1, F. Shimura (ed.). See references therein.

[2] R. C. Newman and R. Jones, in *Semiconductors and Semimetals* **42**, Academic Press Inc., San Diego, p. 289, F. Shimura (ed.). See references therein.

[3] J. C. Mikkelsen, Mater. Res. Soc. Symp. Proc. **59** 19 (1986).

[4] M. Stavola, J. R. Patel, L. C. Kimmerling and P. Freeland, Appl. Phys. Lett. **42**, 73 (1983).

[5] V. P. Markevich, L. F. Makarenko and L. I. Murin, Phys. Stat. Sol. A **97**, K1 73 (1986).

[6] M. Claybourn and R. C. Newman, Appl. Phys. Lett. **51**, 2197 (1987).

[7] U. Gosele and T. Y. Tan, Appl. Phys. A **28**, 79 (1982).

[8] U. Gosele et al., Appl. Phys. A **48**, 219 (1989).

[9] R. C. Newman, J. H. Tucker, A. R. Brown and S. A. McQuaid, J. Phys. C **16**, L667 (1983).

[10] A. Ourmazd, W. Schroter and A. Bourret, J. Appl. Phys. **56**, 1670 (1984).

[11] L. C. Snyder, J. W. Corbett, P. Deak and R. Wu, Mater. Res. Soc. Symp. Proc. **104** 179 (1988).

[12] H. J. Stein and S. K. Hahn, Appl. Phys. Lett. **56**, 63 (1990).

[13] R. C. Newman, J. H. Tucker, A. R. Brown and S. A. McQuaid, J. Appl. Phys. **70**, 3061 (1991). See references therein.

[14] S. K. Estreicher, *Phys. Rev. B* **41**, 9886 (1990).

[15] C. P. Ewels, R. Jones and S. Öberg, Proceedings of the NATO Advanced Research Workshop 'Early Stages of Oxygen Precipitation in Silicon', March 1996.

[16] R. Jones, S. Öberg and A. Umerski, *Mater. Sci. Forum* **83–87**, 551 (1992).

[17] C. G. Van de Walle, P. J. H. Denteneer, Y. Bar-Yam, and S. T. Pantelides, *Phys. Rev. B* **39**, 10791 (1989). See references therein.

[18] M. Ramamoorthy and S. T. Pantelides, *Phys. Rev. Lett.* **76**, 267 (1996). See references therein.

[19] D. Vanderbilt, *Phys. Rev. B* **41**, 7892 (1990).

[20] D. J. Chadi and M. L. Cohen, *Phys. Rev. B* **8**, 5747 (1973).

[21] D. J. Chadi, *Phys. Rev. Lett.* **77**, 861 (1996).

[22] To obtain this configuration, the four principal atoms were moved into positions lying on the dotted lines parallel to the $< 001 >$ direction, as shown in Fig. 2, and were constrained to move only in this direction. All other atoms were allowed to relax to equilibrium.

[23] This was achieved by moving Si(C) towards Si(L), while the other three principal atoms were still constrained as before.

[24] During this motion of the O atom, Si(C) was moved into a position on the dotted line parallel to the $< 001 >$ direction, as shown in Fig. 4, and was allowed to relax only in this direction. All other atoms were allowed to relax to equilibrium.

## FIGURES

FIG. 1. The migration of the O atom in Si. (a) initial equilibrium configuration. (b) O at the mid-point of the path. (c) saddle-point configuration. (d) final equilibrium structure. The small dots are the nominal sites of Si atoms in the bulk. The open circles are the current positions of the left (L), central (C) and right (R) Si atoms. The large shaded circle is the O atom.

FIG. 2. The migration of the O dimer. (a) initial equilibrium configuration. (b) intermediate four-membered ring structure. (c) saddle-point configuration. (d) final equilibrium structure. The dotted lines indicate constraints. See Refs.22 and 23.

FIG. 3. The stable configurations of the oxygen-hydrogen complex. (a) adjacent bond-center configuration (BC). (b) adjacent anti-bonding configuration (AB). (c) OH configuration.

FIG. 4. The migration of the oxygen-hydrogen complex in the neutral charge state. (a) initial equilibrium configuration. (b) intermediate four-membered ring structure. (c) saddle-point configuration. (d) final equilibrium structure. The dotted line indicates constraints. See Ref.24.

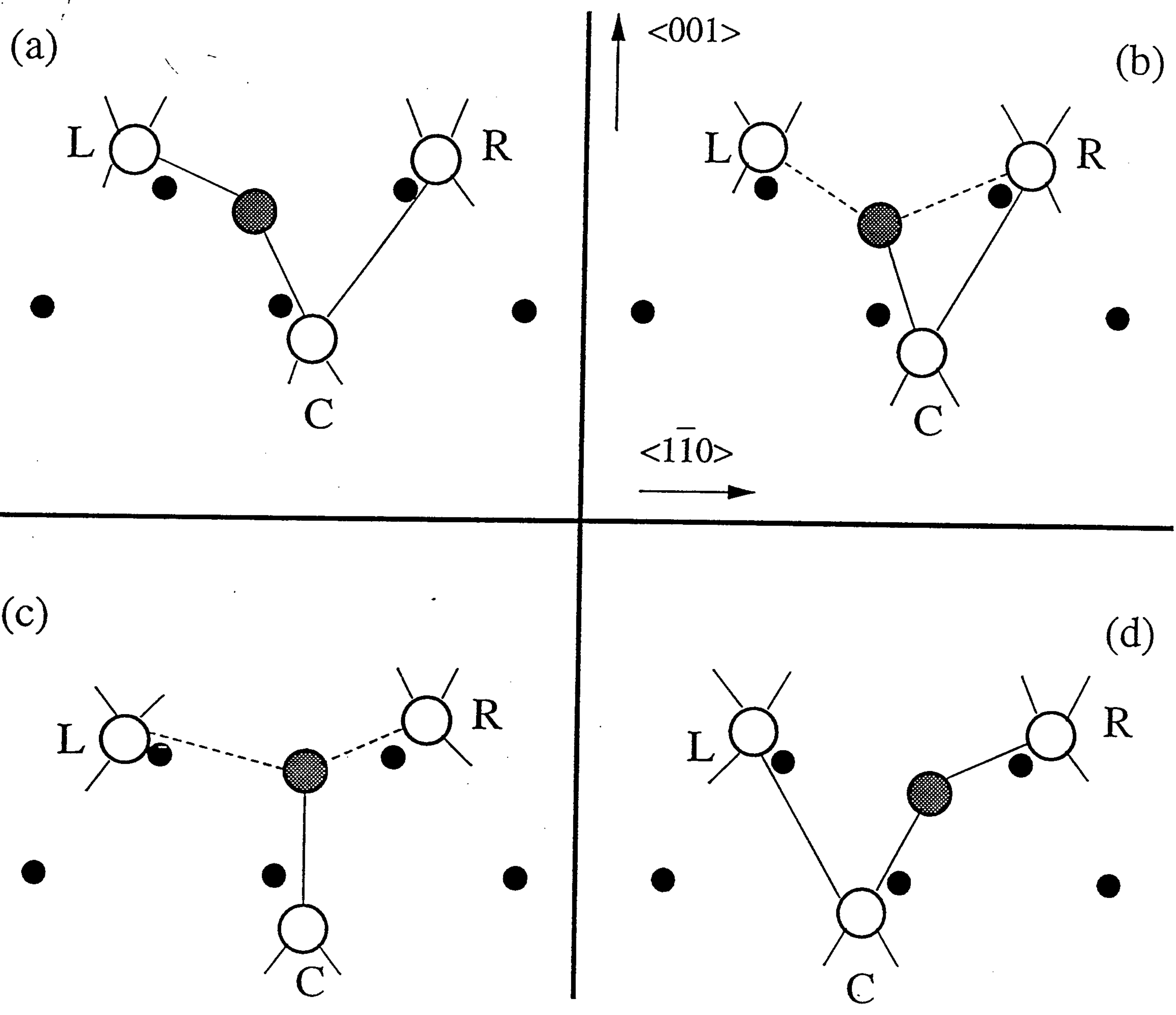


Figure 1

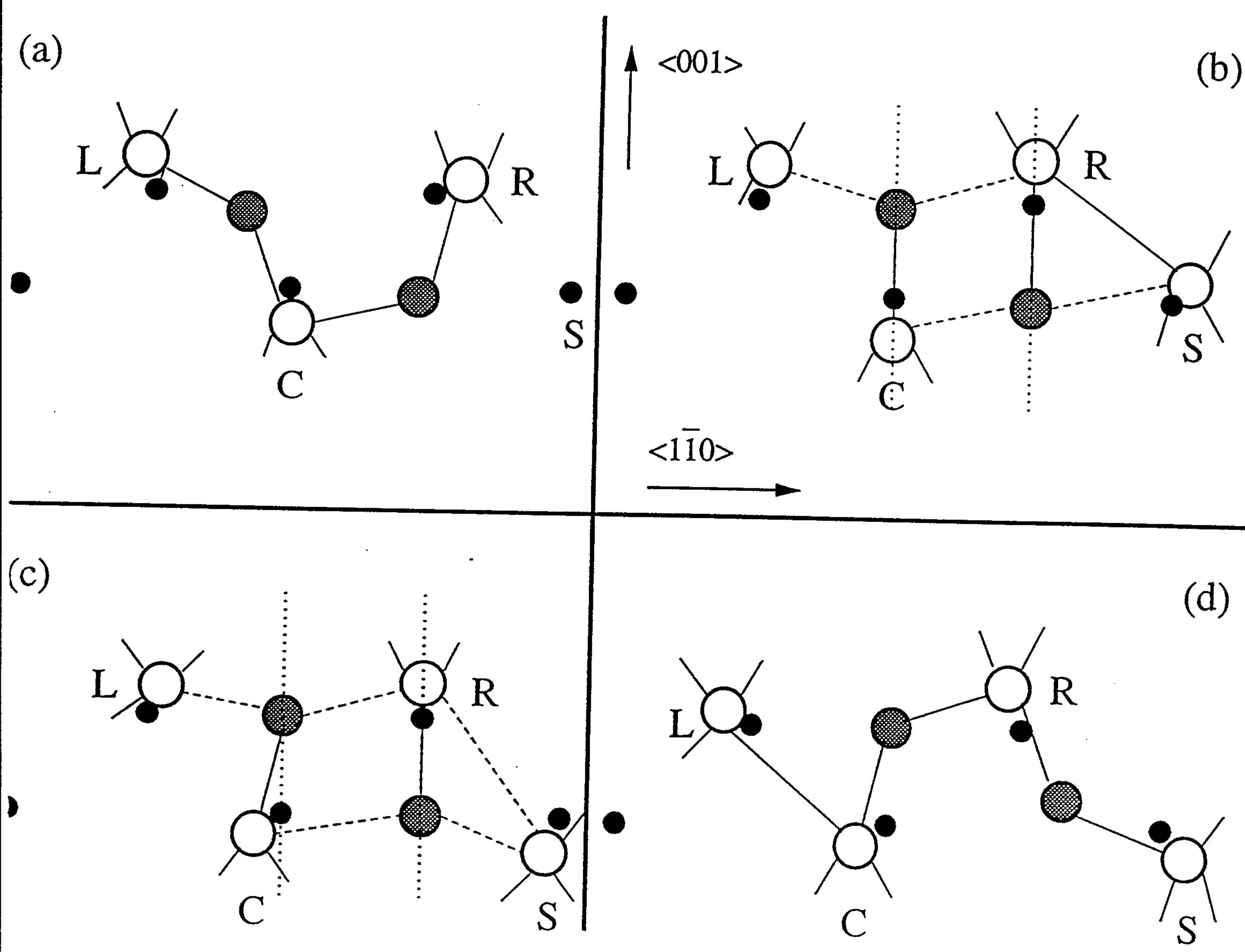


Figure 2

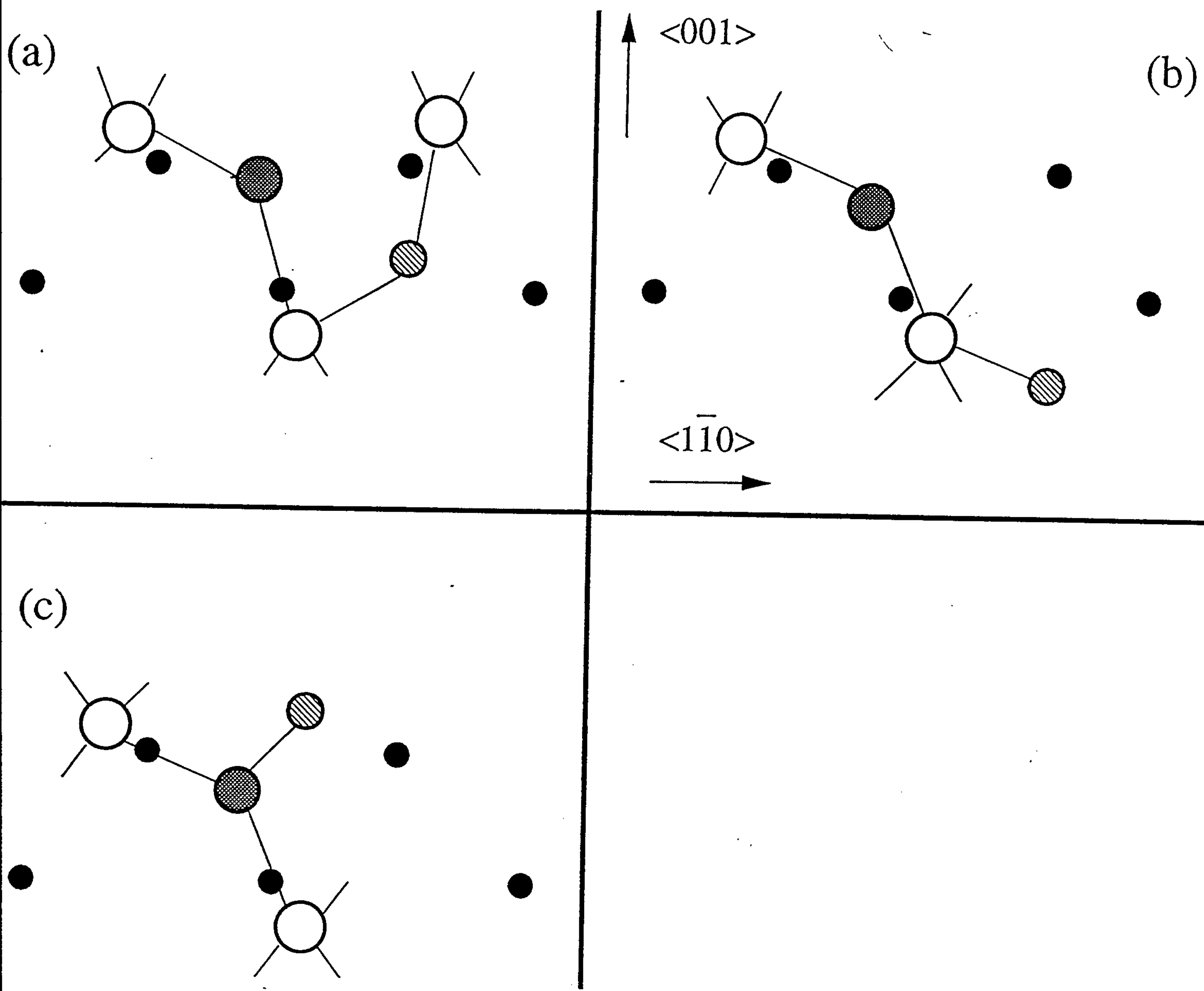


Figure 3

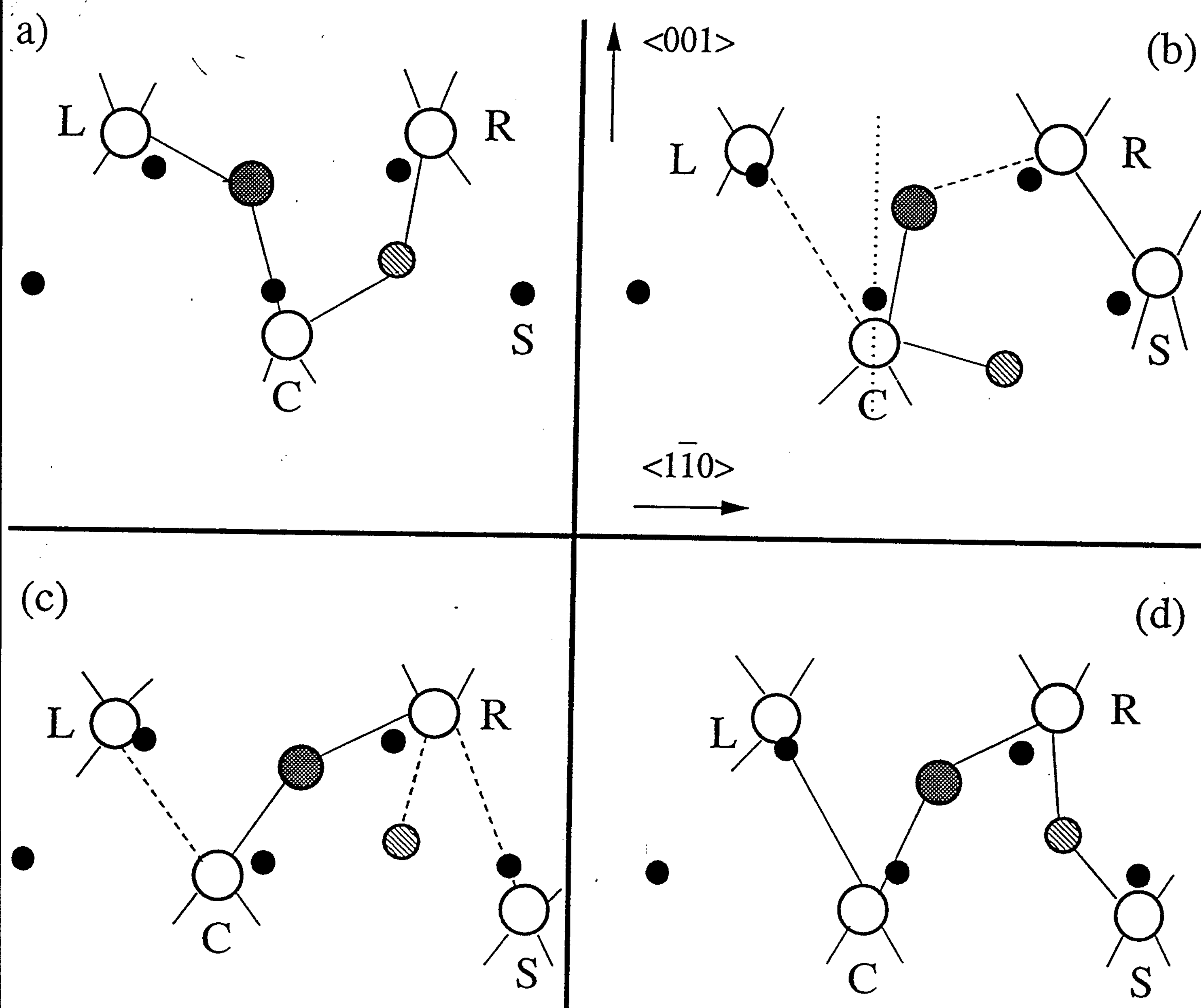


Figure 4

Appendix F

March 25, 1996

**Dynamical simulations of nonequilibrium processes -- Heat flow and the Kapitza conductance across grain boundaries**

A. Maiti,[1,2] G. D. Mahan[1,3] and S. T. Pantelides[1,2]

[1]Solid State Division, Oak Ridge National Laboratory, Oak Ridge, TN 37831

[2]Department of Physics and Astronomy, Vanderbilt University, Nashville, TN 37235

[3]Department of Physics and Astronomy, University of Tennessee, Knoxville, TN 37996

Abstract

We report molecular dynamics simulations of nonequilibrium heat flow in a *solid* system in the local-equilibrium or hydrodynamic approximation, and demonstrate that local equilibrium can be achieved in a surprisingly small number of atomic layers. From the dynamical simulations, we calculate the thermal boundary (Kapitza) conductance that arises from heat flow across Si grain boundaries and compare with the traditional approach based on calculating the transmission and reflection of harmonic phonons at the grain boundary interface.

PACS: 66.70.+f, 44.30.+v, 61.72.Mm, 05.60.+w

Submitted to *Physical Review Letters*.

Molecular dynamics has been a powerful method to study the dynamical evolution of systems of atoms, namely a gas, a liquid, or a solid. The positions $q_i$ and momenta $p_i$ of all the atoms in the system are the dynamical variables whose evolution in time is governed by Hamilton's equations of motion. The classical Hamiltonian (total energy) of the system is determined from a set of interatomic potentials (conventional molecular dynamics [1]) or from density-functional theory (Car-Parrinello dynamics [2]). In principle, simulations are done by assuming one of Gibbs' statistical mechanical ensembles that specify which externally controlled macroscopic variables are kept constant. The resulting $q_i(t)$ and $p_i(t)$ are the trajectories in phase-space of one replica in the ensemble. Typically, one assumes a uniform and constant temperature and either a constant volume, or a constant pressure or stress. The trajectories are then computed with the constraints imposed by the values of the externally controlled variables.

When externally controlled macroscopic variables such as temperature or pressure are non-uniform over a sample, the system is in a nonequilibrium state and irreversible transport occurs. For homogeneous systems, such as liquids or uniform solids, linear transport coefficients can be computed from *equilibrium* simulations [3-5] using the Kubo formalism [6]. This formalism, however, is not useful for inhomogeneous systems (*e.g.* a polycrystal, or an interface between two different solids.). For such systems, one must perform nonequilibrium simulations. Such nonequilibrium simulations, however, present different challenges that have not been systematically addressed so far. For example, for nonequilibrium heat flow, we are aware of only one attempt to establish a steady state in a homogeneous Lennard-Jones liquid [7].

In this Letter, we report the first nonequilibrium dynamical simulation of heat flow in a solid when a temperature difference is externally maintained between two planes. First, we show that it is possible to establish a uniform temperature gradient between the two planes in the case of a single crystal. These results establish that local equilibrium can be achieved in a surprisingly small number of atomic layers. Then, we simulate heat flow in a bicrystal and demonstrate that a temperature discontinuity is

established across the grain boundary. In terms of this discontinuity we are able to compute the Kapitza conductance [8, 9] of the grain boundary. We report such calculations for two different grain boundaries in Si using the Stillinger-Weber classical three-body potential [10].

Traditional calculations of the Kapitza conductance have been based on the lattice dynamical theory in which one computes the transmission coefficient of harmonic phonons at the interface [11-14] (see eqn. (6) below). For this, one needs to match wavevectors and modes of phonons with the same frequency on the incident and the transmitted sides of the interface. The number of such matching conditions is governed by the number of atoms in the surface unit cell containing a periodic segment of the interface parallel to the boundary plane. Although the theoretical formalism of wavevector matching for a general interface exists [12], it has so far been applied to examples with only a few atoms in the surface unit cell. However, even for the simplest case of a twin boundary, there are many atoms in the surface unit cell, and using the traditional mode counting approach becomes a nontrivial exercise. The molecular dynamics method to calculate Kapitza conductance is superior to the traditional method because: (i) it is much simpler to set up for any crystal structure and any interface; (ii) the accuracy of the calculations can be systematically increased by merely increasing the supercell size and the total simulation time; and (iii) all anharmonic effects are included automatically.

Before describing the simulation details, it is relevant to address the major obstacles to a successful nonequilibrium simulation, that would help explain why *not* many such simulations have been reported to date. The major difficulty stems from the fact that in order to establish an accurate thermal profile, one needs to partition the supercell into various sections and define a local-equilibrium temperature for each section. To accurately define a local temperature, one would like to have sections that are long compared to the mean free path (mfp) [5] of the heat carriers, *i.e.*, phonons in our

case. Starting from a Boltzmann transport theory formalism [15], one obtains the following expression for the averaged phonon mfp for an isotropic solid:

$$\langle l_{ph} \rangle = \frac{3\sigma_0}{\rho\, C_v \langle v_{ph} \rangle}\,, \qquad (1)$$

where $\sigma_0$ is the bulk thermal conductivity, $\rho$ the mass density of the crystalline solid, $C_v$ the phonon contribution to the specific heat at constant volume, and $\langle v_{ph} \rangle$ an average phonon velocity. The last two quantities are defined by:

$$C_v = \sum_\lambda \int d^3q\, \hbar\omega(\lambda, q) \frac{\partial f(\omega, T)}{\partial T}\;; \qquad (2)$$

$$\langle v_{ph} \rangle = \frac{\sum_\lambda \int d^3q\, \omega(\lambda, q) \frac{\partial f(\omega, T)}{\partial T} |\nabla_q \omega(\lambda, q)|}{\sum_\lambda \int d^3q\, \omega(\lambda, q) \frac{\partial f(\omega, T)}{\partial T}}\,. \qquad (3)$$

where $\omega(\lambda, q)$ is the phonon frequency corresponding to the mode $\lambda$ and wavevector **q**, $f(\omega, T)$ is the phonon occupation given by the Bose-Einstein factor, and all integrations are defined over the whole Brillouin Zone. We have calculated the phonon spectrum of Si using the Stillinger-Weber potential [10] and obtained values of $C_v$ and $\langle v_{ph} \rangle$. The resulting $\langle l_{ph} \rangle$ is shown in Fig. 1 as a function of temperature. It is clear that the phonon mfp is large, from 20 nm to several microns. Even at the Debye temperature ($\Theta_D \sim 650$ K [16]) the mfp ~ 30 nm. Thus, supercells that are large compared with the phonon mfp should contain thousands of atoms. Another measure of the difficulty is the average phonon lifetime $\tau_{ph} = \langle l_{ph} \rangle / \langle v_{ph} \rangle$, which is ~ 0.01 ns at $T \sim \Theta_D$, and orders of magnitude larger at lower temperatures. Again, in order to generate a good steady-state profile, one would expect simulations to be longer than $\tau_{ph}$ which might be prohibitively long at low temperatures.

In spite of great strides in the understanding of nonequilibrium statistical mechanics [17], there is no established theory to systematically predict the smallest supercell size and the shortest simulation time required to establish a thermal profile with reasonable accuracy. From a practical point of view, it is therefore important to explore these questions with computer experiments on supercells of various sizes and various simulation times. From the foregoing discussion it would seem that simulations in Si are completely unfeasible at very low temperatures ($T \ll \Theta_D$). It seems to be a significantly daunting task even at $T \sim \Theta_D$. As a first step towards a more general investigation we have, therefore, concentrated only at a temperature range just below $\Theta_D$. Results of three such simulations reported below are quite encouraging: it is possible to establish steady-state thermal profiles using sections that are *much smaller than the phonon mfp* with reasonably long simulation times.

We now describe details of the simulation set up. All supercells are in the shape of rectangular parallelopipeds (Fig. 2) with a length of a few tens of nm in the direction of heat flow, taken normal to the grain boundary plane (x-axis of Fig. 2). A few Å of vacuum is left beyond the two end faces parallel to the grain boundary plane; otherwise the application of a temperature gradient would be incompatible with periodic boundary conditions employed in the simulation. The y and z dimensions of the supercell are set equal to the dimensions of one periodic segment of the grain boundary plane. For simulations on (i) uniform Si, (ii) the $\Sigma=5$ twin boundary, and (iii) the $\Sigma=13$ twin boundary, these dimensions are a x a, $\sqrt{5/2}$ a x a and $\sqrt{13/2}$ a x a respectively, a being the Si lattice constant. For simulations with the twin boundaries, the two grains are chosen of equal length so that the grain boundary is located precisely in the middle of the simulation cell. In order to define a temperature profile, the sample solid is equally divided into an odd number of sections parallel to the grain boundary plane, with the grain boundary fully contained in the middle section. For each section S, an average temperature T(S) is defined by:

$$\frac{1}{2}\sum_{i\in S} m\langle v_i^2\rangle = \frac{1}{2}\frac{N_s}{N}\sum_{\lambda}\int\frac{d^3q}{(2\pi)^3}\frac{\hbar\omega(\lambda, q)}{\exp[\hbar\omega(\lambda, q)/k_B T(S)] - 1}, \quad (4)$$

where $N_s$ is the number of particles contained in the section S, N the total number of particles in the system, and <> denotes averaging over the simulation time. The quantity on the l.h.s. of eq. (4) is the time-averaged total kinetic energy of section S, while the sum on the r.h.s. of eq. (4) is the total energy of the phonons corresponding to an equilibrium temperature T(S). The zero-point energy has been excluded from the phonon energy expression, so that T(S) = 0 corresponds to static atoms. In the high temperature limit, i.e. for $T(S) \gg \Theta_D$, the r.h.s. of eq. (4) $\rightarrow 3N_s k_B T(S)/2$, the usual definition of temperature employed in most simulations. For consistency, we have used eq. (4) with the phonon dispersion $\omega(\lambda, q)$ obtained from the Stillinger-Weber potential [10].

The thermal gradient is applied by maintaining the two end sections at constant but different temperatures $T_1$ and $T_2$. For isothermal simulations of the two end sections, we employ Hoover's method [18] in which a velocity-dependent drag term is introduced into the equation of motion. This method of constant temperature is more suitable for the present simulations than the canonical method of Nosé [19] in which there is an inherent temperature fluctuation of order $T/\sqrt{N_s}$, $N_s$ being the number of particles in section S, and T the desired temperature. In all sections other than the two ends, the atoms move according to Newton's equation of motion with forces derived from the Stillinger-Weber potential. The equations of motion are numerically integrated by the Leapfrog Verlet algorithm [1] using a time-step of 0.8 femtoseconds.

Fig. 3 displays the thermal profile for crystalline Si (*i.e.* no grain boundary) after a total simulation time of 1.0 nanosecond, which was found to be adequate to establish a steady-state profile (see discussion below). The supercell is of length 45 nm, and the sample is divided into 21 equal sections each containing 30 atoms. The yz plane is taken to be the [100] plane of the Si crystal. The cold and the hot ends i.e. section #s 1 and 21 are maintained at constant temperatures of 520 K and 630 K respectively throughout the

entire simulation. Even this unrealistically large temperature gradient yields a linearly varying profile across a large part of the sample (section #s 3 through 16), in accordance with Fourier's law. The end effects, also present in a previous simulation for Lennard-Jones liquid [10], are due to enhanced scattering of phonons arising from the additional "drag" terms introduced to maintain constant temperatures [18] at the end sections. The asymmetry about the middle section (# 11) is due to a decrease in the thermal conductivity of Si with increase in temperature[20, 21] in the range considered.

Fig. 4 displays a similar thermal profile when the middle section (# 11) contains a symmetric $\Sigma=13$ tilt boundary, with a supercell of length 25 nm, containing 840 atoms (the profile for a $\Sigma=5$ boundary is qualitatively very similar, and is not shown explicitly). This profile is dramatically different from the pure Si case (Fig. 3) in that a sharp discontinuity in temperature, $(\Delta T)_{GB}$ appears across the grain boundary. In addition, there are pronounced end effects due to the same reasons as for the pure Si case. However, the sample was chosen large enough to extract the linear slope $(dT/dx)_{xtal}$ in the crystalline material away from the ends, as given by the slopes of the two fitted lines AB and CD. The Kapitza conductance can be readily calculated in terms of the bulk thermal conductivity $\sigma_0$ using the formula:

$$\sigma_K = \frac{(dT/dx)_{xtal}}{(\Delta T)_{GB}} \sigma_0 \, . \tag{5}$$

The values obtained by eq. (5) from the lower (AB) and upper (CD) slopes (in conjunction with $\sigma_0$ values for the corresponding lower and higher temperatures) are averaged to yield $\sigma_K = 0.8$ GW/(m$^2$K) for the $\Sigma=13$ boundary. A similar calculation for the $\Sigma=5$ boundary yields $\sigma_K = 0.9$ GW/(m$^2$K).

The smooth thermal profiles of Figs. 3 and 4 are surprising considering the fact that each section is only 1-2 nm long, whereas the mfp ~ 30 nm! In order to obtain a deeper insight into why it works, it is necessary to examine the profile as it develops with time. Monitoring of the time evolution of the profiles reveals that signatures of high temperature gradients, at the ends and across the grain boundary, get established much

earlier than the flatter profiles in the bulk "crystalline" regions. For the simulation on the $\Sigma$=13 boundary, Fig. 5 shows the temperature of a given section (# 7, chosen for concreteness) as a function of the simulation time. Fig. 5 also displays the time evolution of the temperature discontinuity $(\Delta T)_{GB}$ across the grain boundary. Both quantities oscillate significantly for the first few hundred ps, and attain steady-state values in time of order a ns. However, the *fractional* fluctuation of $(\Delta T)_{GB}$ about its steady-state value reduces to less than 10% only after 70 ps. It takes much longer, at least a ns, to achieve the same order of accuracy in the slope $(dT/dx)_{xtal}$, because it entails an *absolute* fluctuation in T(S) less than a fraction of 1 K, for all S in the crystalline region. The observation that thermal profiles get established faster in regions of larger phonon scattering rates, implies that local thermal equilibrium is established presumably by a certain critical number of phonon scattering events, *even if the section is much smaller than the mfp*. Using the Boltzmann relaxation approximation, and an energy independent relaxation time, we have estimated the number of phonon scattering events within each section (in the crystalline region) to be a few thousand for a total simulation time of 1 ns. This number seems to be sufficient to establish a smooth thermal profile.

In order to recast the above values of Kapitza conductance in terms of a lattice dynamical model, we recall that $\sigma_K$ can be expressed as the temperature derivative of the phonon heat current density across the interface [6]:

$$\sigma_K = \sum_{\lambda} \int_{v_x > 0} \frac{d^3q}{(2\pi)^3} \hbar\omega(\lambda, q)\, v_x(\lambda, q)\, \frac{\partial f(\omega, T)}{\partial T}\, t(\lambda, q) \ , \qquad (6)$$

where $t(\lambda, q)$ is the *transmission coefficient* of the $(\lambda, q)$ phonon, *i.e.* the fraction of the energy of an incident phonon of wavevector **q** and mode $\lambda$ that gets transmitted through the boundary, and $v_x$ is the phonon group velocity normal to the boundary. The integration, as before, is over the entire Brillouin Zone, and the condition $v_x > 0$ chooses only those phonons that are incident on the grain boundary from the left side. As indicated earlier, calculating $t(\lambda, q)$ from wavevector matching equations is not

straightforward for the case of a grain boundary. However, once $\sigma_K$ values are obtained by MD simulations, one could estimate an *average transmission coefficient* $\langle t \rangle = \sigma_K / I$, where:

$$I = \sum_{\lambda} \int_{v_x > 0} \frac{d^3q}{(2\pi)^3} \hbar\omega(\lambda, \mathbf{q})\, v_x(\lambda, \mathbf{q})\, \frac{\partial f(\omega, T)}{\partial T} \,. \tag{7}$$

The quantity I can be interpreted as the maximum possible value of $\sigma_K$, which occurs under perfect phonon transmission across the interface, i.e. $t(\lambda, \mathbf{q}) = 1$ for all $\lambda$ and $\mathbf{q}$. Using the Stillinger-Weber phonon dispersion at our mean simulation temperature of 575 K we obtain $I = 1.4$ GW/(m$^2$K), which yields $\langle t \rangle = 0.65$ and 0.57 for the $\Sigma$=5 and the $\Sigma$=13 boundaries, respectively. The fact that $\langle t \rangle < 1$ for both the boundaries is a consistency check on the MD simulations. The relatively large values of the average transmission coefficient are consistent with the fact that all Si atoms in the two grain boundaries are fourfold coordinated [22, 23], and therefore the local phonon modes in the interface region are not expected to be very different from that in crystalline Si. A more systematic study of the variation of $\sigma_K$ with the grain boundary tilt angle is underway.

In summary, we have demonstrated that local equilibrium can be achieved in a nonequilibrium molecular dynamics simulation on sections that are much smaller than the phonon mfp. The technique is illustrated by establishing steady-state thermal profiles in crystalline Si and across two different symmetric tilt grain boundaries in Si. The results establish the validity of Fourier's law even under very large temperature gradients (of order 1 K/Å), and give rise to dramatic temperature discontinuities across interfaces between two different crystals. This allows for the first time a simple method to determine the thermal boundary (Kapitza) conductance associated with a general grain boundary, and opens the door for more nonequilibrium simulations in solid and liquid systems.

This research was supported in part by Lockheed Martin Energy Research Corp. under DOE contract No. DE-AC05-96OR22464, and ONR grant No. N00014-95-1-0906.

References

1. M. P. Allen and D. J. Tildesley, *Computer Simulation of Liquids*, Oxford: Clarendon (1987), and references therein.
2. M. C. Payne, M. P. Teter, D. C. Allan, T. A. Arias, and J. D. Joannopoulos, Rev. Mod. Phys. **64**, 1045 (1992).
3. M. J. Gillan and M. Dixon, J. Phys. C **16**, 869 (1983).
4. D. J. Evans and G. P. Morriss, Comput. Phys. Rep. **1**, 297 (1984).
5. P. Sindzingre and M. J. Gillan, J. Phys.: Condens. Matter **2**, 7033 (1990), P. J. D. Lindan and M. J. Gillan, *ibid.* **3**, 3929 (1991).
6. R. Kubo, Rep. Prog. Phys. **29**, 255 (1966).
7. A. Tenenbaum, G. Ciccotti, and R. Gallico, Phys. Rev. A **25**, 2778 (1982).
8. P. L. Kapitza, J. Phys. USSR **4**, 181 (1941).
9. E. T. Swartz and R. O. Pohl, Rev. Mod. Phys. **61**, 605 (1989).
10. F. H. Stillinger, and T. A. Weber, Phys. Rev. B **31**, 5262 (1985).
11. D. A. Young and H. J. Maris, Phys. Rev. B **40**, 3685 (1989).
12. S. Pettersson and G. D. Mahan, Phys. Rev. B **42**, 7386 (1990).
13. R. J. Stoner, H. J. Maris, T. R. Anthony, and W. F. Banholzer, Phys. Rev. Lett. **68**, 1543 (1992).
14. R. J. Stoner and H. J. Maris, Phys. Rev. B **48**, 16373 (1993).
15. J. M. Ziman, *Principles of the Theory of Solids*, Cambridge (1965), Chap. 7.
16. *Americal Institute of Physics Handbook*, ed. by D. E. Gray, McGraw-Hill, New York (1972).
17. R. Kubo, M. Toda, and N. Hashitsume, *Statistical Physics II: Nonequilibrium Statistical Mechanics*, Springer-Verlag, Berlin (1985).
18. W. G. Hoover, A. Rev. Phys. Chem. **34**, 103 (1983).
19. S. Nosé, Mol. Phys. **52**, 255 (1984).

20. A. Goldsmith, T. E. Waterman, and H. J. Hirschhorn, *A handbook of thermophysical properties of solid materials, vol. I*, Macmillan, New York (1961), pg. 571.

21. Y. S. Touloukian, R. W. Powell, C. Y. Ho, and P. G. Klemens, *Thermal Conductivity of Metallic Elements and Alloys, vol. I,* Plenum, New York (1970), pg. 326.

22. T. A. Arias and J. D. Joannopoulos, Phys. Rev. B **49**, 4525 (1994).

23. A. Bourret and J. L. Rouvière, Springer Proc. Phys. **35**, 8 (1989).

## Figure captions

1. Average phonon mean free path <$l_{ph}$> in crystalline Si as a function of temperature. See text.

2. Schematic showing the shape of supercell employed in all simulations. The supercell is divided into an odd number (13 in this figure) of equal sections parallel to the yz plane. The grain boundary is entirely contained in the middle section (section 7). Periodic boundary condition is employed on all sides. Some vacuum is left beyond the two end sections which are kept at two different temperatures $T_1$ and $T_2$.

3. Thermal profile for pure Si. The supercell is 450 Å along the x-axis and contains 630 atoms (21 sections, each containing 30 atoms). The [100] plane of the Si crystal is oriented parallel to the yz plane. Total simulation time is 1 ns.

4. Thermal profile for a $\Sigma$=13 twin boundary. The supercell is 250 Å long and contains 840 atoms. The grain boundary is obtained by rotating the two "grains" of the original crystal in opposite senses through an angle of 11.31° about the z-axis. Total simulation time is 1 ns.

5. Time evolution during simulation on the $\Sigma$=13 twin boundary: lower (solid) curve monitors the temperature of section #7 measured relative to the cold end (520 K); upper (dashed) line describes the behavior of the temperature discontinuity across the grain boundary (rescaled by a factor of half).

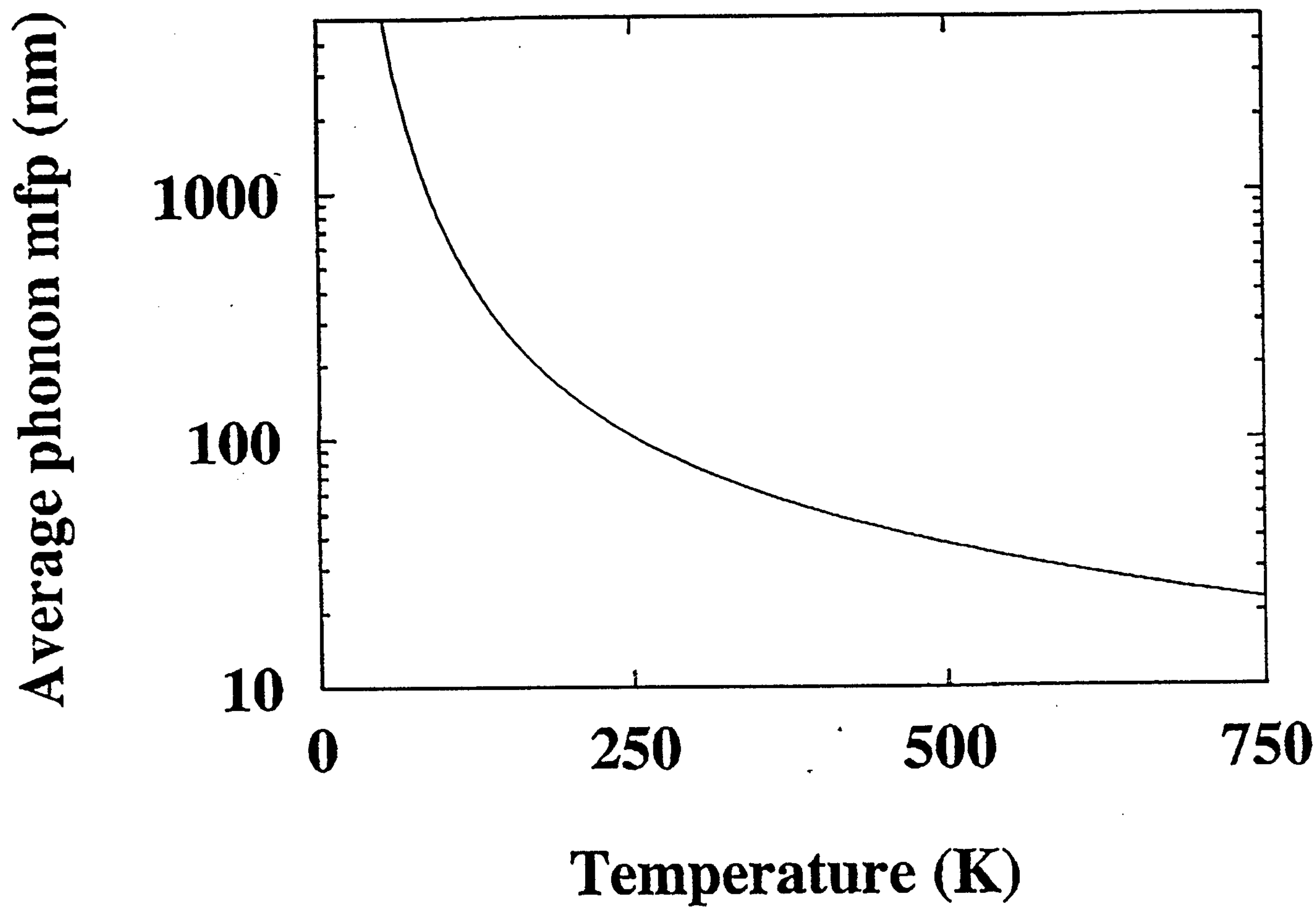


Figure 1

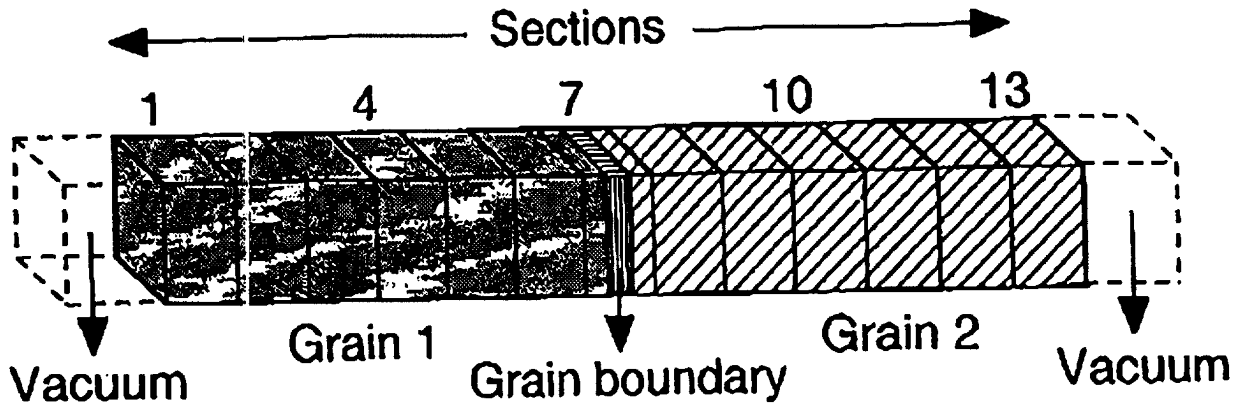


Figure 2

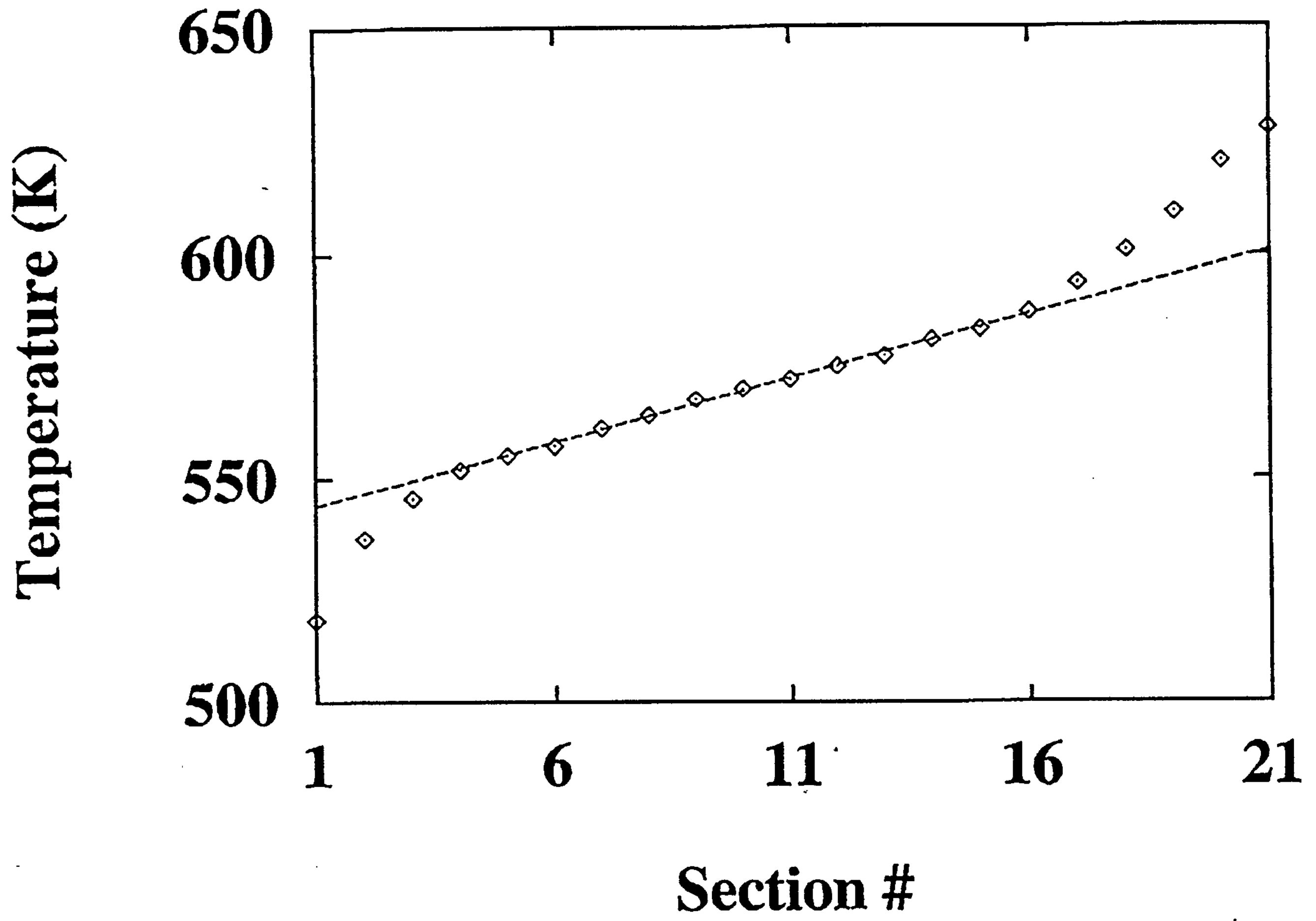


Figure 3

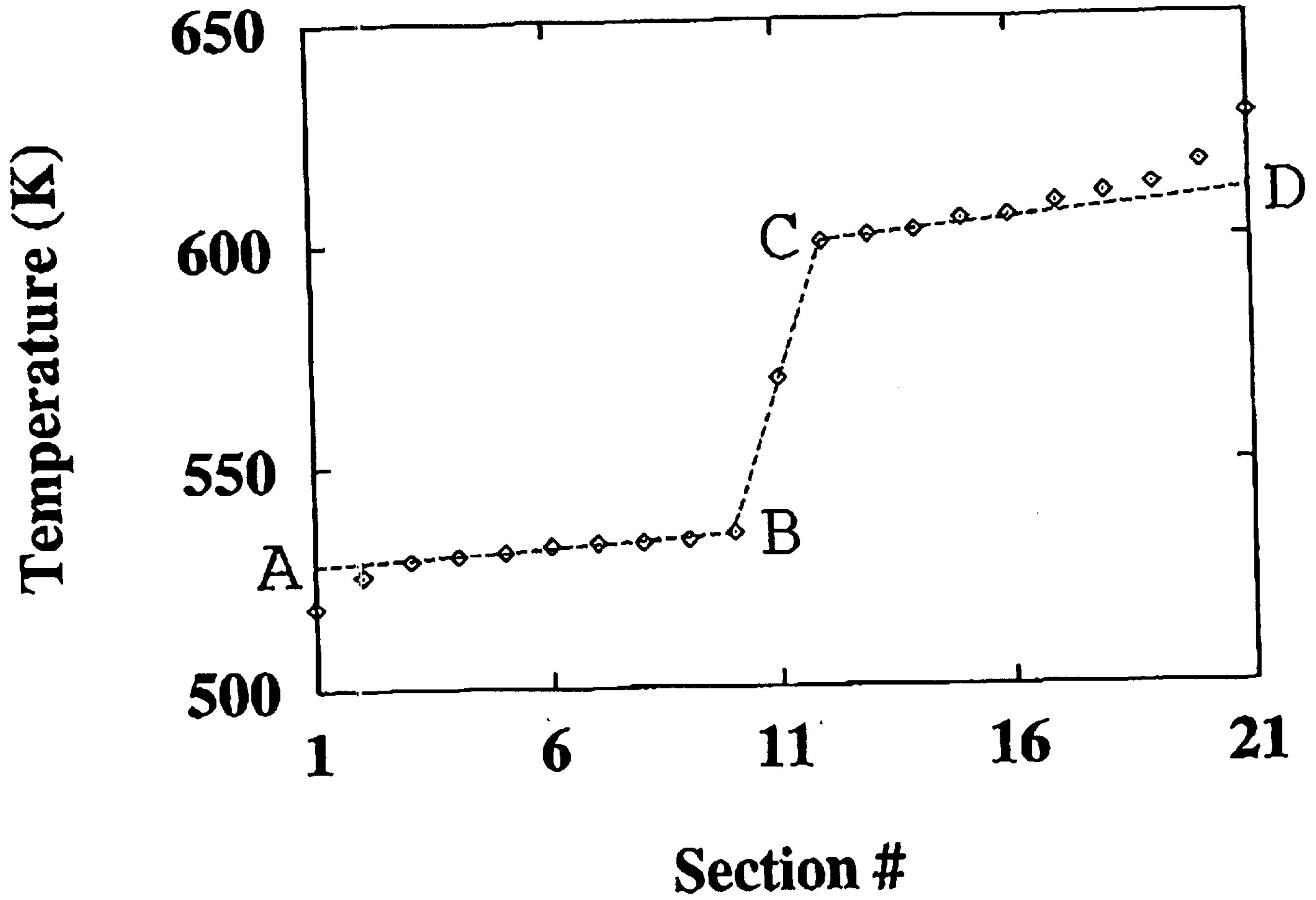


Figure 4

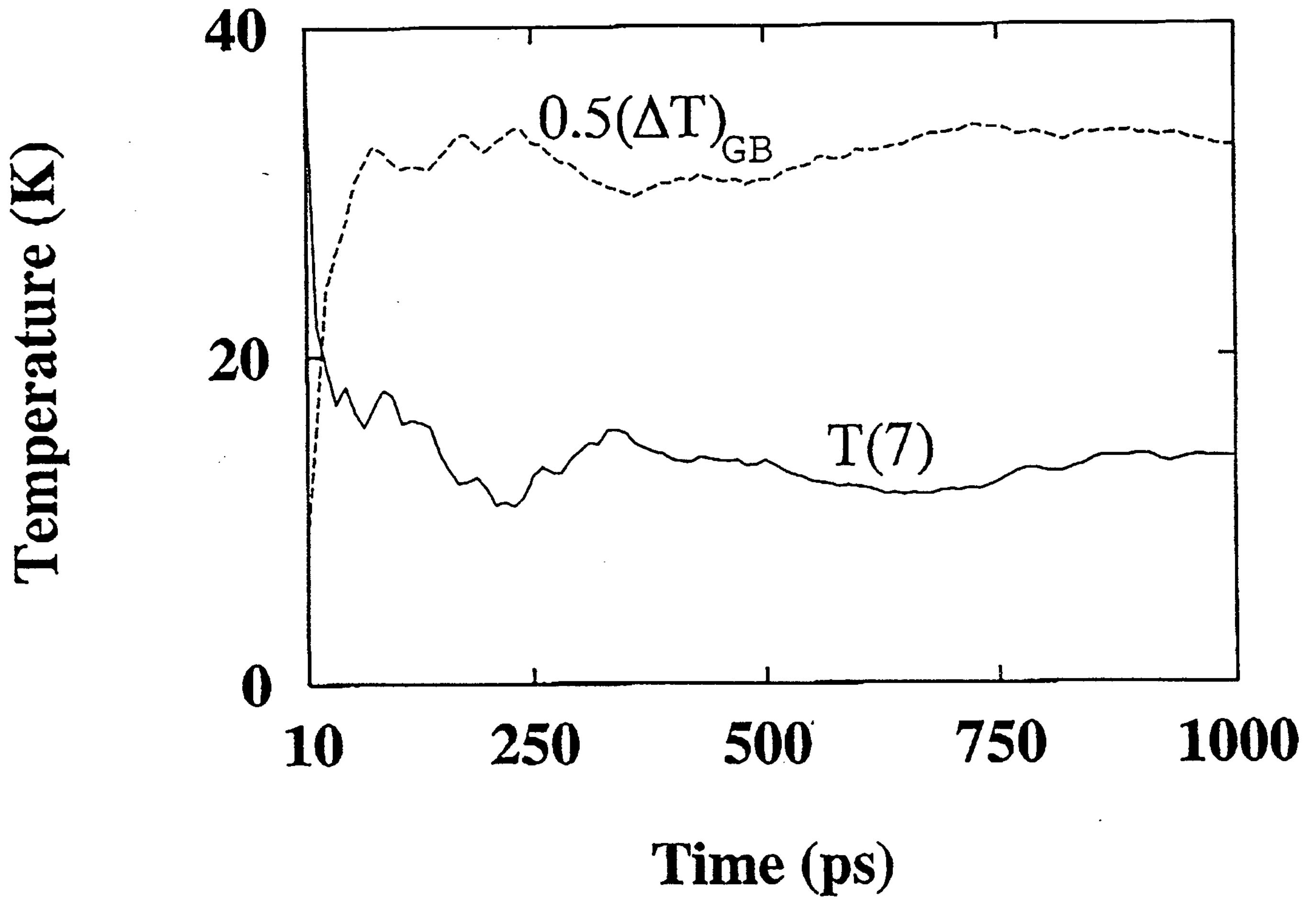


Figure 5

Appendix G

# THEORY AND COMPUTER SIMULATION OF MICROSTRUCTURE EVOLUTION IN POLYCRYSTALLINE METALLIC THIN FILMS

Dimitrios Maroudas[1], Matthew N. Enmark[2], Cora M. Leibig[1], and Sokrates T. Pantelides[3],[4]

[1]Department of Chemical Engineering,
[2]Department of Mechanical Engineering and Department of Materials,
University of California, Santa Barbara, CA 93106,
[3]Department of Physics and Astronomy, Vanderbilt University, Nashville, TN, 37235,
[4]Solid State Division, Oak Ridge National Laboratory, Oak Ridge, TN 37831.

## Abstract

A theoretical and computational analysis is presented of the microstructural dynamics in polycrystalline metallic thin films under the action of external fields. The analysis aims at a systematic modeling of failure mechanisms in Al-based interconnects driven by electric fields and thermomechanical stresses. Emphasis is placed on the formation, dynamics, and morphological stability of microvoids in aluminum thin-film conductors with bamboo grain structure. Simulations of thermal stress development during conductor processing explain the formation of intergranular voids at the intersections of grain boundaries with the conductor/passivation interface. The driving forces for the formation of slit-like cracks on transgranular void surfaces are calculated and the morphological stability of these surfaces is analyzed in detail. The results are in agreement with recent experimental data and explain the morphological evolution of transgranular voids under electromigration conditions.

## Introduction

Microstructure evolution in polycrystalline metallic thin films under the action of mechanical stress and electric current underlies many reliability issues in microelectronics. A serious reliability problem is the current-induced or stress-induced failure of metallic thin films which are used for interconnections in integrated circuits [1-3]. Interconnect technologies are currently based on polycrystalline aluminum thin films, usually with a small alloying addition of copper [1-3]. Failure occurs by formation and propagation of damage, usually in the form of voids, which is driven by the electric current that is conducted through the metal and/or thermomechanical stresses that develop during thin-film processing [3-4]. The continuous shrinking of the interconnect cross-sectional areas toward ultra-large-scale integration (ULSI) results in thin films with submicron-scale dimensions. These films must tolerate increasingly high current densities and levels of mechanical stress, which makes the problem of interconnect reliability very serious.

The development of design strategies for the improvement of interconnect reliability requires a fundamental understanding of the relation between thin-film structure and resistance to failure together with quantitative predictions of the thin-film structural evolution under processing and operation conditions. Self-consistent modeling of the physical mechanisms that drive the microstructural evolution can contribute significantly toward this goal. The general theoretical framework for the description of the microstructural dynamics starting from an atomic-scale description of a heterogeneous solid is available [5,6]. Robust computational tools for self-consistent calculations within the

above framework are provided by finite-element and boundary-integral methods [7,8], while the systematic search of the parameter space for engineering applications can be accomplished by nonlinear continuation techniques [9].

This paper presents a theoretical analysis and computer simulation results of microstructural stability and dynamics in polycrystalline thin-film conductors. Special emphasis is placed on the formation and dynamics of microvoids in Al-based conductors with bamboo grain structure. In particular, the formation of intergranular voids in passivated conductors is investigated through simulation of thermal stress development during the thermal processing of the conductors. The morphological stability and evolution of transgranular voids in unpassivated and passivated conductors under the action of an electric field is analyzed in detail. The analysis focuses on the calculation of the driving forces for morphological instabilities on the void surfaces, the steady-state void morphologies for a given magnitude of the electric field, and the investigation of the morphological evolution beyond the instabilities.

## Theory and Computer Simulation

The basic framework for the analysis of microstructure evolution in metallic thin-film conductors is provided by a self-consistent formulation of diffusional mass transport in a heterogeneous solid under the action of external fields. A detailed overview of this formulation has been given elsewhere [10,11]. The most important element of the formulation is the expression of the total interfacial atomic flux, which consists of both purely diffusional components and field-induced drift fluxes, such as the electromigration flux under the action of an applied electric field. Typical interfaces involved in the formulation for a thin-film conductor are grain boundaries, conductor/passivation interfaces, and the free surfaces of voids present in the conductor. Purely diffusional fluxes are determined by the interfacial gradient of the chemical potential of the atoms in the interfacial region. The chemical potential is a function of the local stress and strain fields, the local curvature, and the interfacial free energy per unit area. The strongest nonlinearities in the analysis arise from the presence of the curvature operator in the formulation. The interfacial dynamics is governed by the continuity equation, which involves the interfacial divergence of the total interfacial flux. The interfacial transport problem is coupled with the stress field distribution in the solid, due to the dependence of the chemical potential on stress. Under the action of an electric field, interfacial transport is also coupled with the electric current distribution in the conductor, due to the explicit dependence of the electromigration flux on the electric field [10,11].

In the general case, therefore, the transport problem should be solved self-consistently with Cauchy's equilibrium equations for the stress field in the solid and Maxwell's equations for the electric field. This is done numerically by employing finite-element or boundary-integral techniques. Most of the numerical simulations presented in this paper are based on the finite-element discretization and the Galerkin method of weighted residuals [7]. The Galerkin finite-element method reduces the weak form of a boundary-value problem to a large set of sparse algebraic equations for the nodal values of the field variables. The resulting linear/linearized equation sets are solved using standard banded-matrix solvers based on direct L U factorization [12].

## Analysis of Stress-Driven Intergranular Void Formation

The development of thermomechanical stresses in the metallic thin film during processing is one of the main driving forces for the formation of voids in the conductor. Here, we present an analysis based on thermal stress modeling that identifies the most



probable sites for void nucleation in bamboo-structure conductor lines avoiding a detailed thermodynamic analysis of void nucleation in a metallic thin film.

In order to understand the development of thermal stresses during the processing of a metallic thin film, let us consider a long conductor line that is deposited on the semiconductor substrate at an elevated temperature. A passivation material, such as $SiO_2$, is used to encapsulate the conductor. A schematic of an encapsulated conductor line with bamboo grain structure is shown in Fig. 1. When the system is cooled down to room temperature or to a temperature typical of accelerated electromigration testing (500 K), thermal stresses develop in the metallic film due to the differences, $\Delta\alpha$, in the thermal expansion coefficients between the metal and the substrate or passivation. The order of magnitude of the induced hydrostatic tensile stresses is $B(\Delta\alpha)\Delta T$, where $B$ is the bulk modulus of the metal and $\Delta T$ is the temperature difference involved in the cooling process.

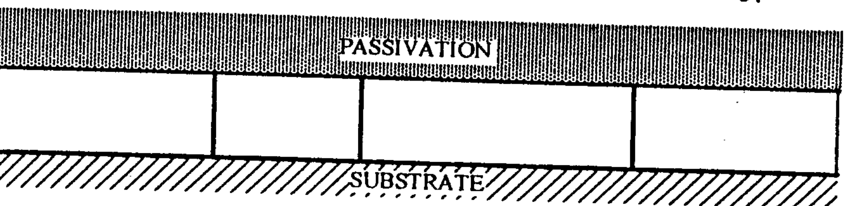


**Figure 1.** Schematic of a passivated bamboo-structure conductor line with the grain boundaries oriented perpendicularly to the conductor axis.

We simulated the development of thermal stresses in the metallic film using the Galerkin finite-element method for a conductor microstructure similar to the structure of Fig. 1. The computational domain employed in our calculations is a simulation cell that contains three grain boundaries that are oriented perpendicularly to the conductor axis with periodic boundary conditions in the direction of the conductor length. We used a nonuniform grain-boundary spacing with a variation from $2w$ to $6w$, where $w$ is the width of the conductor line. The periodic boundary conditions implemented here result in a regular but representative distribution of grain boundaries in a conductor line with bamboo grain structure.

In our finite-element simulations, the substrate and the passivation were modeled as perfectly rigid materials, while the constitutive equations of linear thermoelasticity [13] were implemented for the metallic conductor. A two-dimensional displacement formulation within the plane-stress approximation was adopted for the solution of Cauchy's equilibrium equations for the stress field in the conductor. In addition to this routine formulation of the thermomechanical boundary-value problem, we assigned a finite grain-boundary width, $\delta_b$, to each grain boundary in the computational domain. In the simulations presented here, $\delta_b$ was taken to be equal to 1% of the linewidth; for a typical linewidth, $w$=0.5 μm, the corresponding grain-boundary width is $\delta_b$=5 nm. In the grain-boundary region of size $\delta_b$, we used elastic constants different from the ones used in the grains according to recent atomistic simulation results in *fcc* metals [14]. In particular, we adopted atomistic-simulation predictions for copper bicrystals, which suggest that the Young modulus in the grain-boundary region is higher by 40% than the Young modulus in the grains [14]. Thermophysical properties typical of pure aluminum were used for the grains.

In the finite-element simulations, the components of the displacement field were approximated using Lagrangian interpolation with biquadratic basis functions [7]. The direct treatment of the grain-boundary regions required extreme refinement of the finite-

element mesh in these regions and was the main source of computational intensity for the calculation. Additional mesh refinement close to the conductor/passivation interfaces resulted in a total number of about 50,000 degrees of freedom for a typical calculation.

Figure 2 shows representative results for the distribution of the stress component, $\sigma_{xx}$, normal to the grain boundaries. The results are given in terms of isostress contours for a temperature difference $\Delta T$=375 K, which is typical of the cooling process under investigation. The variation of the normal stress component along the grain-boundary plane for the middle grain boundary in the computational domain is shown in Fig. 3. The stress is scaled with the appropriate elastic modulus in the plane-stress formulation of the problem [13]. The normal stress distributions along the other two grain boundaries in the simulation cell are very similar to that of Fig. 3.

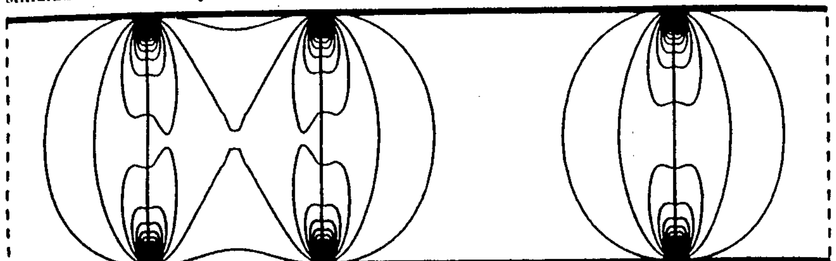

**Figure 2.** Distribution in terms of isostress contours of the stress component normal to the grain boundaries in the conductor of Fig. 1.

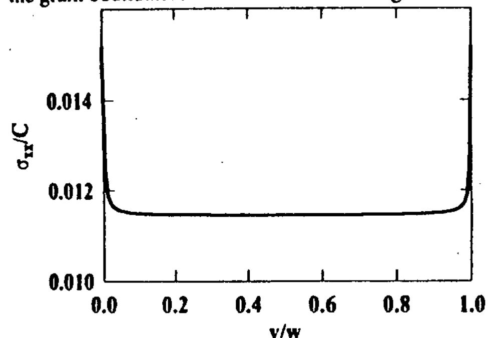


**Figure 3.** Variation of stress component normal to the grain boundaries along one of the grain boundaries in the conductor of Fig. 1.

Both the contours of Fig. 2 and the normal stress distribution of Fig. 3 show the development of very high stress concentrations at the intersections of the grain boundaries with the conductor/passivation interface. Due to these high tensile stress concentrations, the sites at such intersections become primary candidates for the nucleation of voids in order to lower the overall free energy of the conductor. This qualitative result is fully consistent with experimental observations of void formation at such regions of the conductor [15] and explains the role of the induced mechanical stress in intergranular void nucleation. Currently, we are performing three-dimensional simulations with realistic mechanical properties of the substrate and passivation materials for quantitative predictions of the induced thermal stress field in the thin-film conductor.



## Dynamics of Transgranular Voids Under Electromigration Conditions

In thin-film conductors with bamboo grain structure, transgranular voids, i.e. voids in the grains of the conductor not associated with grain boundaries, have been identified as major forms of damage that can cause conductor failure under electromigration conditions [16,17]. Frequently, conductor failure occurs after a transgranular void undergoes a current-induced morphological instability, such as the slit-like instability [18]. This morphological instability, which is expressed by the formation of a slit-like crack that propagates from the void surface, is demonstrated in Fig. 4 for two void surface geometries. The fundamental theoretical problem in transgranular void dynamics under electromigration conditions is the prediction of current-induced instabilities and of the void-surface morphological evolution beyond the instability. Such predictions are based on the solution of the mass transport problem on the void surface coupled with the electric field distribution in the conductor. These calculations can provide valuable answers regarding the electromigration resistance of a conductor as a function of the magnitude of the applied electric field and of material and interface properties.

In our analysis, we distinguish between wedge-shaped and rounded transgranular void morphologies, both of which are observed experimentally in unpassivated or passivated bamboo-structure conductor lines. In our calculations, we adopt a two-dimensional representation of the conductor microstructure. In such a representation, the voids are assumed to extend throughout the line thickness, thus maintaining an overall *cylindrical* shape. The analysis focuses on the morphology and dynamics of the transgranular void surface neglecting the presence of grain boundaries in the conductor away from the void surface.

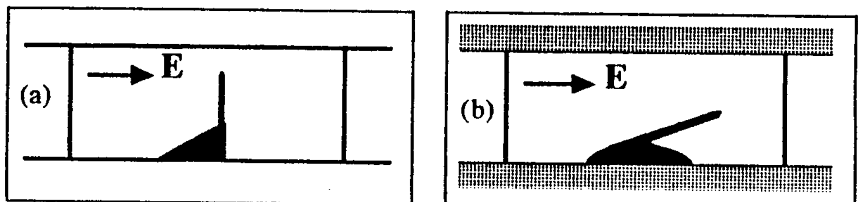


**Figure 4.** Formation of slit-like cracks that emanate from the surface of transgranular voids that are either (a) wedge-shaped or (b) rounded in bamboo-structure conductors that are (a) unpassivated or (b) passivated.

## Wedge-Shaped Transgranular Voids In Unpassivated Conductors

Wedge-shaped voids are common in aluminum conductors. These voids consist of two planar surfaces. Under the action of an electric field, it is frequently observed that one of these surfaces is oriented almost perpendicularly to the direction of the field, while the second surface forms either a positive or a negative slope with respect to the direction of the field. The morphological evolution of such voids under electromigration conditions was demonstrated in some recent experiments in unpassivated aluminum lines [19,20]. More recently, we have shown that the tilted planar surface of these voids is morphologically *stable* if it is negatively tilted with respect to the field direction. In the opposite case, a perturbation from the planar surface may grow *unstably* if the wavelength of the perturbation is longer than a critical wavelength [21]. Steady-state morphologies that

bifurcate from the tilted planar surface have also been predicted [10,11]. Here, we focus our attention on the driving forces responsible for the formation and propagation of slit-like cracks from wedge-shaped void surfaces; such slit-like crack formation is observed experimentally at wedge-void tips, even for voids with negatively tilted surfaces. Our study is based on finite-element simulations of current crowding around the surfaces of wedge-shaped voids in unpassivated aluminum conductors.

In our simulations, we solved Laplace's equation, $\nabla^2\Phi = 0$, for the electric potential $\Phi$ and computed the distribution of the electric field, $\mathbf{E} = -\nabla\Phi$, in the conductor under the boundary conditions that the field does not penetrate the void surface and the external surface of the conductor. The void was placed in the middle of the conductor and the length of the computational domain in the direction of the applied electric field was determined by a series of convergence tests. The far field condition $E=E_\infty$, where $E_\infty$ is the magnitude of the applied electric field away from the void surface, was posed at the edges of the computational domain. In the simulations, $\Phi$ was approximated through Lagrangian interpolation using biquadratic basis functions. Mesh refinement near and along the void surface resulted in a number of degrees of freedom on the order of $10^4$.

Figure 5 shows the distribution of the electric field magnitude $E$ around three wedge-shaped voids with tilted surfaces at angles $\theta_w$ with the electric field direction of 30°, 45°, and 60°, respectively. The void sizes in the direction of the field are equal to one third of the linewidth. The results are presented in terms of contours of $E/E_\infty$. In particular, 50 contours of constant $E/E_\infty$ are shown for each case. The contour levels are equidistant ranging from zero at the intersections of the void surface with the external surface of the conductor to a maximum value at the void tip. These results show the significant variation of the electric field along the void surface. The wedge edges, i.e. where the void surface meets the external surface of the conductor, correspond to stagnation points in the current flow. In general, the simulations predict a maximum in the tangential component $E_s$ of the field right at the void tip. This variation of $E_s$ along the void surface of total peripheral length $s_t$ is shown in Fig. 6 including both the perpendicular and the tilted plane of the wedge for $\theta_w=60°$. Excluding the sharp maximum of $E_s(s)$ exhibited at the tip, the variation of $E_s$ along the tilted surface of the void is fairly smooth and symmetric about the value $E_s=E_\infty \cos\theta_w$.

The sharp maximum of $E_s$ in the vicinity of the void tip predicted by our finite-element simulations has important implications for the dynamical behavior of wedge voids. Specifically, very high electromigartion fluxes and flux divergences develop in the vicinity of the void tip. This makes the void tip a site for nucleation of finer-scale void forms, such as slits or cracks, which can subsequently propagate very fast and cause conductor failure. This is a very important result of our simulations and explains the formation of slits at wedge-void tips which has been observed experimentally [19,20].

For further investigation of the effects of current crowding around the void surfaces, we carried out simulations of the electric field distribution in the presence of narrow slits that emanate from the void tip. Results are presented in Fig. 7 for the case of a wedge void with $\theta_w=45°$, where the size $a$ of the void in the direction of the field is equal to one third of the linewidth. In particular, two cases are analyzed, where the slit tip is located at 50% and 80% of the linewidth, respectively, and for a slit width equal to 0.2 $a$. About 40,000 degrees of freedom are involved in these numerical calculations. The results are presented again in terms of contours of $E/E_\infty$; 50 contours of constant $E/E_\infty$ are shown for each case. The contour levels are equidistant ranging from zero at the intersections of the void surface with the external surface of the conductor to 4 at a region around the slit tip. The (contour-free) region right above the slit tip corresponds to field magnitudes that



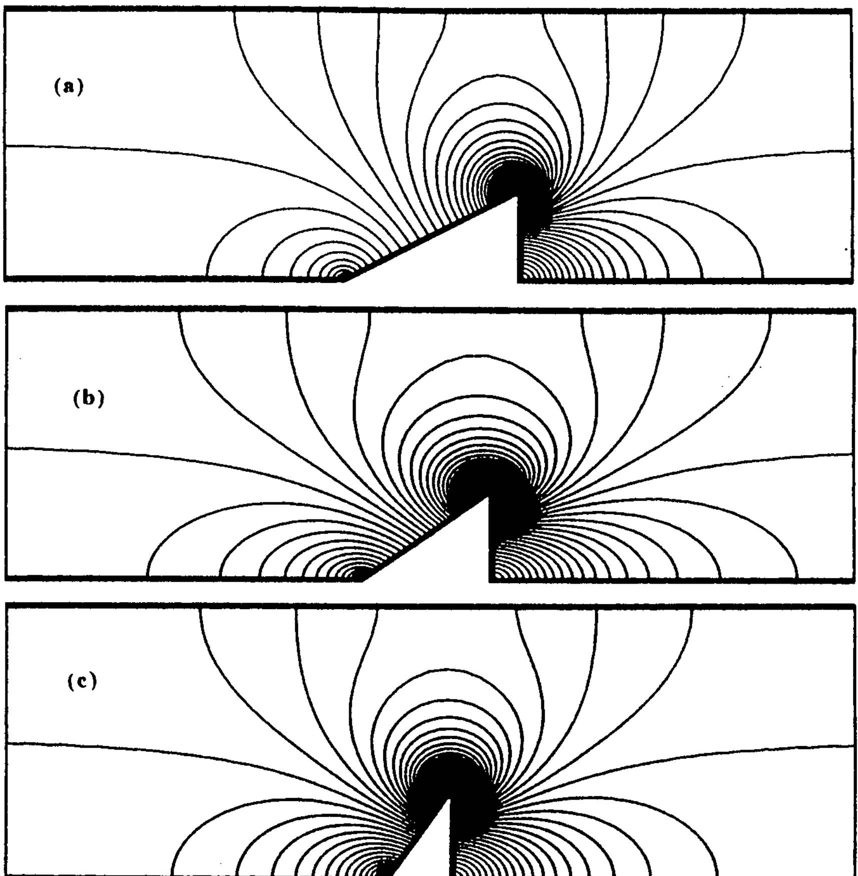


**Figure 5.** Distribution of the magnitude $E$ of the electric field around wedge-shaped transgranular voids. The tilted surface of the wedge forms an angle of (a) 30°, (b) 45°, and (c) 60°, with respect to the field direction, which is from the right to the left.

satisfy $E/E_\infty > 4$. A very sharp maximum in the distribution of the field magnitude occurs right at the slit tip. For the slit-like cracks simulated here, the maximum of $E_s$ at the tip is higher by about one order of magnitude compared to the maximum value at the tip of the wedge void in the absence of the slits. In addition, this maximum value of the field magnitude keeps increasing monotonically with the height of the slit. As a result, the electromigration flux and its surface divergence, which controls the rate of slit propagation, increase significantly, thus making the open-circuit failure of the line inevitable.

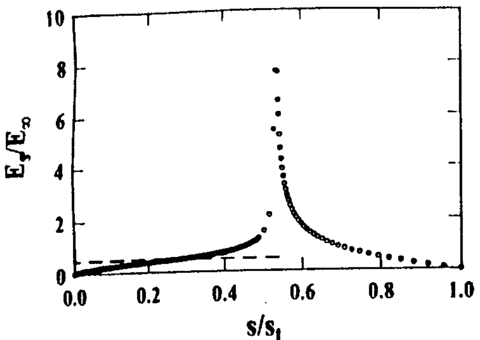


**Figure 6.** Variation of the tangential component of the electric field along the wedge-shaped void of Fig. 5c. Here, $s/s_t$=0 corresponds to the intersection of the tilted surface of the wedge with the outer surface of the conductor. The dashed line represents the projection of the far field on the tilted surface of the wedge.

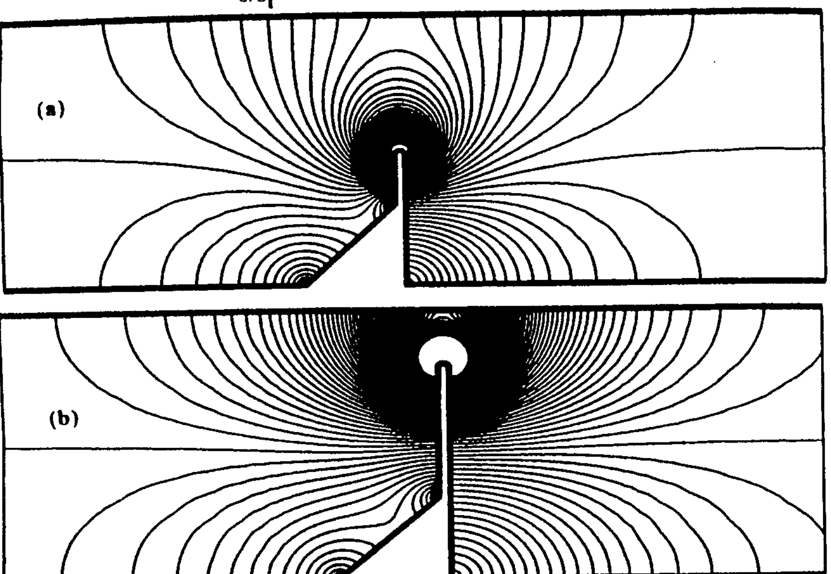


**Figure 7.** Distribution of the magnitude $E$ of the electric field around wedge-shaped voids with slits emanating from the void tips. The slit tip is located at (a) 50% and (b) 80% of the linewidth. In both cases, the field direction is from the left to the right.

**Rounded Transgranular Voids In Passivated Conductors**

Rounded transgranular voids are common forms of damage in passivated conductor lines [22]. Here, we present an analysis of the nonlinear free-boundary surface transport problem that determines the morphology and morphological stability of the transgranular void surface. The analysis is based on the integration of the steady-state form of the



continuity equation, $\nabla_s \cdot \mathbf{J}_s = 0$, where the total surface flux of atoms $\mathbf{J}_s$ includes curvature-driven surface diffusive fluxes and electromigration fluxes. We solved the problem numerically by implementing the shooting method within a Newton iterative scheme [12] under boundary conditions that specify the points of intersection of the void surface with the passivated surface and the equilibrium contact angle $\theta_c$ at the points of intersection. The contact angle is a thermodynamic property of the system determined by the interfacial free energies of the interfaces that are involved in the formation of the angle; our incomplete knowledge of such thermodynamic properties made us use $\theta_c$ as a parameter in our investigation.

In order to accelerate our analysis of void morphological stability, we decoupled the calculation of the electric field distribution in the conductor from the nonlinear surface transport problem. This was done by employing for the component $E_s$ of the electric field tangent to the void surface the analytical approximation $E_s=2E_\infty \cos\theta$, where $\theta$ is the angle formed between the direction of the far field and the tangent to the void surface. This analytical expression is the exact potential-flow result for the tangential component of the field around a perfectly cylindrical void [10]. In the application of this approximate analytical expression, the actual computed shape function $\theta(s)$ from the solution of the nonlinear transport problem was used, where $s$ is the arc-length coordinate along the void surface.

We carried out a systematic parametric study of the steady-state void morphology based on the pseudo-arc-length continuation technique [9] with the surface electrotransport number $\Gamma$ [23] as the controlling parameter. $\Gamma$ is a dimensionless parameter that scales electric forces with surface forces and is defined as $\Gamma=E_\infty q_s^* a^2/(\gamma\Omega)$, where $q_s^*$ is the surface effective charge, $\gamma$ is the surface free energy per unit area, and $\Omega$ is the atomic volume. Representative results of this parametric study are shown in Fig. 8, in terms of a response (bifurcation) diagram, where the total length of the void periphery $s_t$ is plotted as a function of $\Gamma$ for two values of the contact angle, $\theta_c$=80° and $\theta_c$=70°, respectively. The solution families exhibit a regular turning point at critical values $\Gamma=\Gamma_c$, which expresses the presence of multiple steady states. The steady states that correspond to the lower branch of $s_t(\Gamma)$ are stable, while those that correspond to the upper branch are unstable. The stability of the steady-state solutions is determined by calculating the eigenvalues of the Jacobian matrix involved in our Newton-shooting method.

The void morphologies that correspond to points A and B of the solution curve of Fig. 8 are shown in Figs. 9a and 9b, respectively. The basic morphological characteristic is the distortion of the void surface in the direction of the electric field with respect to the ideal cylindrical shape; the distortion is much more pronounced for the unstable void morphology. These are generic morphological characteristics of rounded transgranular voids under the action of an electric field and do not arise as a result of the specific choice of the equilibrium contact angle. These qualitative characteristics are fully consistent with void morphologies that have been observed experimentally during accelerated electromigration tests in Al-based passivated conductor lines [22].

The results of the nonlinear analysis have important implications regarding the morphological evolution of rounded transgranular voids under electromigration conditions. The results of Fig. 8 explain the experimentally observed morphological evolution of the void surface beyond the instability. At a given value of $\Gamma$, perturbations from the unstable void shape grow toward either lower or higher values of the void peripheral length $s_t$. In the former case, the void surface evolves ultimately to the stable morphology. In the latter case, however, the perturbation leads to the propagation of an elongated shape, such as a slit, which is a common observation in electromigration testing experiments [16,17]. Quantitatively, the analysis predicts the actual size of the void as a function of the

magnitude of the applied electric field and material properties. Using the defnition of $\Gamma$, values of $\Gamma$ in the vicinity of the turning point, field magnitudes on the order of 500 V/m that are typical of electromigration testing, and material properties that are typical of pure Al gives void sizes over the range of 0.35 µm $\leq a \leq$ 0.65 µm. This is the correct order of magnitude for experimentally observed void sizes and can be compared, to within a factor of two, with most of the data from electromigration testing experiments [22,24].

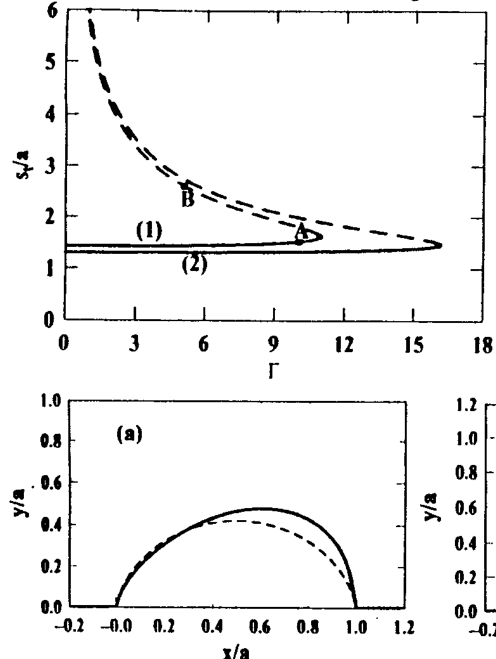


**Figure 8.** Dependence of the steady-state peripheral length of a rounded transgranular void on the surface electrotransport number $\Gamma$ for contact angles of (1) 80° and (2) 70°. Solid and dashed lines indicate stable and unstable steady-state solution families, respectively.

**Figure 9.** Calculated steady-state void morphologies that correspond to points (a) A and (b) B on the solution family of Fig. 8. The dashed circular arc corresponds to the perfectly cylindrical void morphology.

We have tested the validity of the analytical approximation for the decoupling of the electric field distribution from the surface transport problem by numerical simulations of current crowding in passivated aluminum conductors that contain transgranular voids with the morphological characteristics predicted by our nonlinear analysis. In particular, we have performed a sequence of finite-element simulations for various linewidths, $w \geq 2a$, and contact angles over the range $45^{\circ} \leq \theta_w \leq 120^{\circ}$. The simulation procedure that we followed is the same procedure that was followed in the simulations of current crowding around wedge-shaped voids.

The qualitative characteristics of the field distribution are similar in all of the cases that we simulated. Figure 10 shows the distribution of the electric field magnitude $E$ around the stable and unstable void surfaces with the morphologies of Fig. 9a and 9b, respectively. The void sizes in the direction of the field are equal to one third of the linewidth. The results are presented in terms of contours of $E/E_\infty$. In particular, 25 contours of constant $E/E_\infty$ are shown for each case. The contour levels are equidistant ranging from zero at the intersections of the void surface with the conductor/passivation interface, which are stagnation points for the current flow, to a maximum value at the top of the void surface, $\theta(s)=0$. Therefore, the field distribution results in increased current densities in the region of the conductor above the void surface; quantitatively, the current crowding is generally consistent with the prediction of the analytical potential-flow approximation.

A detailed comparison between the analytical approximation and the fully numerical results was presented in previous publications for stable rounded void morphologies [10,11]. The agreement is overall satisfactory in all of the cases that we investigated. In general, the analytical approximation is better for the stable morphologies, in the wider conductor lines, and for contact angles closer to $\theta_c=90^{\circ}$.

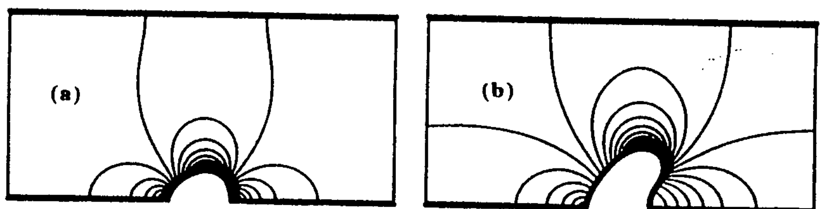


**Figure 10.** Steady-state distribution of the electric field magnitude $E$ around surfaces of rounded transgranular voids with (a) the stable morphology of Fig. 9a and (b) the unstable morphology of Fig. 9b. In both cases, the field direction is from the left to the right.

## Summary and Conclusions

A theoretical and computational analysis was presented of microstrutural dynamical processes in aluminum thin-film conductors under the action of thermomechanical stresses and electric fields. The analysis focused on the formation of intergranular voids and the morphological stability and evolution of transgranular voids in conductors with bamboo grain structure. Reasonable approximations of the actual conductor microstructure yielded results that are in general agreement with experimental observations of void formation, morphological stability, and morphological evolution. Such simplified models that include the dominant microstructural features of the conductor and a description of the underlying physical mechanisms at a sufficient level of approximation are, therefore, capable of qualitative and quantitative predictions of microstructure evolution and its implications for thin-film reliability.

For the development of systematic engineering strategies to improve interconnect reliability, however, accurate predictive modeling is required of the microstructure evolution and its dependence on the film composition, material and interface properties, and processing conditions. Therefore, the details of the conductor grain structure is required in conjunction with an accurate description of the physical mechanisms that govern the mechanical behavior of the grains and the interfacial dynamics. In addition, accurate quantitative predictions require the development of an accurate material and interface property database. These properties determine the stability of surfaces and interfaces and

set the time scales that determine the microstructural dynamics. Incorporation of this realistic level of complexity into a self-consistent calculational scheme introduces significant computational problems and requires optimal algorithmic approaches for its computationally efficient implementation. This is a task that we have undertaken and we are currently implementing using atomic-scale simulations for property predictions and a fully self-consistent dynamical scheme for the simulation of microstructure evolution based on a boundary-integral formulation.

## Acknowledgements

D.M. acknowledges the support of the NSF (ECS-95-01111) through a CAREER award. S.T.P. acknowledges the support of the ONR under contract No. N00014-95-1-0906.

## References

[1] P. S. Ho and T. Kwok, *Rep. Prog. Phys.* **52**, 301 (1989).
[2] F. M. d'Heurle and R. Rosenberg, in *Physics of Thin Films* (Academic Press, New York, 1973), vol. 7, p. 257.
[3] C. V. Thompson and J. R. Lloyd, *MRS Bulletin* **18**, No. 12, 19 (1993).
[4] P. A. Flinn et al., *MRS Bulletin* **18**, No. 12, 26 (1993).
[5] S. T. Pantelides, *J. Appl. Phys.* **75**, 3264 (1994).
[6] S. T. Pantelides, D. Maroudas, and D. B. Laks, *Mater. Sci. Forum* **143-147**, 1 (1994); in *Computational Material Modeling*, edited by A. K. Noor and A. Needleman (ASME, New York, 1994), p. 1.
[7] G. F. Carey and J. T. Oden, *Finite Elements. A Second Course* (Prentice-Hall, Englewood Cliffs, NJ, 1983).
[8] C. A. Brebbia, J. C. F. Telles, and L. C. Wrobel, *Boundary Element Techniques* (Springer-Verlag, New York, 1984).
[9] M. Kubicek and M. Marek, *Computational Methods in Bifurcation Theory and Dissipative Structures* (Springer-Verlag, New York, 1983).
[10] D. Maroudas, M. N. Enmark, C. M. Leibig, and S. T. Pantelides, *J. Comp.-Aid. Mater. Des.*, in press (1996).
[11] D. Maroudas and S. T. Pantelides, *MRS Symp. Proc.* **391**, 151 (1995).
[12] G. Dahlquist and A. Björck, *Numerical Methods* (Prentice-Hall, Englewood Cliffs, NJ, 1974).
[13] L. D. Landau and E. M. Lifshitz, *Course on Theoretical Physics, vol. 7: Theory of Elasticity* (Pergamon Press, Oxford, 1986).
[14] M. Nomura and J. B. Adams, private communication.
[15] M. A. Korhonen, P. Borgesen, and C.-Y. Li, *MRS Bulletin* **17**, No. 7, 61 (1992).
[16] J. E. Sanchez, Jr., L. T. McKnelly, and J. W. Morris, Jr., *J. Appl. Phys.* **72**, 3201 (1992).
[17] J. H. Rose, *Appl. Phys. Lett.* **61**, 2170 (1992).
[18] Z. Suo, W. Wang, and M. Yang, *Appl. Phys. Lett.* **64**, 1944 (1994).
[19] O. Kraft, S. Bader, J. E. Sanchez, Jr., and E. Arzt, *MRS Symp. Proc.* **309**, 351 (1993).
[20] E. Arzt, O. Kraft, W. D. Nix, and J. E. Sanchez, Jr., *J. Appl. Phys.* **76**, 1563 (1994).
[21] D. Maroudas, *Appl. Phys. Lett.* **67**, 798 (1995).
[22] M. C. Madden et al., *MRS Symp. Proc.* **265**, 33 (1992).
[23] D. Maroudas and S. T. Pantelides, *MRS Symp. Proc.* **309**, 333 (1993).
[24] W. D. Nix and E. Arzt, *Metall. Trans. A* **23A**, 2007 (1992).